ANALYSIS OF BRIDGE SOIL INTERACTION UNDER SEISMIC LOADING

MD. MOZAMMEL HOQUE

DEPARTMENT OF CIVIL ENGINEERING
BANGLADESH UNIVERISTY OF ENGINEERING AND TECHNOLOGY
DHAKA

SEPTEMBER, 2001

ANALYSIS OF BRIDGE SOIL INTERACTION UNDER SEISMIC LOADING

A THESIS BY
MD. MOZAMMEL HOQUE

Submitted in partial fulfilment of the requirements
for the degree of

MASTER OF SCIENCE IN CIVIL ENGINEERING

DEPARTMENT OF CIVIL ENGINEERING
BANGLADESH UNIVERISTY OF ENGINEERING AND TECHNOLOGY,
DHAKA

SEPTEMBER, 2001

ANALYSIS OF BRIDGE SOIL INTERACTION UNDER SEISMIC LOADING

A THESIS BY

MD. MOZAMMEL HOQUE

Approved as to the style and content by the Examination Committee

Mehedi Ahmed Ansary

Dr. Mehedi A. Ansary
Associate Professor
Derpatment of Civil Engineering
BUET, Dhaka

Chairman
(Supervisor)

Dr. Md. Abdur Rouf
Professor & Head
Department of Civil Engineering
BUET, Dhaka

Member

T.M. Al-Hussaini

Dr. T.M. Al-Hussaini
Associate Professor
Department of Civil Engineering
BUET, Dhaka

Member

Md. Nuruzzaman
Professor
Department of Civil Engineering
BIT Dhaka,Gazipur

Member
(External)

Dedicated

To

Almighty Allah

CONTENTS

DECLARATION

Declared that, except where specified references are made to other investigators, the work embodied in this thesis is the result of investigation carried out by the author under the supervision of Dr. Mehedi A. Ansary Associate Professor of Civil Engineering Department, BUET.

Neither the thesis nor any part thereof has been submitted or is being concurrently submitted in candidature for any degree at any other institution.

Author.

ACKNOWLEDGEMENT

The author wishes to express his deepest gratitude to Dr. Mehedi A. Ansary, Associate Professor of Civil Engineering Department, BUET for his guidance, invaluable suggestions and affectionate encouragement at different stages of the study.

The author is grateful to Dr. T.M. Al-Hussaini, Associate Professor of Civil Engineering Department for his constructive suggestion at some stages of the study.

The author expresses his profound gratitude to Dr. M.S.A.Siddiqee, Associate Professor of Civil Engineering Department for his constructive suggestion at different stages of the study.

The author is grateful to Dr. Md. Abdur Rouf, Professor & Head of the Department of Civil Engineering Department for his encouragement and co-operation.

Acknowledgement is also made to Prof. Md. Nuruzzaman , Professor, Department of Civil Engineering BIT Dhaka, Gazipur for his advice ,help and encouragement during the course of the study.

ABSTRACT

Deformation of soil due to seismic load imposed by the structures above can result in the change in stresses and deformation of the structures. Considering the interaction between soil and structure is important especially for the design of large structures with embodiment such as nuclear power plant containment and foundations of bridges. Engineering experience has shown that under dynamic loading and particularly during earthquakes the bridge-soil systems undergo significant alterations. These alternations cannot be taken into account using the classical methods of design. Consequently, to prevent major disasters and material loss it is imperative to perform adequate soil structure interaction analysis. Furthermore, as some interaction phenomena have favorable effect on the structural resistance, their consideration enables design and construction with economy and elegance.

Three multiple span simply supported bridges, representative of typical bridges in Bangladesh, has been analyzed. Soil supports are explicitly modeled with equivalent springs. Radiation damping associated with wave propagation between the masses of the superstructure and foundation-soil is one form of energy dissipation due to soil-structure interaction(SSI). In this study, damping due to material nonlinearly in the foundation-soil is explicitly modeled, while the radiation damping is implicitly accounted for through equivalent viscous damping. Beam column elements are used to model the columns and simple connection elements are employed in modeling bearings and soil-structure springs. Extensive parametric studies are also performed to show the influence of soil shear modulus (400 psi, 4000 psi and 40000 psi), backwall condition (intact and broken), bearing performances (intact and failed with two different coefficient of friction equal to 0.2 and 0.6). Results are presented in terms of time histories of shear force at pier columns, top displacement of pier, gap width of abutment, plastic rotation at base of pier column and deck displacements due to variation of bearing performances, SSI models, boundary conditions of the pier column footings and soil conditions.

Time history analysis of bridges has considered both the fixity and flexibility of the supports using 5% damping. Push over analysis and nonlinear time history analyses of bridges have also been performed using both 2-D and 3-D computer models by DRAIN-2DX and DRAIN-3DX. Raleigh's damping proportional to both stiffness and mass matrices is used. Under peak ground acceleration (PGA) of 0.18g and 0.4g bridges were analyzed under three different earthquake records (Parkfield, El-Centro and Nahanni).

LIST OF TABLES

LIST OF FIGURES

NOTATION

f'_c	Ultimate strength of conrete of Cylindrical Specimen at 28 days
f_y	Yield strength of steel.
α	Shape correction factor
β	Foundation embodiment factor
K_{11} & K_{22}	Stiffness coefficients for horizontal translation
K_{33}	Stiffness coefficient for vertical translation.
K_{44} & K_{55}	Stiffness coefficients for rocking rotations
R	Radius for circular footing Shear modulus of Soil
ν	Poisson's ratio of soil.
K_w	Stiffness coefficient for abutment
K_{RW}	Rotational stiffness coefficients for abutment
E_S	Young's modulus of soil
G_S	Shear modulus of soil
B	Width of the abutment wall
H	Height of abutment wall
K_T	Resultant transnational stiffness.
K_{f1}	Stiffness of backwall footing
K_{f2}	Stiffness for wing wall footing
K_{r1}	Rotational stiffness coefficients for backwall footing
K_{r2}	Rotational stiffness coefficients of equivalent translational stiffness
H_r	Height of backwall
K_0	Stiffness matrix of structures
K_a	Coefficient of equivalent translational stiffness
μ	Coefficients of friction at bearing
φ	Angle of internal friction of soil
C_y	Compression yield capacity
N	Total weight of abutment
P_D	Dead weight of super structure

W_W	Weight of abutment wing wall
W_m	Weight of abutment main wall
W_s	Weight of soil over abutment footings
δ	Angle of internal friction between abutment footing and foundation soil
T_y	Tensile yield strength at the abutment
β	Backfill slope
K_h	Horizontal acceleration coefficient
K_v	Vertical acceleration coefficient
γ	Unit weight of soil
K_{PE}	Coefficient of passive earth pressure

CHAPTER 1

INTRODUCTION

1.1) RATIONALE OF THE STUDY

Earthquake engineering can be considered to be a semi-empirical science. But it is very important to predict the behavior of structures within engineering accuracy. As earthquakes cannot be predicted and even much less prevented, we must learn how to live with them. It is an engineering task to design the structures in the way to prevent the disaster and casualties.

Deformation of soil due to seismic load imposed by the structures above can result in the change in stresses and deformation of the structures. Considering the interaction between soil and structure is important especially for the design of large structures with embodiment such as, for instance, nuclear power plant containment and foundations of bridges. Engineering experience has shown that under dynamic loading and particularly during earthquakes the bridge-soil systems undergo significant alterations. These alternations cannot be taken into account using the classical methods of design. Consequently, to prevent major disasters and material loss it is imperative to perform adequate soil structure interaction analysis. Furthermore, as some interaction phenomena have favorable effect on the structural resistance, their consideration enables design and construction with economy and elegance.

The behavior of bridge structures under the influence of seismic load has been a major point of interest for engineers over a long period of time. The 1971 San Fernando earthquake was a major turning point in the development of seismic design criteria for bridges; in as much the same way as the Long Beach earthquake was for the earthquake response of buildings.

Although significant advances have been achieved since that time in the design and construction of earthquake resistant bridges, numerous gaps including soil structure interaction still remain in the understanding of the seismic behavior of the bridges. Evaluation of dynamic response of bridges in conjunction with the supporting soil presents a challenging as well as multi-facetious task.

It can be seen from the overview presented in the next section, there is a number of sophisticated analytical and numerical techniques, which offer high accuracy and can account off various interaction effects. However, to simulate precisely the behavior of a soil-structure system, a rigorous approach by itself is not sufficient. In practical cases, adequate results can be obtained only if the influence of each interaction phenomenon is considered to an appropriate extent and correct input parameters are supplied. To exercise proper judgement, the analyst needs to understand in depth the soil-structure interaction effects and the complex aspects of system behavior. Only observation and analysis of response of actual soil-structure systems can achieve such understanding. However, even though structures can be more or less standardized, actual soil-structure systems vary greatly due to the great diversity of soil conditions and their behavior is hardly subject to generalization from the point of view of contemporary science and engineering practice. This necessitates extensive experimental and observation work and accumulation of case studies. The knowledge, amassed through such work, will in short term enable the practicing engineer to deal in a more efficient way with a given class of problems. In long term, it can lead to eventual improvement of the theoretical basis of soil structure interaction analysis and contribute to the achievement of desired generality and standardization.

At present, publicized data from observation of actual response of structures including free field motion and soil pressure are still rare. A comprehensive analysis on the seismic response of highway bridges is very essential to perform considering the interaction of real bridges and the supporting soil.

As most high way bridges are multi-span simply supported and interaction between such bridges and their supporting soil is prominent (Andrej and Matjaz, 1999) detailed seismic analysis of such bridges should consider soil structure interaction phenomena.

1.2) OVERVIEW OF ANALYSIS AND RELATED RESEARCH

Evaluation of dynamic response of a structure in conjunction with the supporting soil presents a challenging and multi-facetious task. As such, it has attracted the attention of many scientists in the past years. The complexity of the problem comes from the fact, that the interaction between soil and structure engenders various phenomena of different physical nature often with mutually opposing influence. The analytical and numerical approaches applied in the engineering practice typically employ-simplifying assumptions, which preclude them from handling all these effects simultaneously. This accounts for considerable difficulty in analyzing the problem entirely.

The existing soil-structure interaction analysis methods can be categorized in various ways. For the reason specified above each approach is more successful in accounting for a given class of phenomena and less rigorous with respect to others. Comprehensive reviews on the available techniques and models for analysis can be found in Gazetas (1983) and Proceedings of EPRI/NRC/TPC workshop on Seismic Soil-Structure Interaction Analysis Techniques using data from Lotung, Taiwan, 1987. The summary, given here, includes mainly works related to the present study.

1.2.1) Generic Methods of Analysis

The basic problem in soil-structure interaction analysis is the modeling of the soil. Unlike the commonly used construction materials, the soil is most often highly nonlinear, anisotropic and non-homogeneous. Most of the existing approaches assume, with some reservation, that the soil is isotropic.

The problem of non-homogeneity in the vertical direction is typically overcome by dividing the soil into multiple homogeneous layers with different properties.

In the case of earthquake analysis, the soil is an infinite unbound medium in which the seismic waves travel. This means that the soil model must permit adequate propagation, reflection and refraction of these waves. Particularly, the soil-structure interface will emit such waves in all directions towards infinity and this will lead to the increase of the damping of the final dynamic system.

This effect is called "radiation damping" (Wolf 1985,1994). Conversely, no radiation of reflected waves from the infinity towards the structure can be allowed. Depending on the analysis approach, this necessitates modeling of an infinite or at least a sufficiently large region of the soil around the structure. If the above requirement is not followed, the model may erroneously simulate an excessive input of energy into the system. If only a finite soil region is modeled, the problem may be alleviated by introduction of artificial energy transmitting boundaries around the region (Wolf, 1985, 1994: Lysmer et al., 1988).

In view of the existing theory of wave propagation and the above considerations it is convenient to regard the soil as a layered continuous viscoelastic half space and the structure as an inclusion in this half space. In this way, the analyzed system combines two subsystems with substantially different features: the soil, which is an infinite unbounded medium and the structure, which is an object with finite dimensions.

If we consider an earthquake wave traveling through the viscoelastic halfspace, it is obvious that an inclusion, i.e. a structure would interfere with its propagation. The structure will then be set in motion due to the energy input from the seismic wave and this motion in its turn will have a feedback on the behavior of a limited portion of the soil around the foundation in compliance with Saint-Venant's principle. This effect is known as dynamic or inertial interaction (Wolf, 1985, 1994). The finite region whose response is altered by the structural motion is termed "the near field" and conversely, the rest of the soil is termed "the far field". The hypothetical viscoelastic halfspace, which existed before the structure was inserted, is called the free field and its dynamic response is known as "the site response".

Since theoretically the motion of the far field should be the same as that of the free field, sometimes the term free field is loosely used to designate both. Proceeding from the above considerations, there are several ways to model the soil as described below. The relations between the different approaches are illustrated in figure 1.1.

Boundary integral equation approach:

The boundary integral equation approach is a natural and straightforward way to model a continuous viscoelastic halfspace with a rigid inclusion. This technique is highly accurate and yields analytical forms of the soil impedance through application of Green's functions. A variety of such analysis methods is available. Dominguez (1987a,b) has obtained the response of a rectangular foundation embedded in elastic half-space by using the Green's functions for multi-layered viscoelastic half space. Luco and Wong (1987), and Apsel and Luco (1987) have obtained the impedance functions for hemispherical and cylindrical foundations.

The main disadvantages of the usage of the boundary integral equation approach are that it cannot easily consider soil nonhomogeneity in lateral direction neither can it account for secondary nonlinear effects as, for example, separation of the structure from the soil. Also, it involves extremely sophisticated mathematical apparatus. Particularly, if no geometrical restriction on the shape of the foundation is imposed, the Green's functions must be calculated for a large number of combinations of sources and receivers and this requires a considerable computational effort.

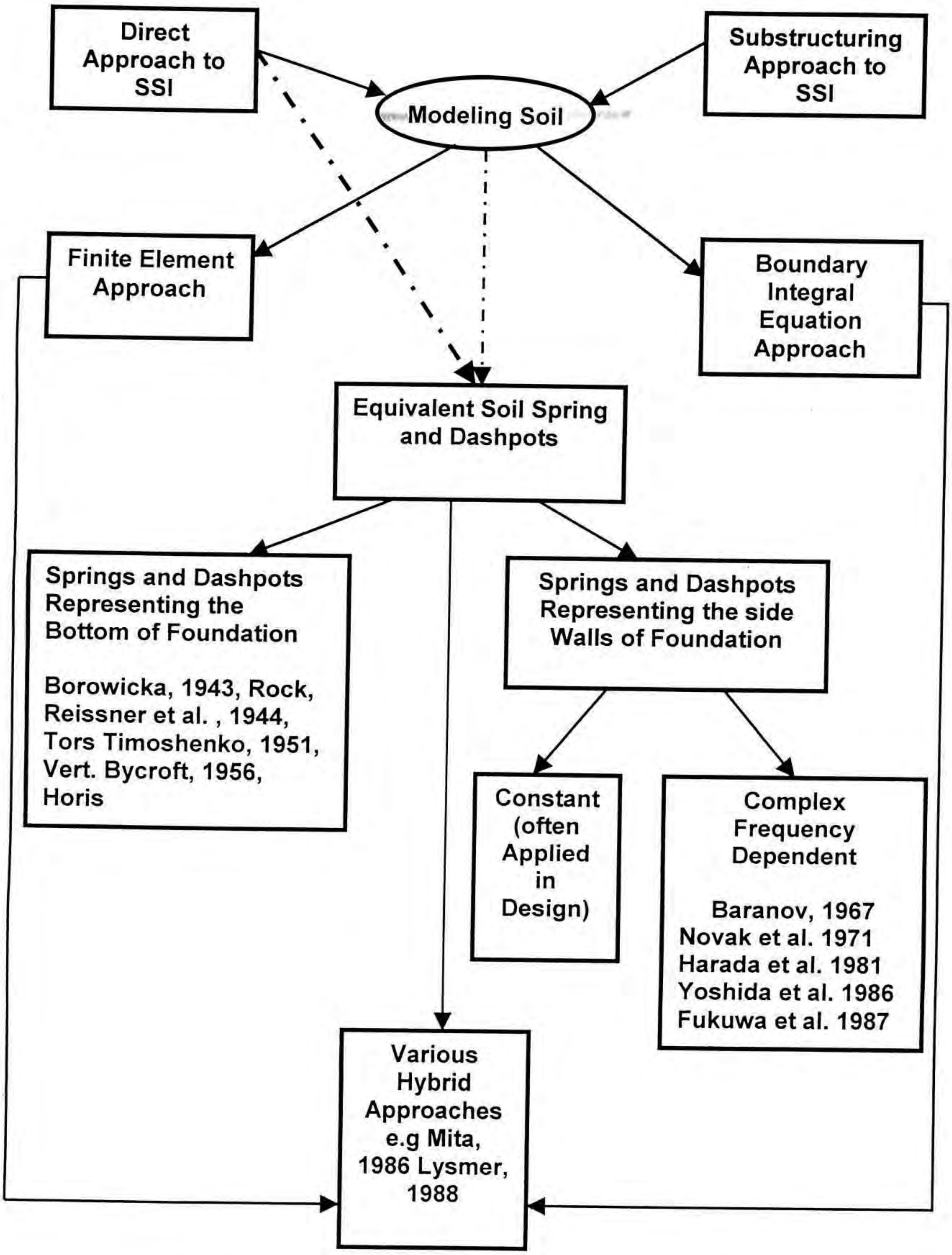

Figure 1.1. Soil-structure interaction analysis approaches

Finite element approach:

The finite element approach is very rigorous and very flexible. Using appropriate finite elements and shape functions can account precisely for irregular soil zones as well as for various nonlinear effects.

There is no restriction on the shape of the foundation. However, modeling of an infinite medium with finite elements creates some problems. As discussed above, to a void energy buildup, a large portion of the soil up to a sufficient distance from the structure must be included in the model and artificial energy transmitting boundaries around the modeled soil region need to be introduced. In addition, in dynamic FEM analysis restrictions are imposed on the maximum size of the elements to ensure proper propagation of the seismic waves.

This necessitates a sophisticated discretization of a massive soil region into an enormous number of small elements. The task often can become extremely heavy and very long processing time may be needed even if a supercomputer is used. Preparation and input of data could require a serious effort and storage and handling of output might present a technical problem.

The disadvantages of this approach are discussed with the implicit presumption that earthquake response analysis is addressed. The problems related to the usage of finite elements may be less significant if machine vibrations, wind or transient impact causes the excitation loads.

Equivalent soil springs and dashpots:

Modeling of the soil support with equivalent springs and dashpots is a simple and economical approach, which offers reasonable accuracy. It is very often used when the performance of the system must be evaluated expediently and at low cost. This approach permits consideration of soil nonlinearities both in the frequency and the time domain, albeit not simultaneously. Also, it is possible to account for separation of structure from the soil under large dynamic loads.

The soil spring and dashpots are global characteristics of the soil support. A spring and dashpot are associated with each mode of motion. Such a group of a spring and dashpots related to a given mode of motion (i.e. rocking or sway) is often referred to as "a generalized spring". Typically, for embedded foundations, the contributions of the soil below the foundation and the soil around the walls of the foundation to the overall support are evaluated separately.

The contribution of the soil below the foundation is easier to evaluate as it is generally constant in the frequency domain for given structure and soil properties. The formulations of the soil reactions have been derived from analysis of structures with shallow embodiment, whose foundations can be assumed to rest on the surface of the viscoelastic halfspace. They have been first evaluated by Borowicka (1943) for rocking motion; Reissner (1944), for torsion; Timoshenko (1951), for vertical motion and Bycroft (1956), for horizontal motion (sway). The formulations of these researchers have been summarized and, in some cases, expanded by Beredugo and Novak (1972) and Kausel (1974).

The reactions of the soil around the walls of the foundation present as much more complicated problem. The equivalent springs and dashpots are nonlinear in the frequency domain. The pioneering work for evaluating the sidewall reactions has been done by Baranov (1967). His results have been expanded by Berdugo and Novak (1972). Since then, the approach has been constantly improved by many researchers. A significant advancement in this direction is the creation of the continuum Formulation method by Harada et al. (1981). Subsequent developments have been done by Yoshida et al. (1986) and Yoshida et al.(1994a,b). Fukuwa and Nakai (1987) have developed a simplified technique of analysis using soil columns with lateral dashpots.

Modeling of the soil support with equivalent springs and dashpots is, in general, less accurate than the previously described approaches. It is difficult to account for soil irregularities and there is a pronounced tendency to overestimate the damping and underestimate the soil stiffness as discussed in Chapter 2. The evaluation of soil springs and dashpots is a serious computational task, which involves integration of Bessel differential equations. In view of this, for practical purposes the stiffness and damping of the side soil are often assumed constant.

1.2.2) Hybrid Approaches

From the above overview it is evident that there is no perfect single approach which can account for all soil-structure interaction effects simultaneously and with reasonable efficacy. Most often, a model would be suited to simulate properly some effect of primary concern and the influence of the others will be included in an approximate manner. To overcome this deficiency, a vast variety of hybrid models have been created on the basis of the generic approaches to combine the advantages of different techniques.

An example of successful development of such a hybrid model is the study of Mita (1986) in which the dynamic response of foundations of arbitrary shape embedded in a viscoelastic halfspace is evaluated with high accuracy. The approach is based on the use of Green's functions for the half-space continuum combined with a finite element discretization of the excavated soil.

1.2.3) Direct and Sub-structuring Approaches

Conceptually, the simplest and most straightforward way to analyze the response of the soil-structure system is to model the structure together with a sufficiently large portion of the surrounding soil, using, for example, finite elements. In this way, various nonlinear effects can be considered accurately. If the excitation is caused by machine vibrations, wind or transient impact loads, this direct approach can be applied effectively, since the modeled soil region need not be very large. However, if earthquake response analysis is performed, the modeled soil region must extend much farther from the structure and the computational time and data storage requirements will increase immensely as explained previously.

If the principle of superposition is implicitly assumed to be valid, more effective substructuring approaches can be applied with sacrifice of little precision with regard to nonlinearity. The soil structure system can then be divided into several simpler subsystems. Each of the subsystems is analyzed separately and the results are combined according to the principle of superposition to yield a complete solution.

There are several ways to define the substructures (Lysmer et al., 1988).

1) the rigid boundary method (Kausel and Roesset, 1974).
2) the flexible boundary method (Gutierrez, 1976; Gutierrez and Chopra, 1977,1978).
3) the flexible volume method (Lysmer et al, 1988).

the concepts of the three substructuring methods are illustrated in Figure 1.2 after Lysmer et al.(1988).

In the cases of the rigid boundary and the flexible boundary methods the division is done in a straightforward way into; a) original site, b) original site minus excavated soil and c) structure. Regarding substructure b), the motion of the points on the boundary of the excavation which will subsequently lie on the soil-structure interface is known as the scattered motion. Thus, the boundary substructuring methods require solutions for the site response, the scattering and the impedance problems.

The flexible volume method is based on a more complicated logic. The system is divided into a) original site and b) structure and basement minus the excavated soil (Figure 1.3, after Lysmer et al., 1998). Irregular soil regions in the near field can be

Method	Rigid Boundary	Flexible Boundary	Flexible Volume
Site Response Problem	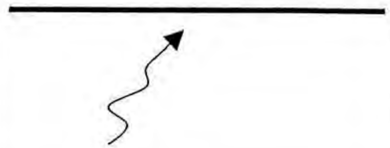	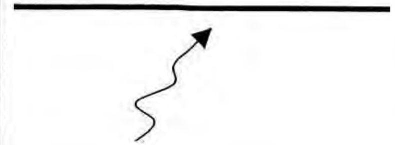	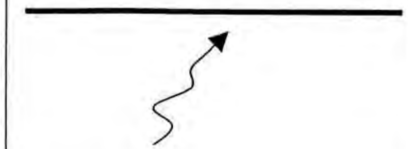
Scattering Problem	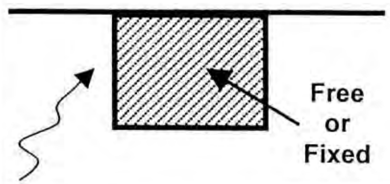	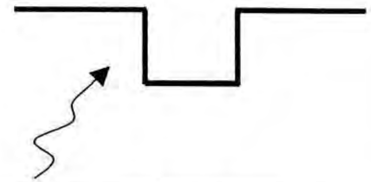	None
Impedance Problem (● Loaded node)	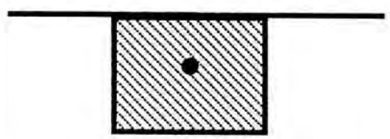	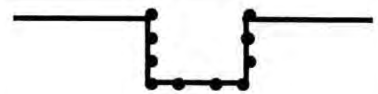	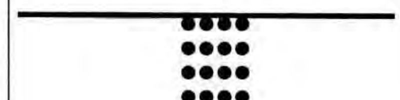
Structural Analysis	Standard	Standard +	Standard +

Figure 1.2. Summary of substructuring methods(after Lysmar et al.,1998)

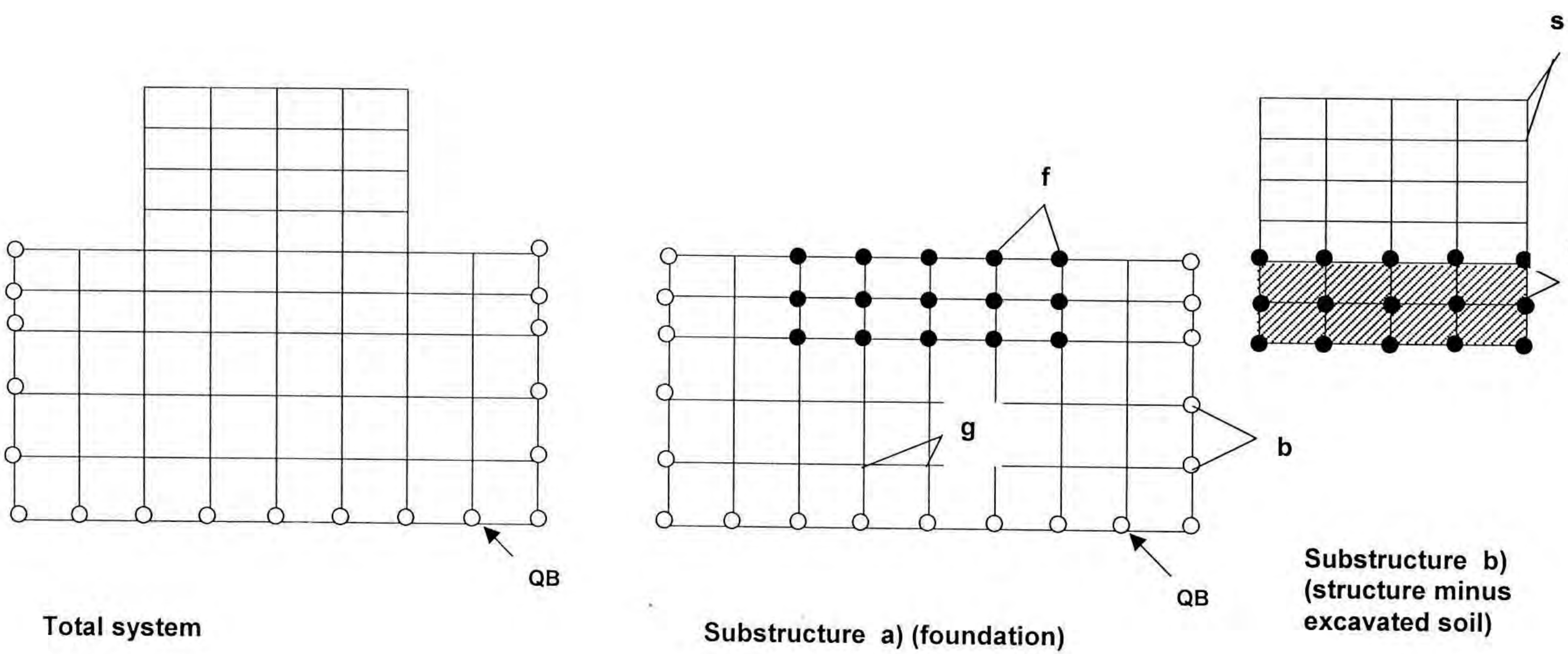

Figure 1.3. Flexible volume substructuring method

modeled as a part of the structure. In this way, the method requires solution for the scattering problem is eliminated. If FEM were to be used for the solution of the scattering problem, it would be burdened with the previously explained deficiencies of modeling of infinite domain with finite elements. In this way, the elimination of the scattering problem results not only in considerable saving of computation time and effort, but often in a more precise complete solution.

Modeling of the soil support with equivalent springs and dashpots is inherently a direct approach to which these considerations are not applicable.

1.3) TIME DOMAIN AND FREQUENCY DOMAIN ANALYSIS

The above described analysis techniques can be used to solve the problem either in the time domain or in the frequency domain.

In general, analysis in the frequency domain is more efficient and requires less effort. Impedance and transfer functions of a soil-structure system which have been once evaluated in the frequency domain can be used repeatedly to simulate the response of the system to loads with different magnitudes and time histories utilizing the Fourier transform techniques. In addition, the soil stiffness and damping vary with respect to the frequency of excitation and consequently this nonlinearity is readily handled by frequency domain analysis.

However, some nonlinear effects can be simulated only in the time domain. Such are, for example, separation of the structure from the soil during large earthquakes, alternation of soil properties under cyclic loading, elasto-plastic behavior, brittleness and structural material fatigue. The time domain analysis offers the choice between modal analysis or direct integration methods. Even though some research has been successfully conducted in the past using modal analysis (Roesset et al., 1973, Bielak, 1976), there is a considerable difficulty in evaluating modal parameters, especially under the influence of soil structure interaction. Consequently, direct integration methods in the time domain as, for example, the Newmark's ß-method and the Wilson Q-method (Bathe and Wilson, 1976) are more rigorous and therefore preferable.

It is possible to combine the advantages of time and frequency domain techniques. For example, in the study of Hayashi and Takahashi (1992) the far-field subsystem is analyzed in the frequency domain and the near field subsystem is analyzed in the time domain.

1.4) *OBJECTIVE* OF THE STUDY

The overall objectives of the present research were to evaluate the seismic response of three bridges set as example with emphasis on soil-structure interaction and three-dimensional effect of ground excitation. Therefore, the research objectives were:

- To identify/develop suitable methodologies to determine the properties (strength and stiffness) of boundary springs to model soil-structure interaction at the abutments and at the base of column piers.

- To perform non-linear dynamic analysis on appropriate dynamic model of bridge, subjected to a variety of earthquakes, different in magnitude and frequency content.

- To perform parametric study to investigate the nonlinear response of bridges in the longitudinal direction considering soil structure interaction.

- To evaluate the combined effect of longitudinal and transverse earthquake excitations on the response of the bridges using 2-D and 3-D models.

1-5) ORGANIZATION OF THE THESIS

In this study the results of research carried out have been divided into different topics and presented in six chapters.

A brief introduction to soil-structure interaction phenomenon, overview of analysis methodology and related research has been presented in the first chapter. The objectives of the work are also outlined in this chapter.

In chapter 2, detailed descriptions of three bridges are presented. For these bridges the number of spans are equal to two, three and four. These are expected to represent the majority of bridges in Bangladesh. Information provided include material properties; weight of various components; and geometry and descriptions of decks, pier bents, abutments, footings, and columns. This chapter also provides the details of how to model the soil-structure interaction. This includes footing stiffnesses, abutment wall stiffness, how to arrive at simplified equivalent stiffness in the longitudinal direction, and determination of abutment strength in the longitudinal direction. Furthermore, the procedures to determine the abutment transverse and vertical stiffnesses are also described.

In chapter 3, features and limitation of program DRAIN-2DX and DRAIN-3DX,the computer program used in this study for numerical analysis, are outlined. Details of the computer models used for 2-D and 3-D analyses are provided. The input earthquake records are also described in this section.

Chapter 4 and 5 present the results of 2-D and 3-D analyses, respectively. Each chapter includes explanation of individual bridge response as well as overall behavioral characteristics that was observed. Furthermore, these chapters also include a comparison between the nonlinear time history analysis and pushover analysis.

Finally, in Chapter 6 the conclusions and recommendations of this research investigation are presented.

CHAPTER-2

MODEL BRIDGES AND SOIL STRUCTURE INTERACTION MODEL

2.1) MODEL BRIDGES

Three multiple span and simply supported (MSSS) bridges, representative of typical bridges in Bangladesh, are analyzed under this research. For these bridges the number of spans are equal to two, three and four designated as Bridge-1, Bridge-2 and Bridge-3 respectively. They have concrete slab on steel girder decks and reinforced concrete pier bents and abutments. The pier columns are all circular with spiral or circular lateral reinforcements and footings are rested on soil without any pile. The spread footings for each abutment, beneath two wing walls and one back wall, are continuous U-shaped foundations. Detailed descriptions of the bridges as follows :

2.2) DECKS AND PIER BENTS

The bridge decks are composite concrete slab on steel girders and pier bents consist of reinforced concrete circular columns and one or two cap beams .The cross section of deck steel girders varies along the length. For each bridge a typical girder with a pertinent concrete slab is shown in Figure 2-1. The cross-sectional properties of the deck are obtained by multiplying the properties of this unit by the number of girders in the deck (NG).

Bridge-1

This bridge has three spans in lengths of 140 ft, 95 ft and 140 ft. The width of the bridge is 45 ft. Deck of the bridge has 6 girders 7 ft 5 inch apart supporting a 9.5-inch thick concrete slab. Separate pier bents beneath the deck consist of two 4-ft diameter circular columns and a cap beam (Figure 2-2a). The deck steel girder dimensions in the mid-span and adjacent to the end-span segments are presented in Table 2-1. Concrete f'_c=3.0 ksi, reinforcing bars, f_y=60 ksi has been considered.

Bridge-2

This bridge has two equal spans in length of 97-ft 4-inch. Each deck has 15 girders 7 ft 11.5 inch apart, supporting an 8.75-inch thick concrete slab. The deck cross section has two separate parts, namely parts 1A and 1B (Figure 2-2b). Correspondingly, the pier bent consists of two parts with a total of ten 3-ft diameter circular columns. The girder dimensions in the mid-span and adjacent to the end-span segments are presented in Table 2-1. Concrete f'_c=4.0 ksi, reinforcing bars, f_y=60 ksi has been considered.

Bridge-3

This bridge has four spans in lengths of 42.0 ft, 130.0 ft, 120.0 ft and 88.0ft. Each deck has 7 girders 7-ft 2-inch apart, supporting an 8 in thick concrete slab. Each column bent consists of five 3.5ft diameter circular columns and a cap beam (Figure 2-2c). Concrete f'_c=3.0 ksi , reinforcing bars, f_y=60 ksi has been considered.

2.3) ABUTMENTS AND FOOTINGS

Each abutment is considered to be supported on continuous U-shaped foundation under its wing walls and back wall. Figure 2-3 shows the dimensions of the abutment footings. Also Figure 2-4 and Table 2-2 present the geometrical information (dimensions and area) of the abutment walls cross sections.

All bridges have continuous rectangular spread footing at each pier bent. The dimensions for pier footings are shown in Table 2-3.

2.4) COLUMNS

All bridges have circular columns with spiral or circular lateral reinforcements. The level of concrete confinement varies for each bridge. The lowest confinement belongs to the Bridge-1 with #3 circular hoops at 12" c/c spacing. On the other hand Bridge-2 and Bridge-3 both have well confinement details for their pier columns, which consist of spiral reinforcement at small pitch (3.5" to 2.25"). Table 2-4 shows the cross sectional properties and reinforcements in the pier columns for all three bridges.

2.5) BEARINGS AND EDGE DISTANCES

A typical fixed bearing is shown in Figure 2-5, which consists of a parted metal casing with each part welded to the top and bottom steel plates. The top steel plate is connected to the deck steel girder by connection bolts and the bottom steel plate is connected to the concrete support by anchor bolts. For roller bearings, except the casings, which have a special configuration for allowing free movement to the supported deck in longitudinal direction, the details are similar to the fixed bearings. Table 2-5 shows the fixed bearings dimensions and connection bolts and welding.

Considering the shear failure at fixed bearings or excessive movement over roller bearings, one of the important parameters in preventing the deck from falling off of its support is the edge distance "e" (Figure 2-6). This distance can be compared to the deck relative movement to its support and if this relative movement is greater than the edge distance then there is a possibility of falling off the deck. Table 2-6 presents the edge distances of the studied bridges at pier bents and abutments. Edge distances are measured from the corner of bearing casings to the edge of the support in the bridge longitudinal direction.

2.6) ESTIMATED WEIGHTS FOR DIFFERENT BRIDGE COMPONENTS

Table 2-7 shows the estimated weight for various structural components for all three bridges. The deck dead weight was increased by 10% to account for additional attached elements and the simplified geometry assumption in the weight calculations.

Table 2.1 Cross-section of composite decks at mid-span and supports

Bridge Name	Span No.	Girder cross section		(Modula Ratio) n	Composite equivalent sec. Area in^2	N_G
		At support	At mid-span			
Bridge-1	1 & 3	20" * 7/8" 60" * 5/8" 18" * 1.375" X-sectional area = 79.75 in^2	20" *1.5" 60" * 5/8" 24" * 2.5" X-sectional area= 127.5 in^2	8.824 FHWA	L_s = 2 *28ft L_m = 84ft 1777 in^2	6
	2	16" * .75" 48" * 0.5" 18" * 1.375" X-sectional area = 60.75 in^2	16" * 1.125" 48" * 0.5" 18" * 2" X-sectional area = 78 in^2		L_s = 2 *27ft L_m = 41ft 1443.4 in^2	
Bridge-2	1 & 2	20* 7/8 42* 7/16 24 * 1.375	20* 1.5 42* 7/16 24*2	7.642 FHWA	L_s = 2 *18ft L_m = 60ft 1486.1 in^2	15
Bridge-3	1	X-sectional area = 64 in^2	X-sectional area = 85 in^2	8.255 FHWA	970	7
	2				1700	
	3				1700	
	4				1400	

Table 2.2 Dimensions and cross sectional areas of abutment walls.

Bridge	Abut. #	Wing Wall cross section			Abutment wall Cross Section			
		H_W (ft)	t_W (ft)	$A_W(ft^2)$	H_m (ft.)	t_m (ft)	C (ft.)	$A_m(ft^2)$
Bridge-1	1	41.0	2.0	51.5	14.0	2.0	7.5	64.6
	2	21.0	2.0	54.0	21.0	2.25	7.5	95.4
Bridge- 2	1	16.	3.0	79.4 99.4	17.0	3.0	5.9	89.5
	2	16.3	3.0	80.8	13.9	3.0	5.7	78.3
Bridge -3	1	13.0	2.5	58.4	13.0	2.5	7.5	49.9
	2	13.0	2.5	67.8	16.0	2.5	6.7	68.1

Table 2.3 Pier footing dimensions

Bridge Name	Footing	Length (ft.)	Width (ft.)	Thickness
Bridge-1	Pier # 1	50	15	3'-3"
	Pier # 2	50	18	3'
Bridge-2 (Whole width)	Pier # 1	115	14	3'
Bridge-3	Pier # 1, # 2 & #3	71	8	3'

Table 2.4 Pier column reinforcement.

Bridge name	D(ft.)	Longitudinal steel	Transverse Steel
Bridge-1	4	0.011	#3@1' A_b=.11in^2 D_b=0.375-inch circular hoop
Bridge –2	3	0.02	#5@3.5' A_b=.31in^2 D=.625 in spiral
Bridge-3	3.5	0.01	#4@2.25' A_b=.20in^2 D=.5 in spiral
	3.5	0.02	#4@2.25' A_b=.20in^2 D=.5 in spiral
	3.5	0.017	#4@2.25' A_b=.20in^2 D=.5 in spiral
	3.5	0.023	#4@2.25' A_b=.20in^2 D=.5 in spiral

Table 2-5 Fixed bearing dimensions

Bridge No	Bearing Type No	L (in)	b (in)	h_1 (in)	h_2 (in)
Bridge-1	1	18	5	10	3.75
	2	18	5	5	3.75
Bridge-2	1	20	5	4.5	4.0
Bridge-3	1	11	5	4.0	4.0
	2	17	5	4.0	4.0
	3	19	5	4.0	4.0

Note : For notations used in the table refer to Figure 2-5

Table 2-6 Fixed bearing edge distances.

Bridge Name	Location support	α (Deg)	c(in)	e(in)
Bridge –1	Abutments	33	7	8
	Piers	33	7	10
Bridge-2	Abutments	3	5	7
	Piers	3	5	7
Bridge –3	Abutments	45	5.7	9.3
	Piers	45	#1 5.7 #2 8.5 #3 7.8	9.3 9.5 10.2

Notes:

1) $c=(L/2)^* \sin(\alpha)+(b/2)^*\cos(\alpha)$
2) For notations used in the table refer to Figure 2-6.

Table 2-7 Weight of various bridge components

Bridge Name	Element	Weight (kips)	Unit Weight (kips/ft)
Bridge -1	Deck # 1 and # 3	1381.5	9.85
	Deck # 2	838.5	8.85
	Columns of Pier # 1 (2columns)	70.4	0.8
	Cap Beam # 1	146.3	1.7
	Abutment # 1	680.0	7.9
	Abutment # 2	1200.0	13.95
Bridge-2	Deck # 1 and # 2	2110.3	21.7
	Columns of the Pier (10 col.)	188.9	1.7
	Cap Beam	258.3	2.3
	Abutment # 1	1850.0	16.6
	Abutment # 2	1500.0	13.4
Bridge –3	Deck # 1	440	10.5
	Deck # 2	1500	11.5
	Deck # 3	1380	11.5
	Deck # 4	910	10.3
	Columns of Pier # 1 (5 columns)	110	2.3
	Columns of Pier # 2 (5 columns)	115	2.4
	Columns of Pier # 3 (5 columns)	90	1.9
	Cap Beam	181	3.7
	Abutment # 1	1100	22.7
	Abutment # 2	1230	25.4

Notes:

1) For Bridge-3, deck weights are based on the estimated values.
2) For decks unit weight is per span length and for other components is per bridge width.

and Tan (1990) are used to determine the parameters of the boundary springs at the abutments and at the base of the column piers. An important aspect of soil-structure interaction is foundation damping which is a complex problem. Radiation damping associated with wave propagation between the masses of the superstructure and foundation-soil is one form of energy dissipation due to soil-structure interaction. Material nonlinearity in the foundation-soil is another form of damping. In this study, the latter form of energy dissipation is explicitly modeled, while the radiation damping is implicitly accounted for through equivalent viscous damping. Descriptions of the procedure used to obtain soil spring properties are described below.

2.8) FOOTING STIFFNESS

FHWA's procedure (FHWA,1986) for rigid footing foundation on semi-infinite elastic half-space is used to determine translational and rotational stiffnesses for abutment and pier foundations. It is reported that for most highway bridges in evaluating the stiffness characteristics of footings the dynamic effects can be ignored. The static stiffness can be determined using the following procedure:

General Form of Stiffness matrix:

The 6 X 6 stiffness matrix for a circular rigid footing along with the directions of translational degrees of freedom is shown in Figure 2-7. The vertical translation and torsional rotation degrees of freedom are uncoupled from the other degrees of freedom. The two components of translations in the horizontal plane are coupled with the rotational degrees of freedom in this plane resulting in off-diagonal terms. However, the values of these off-diagonal terms are very small, especially for a typical highway bridge where the footings are shallow.

Stiffness Coefficients:

The following general equation is recommended by FHWA(1986) for stiffness matrix, K, of an embedded footing:

$$K = \alpha^* \beta^* K_0 \qquad (2.1)$$

Where, K_0 is the stiffness matrix of an equivalent circular footing bonded to the surface of elastic half-space, α is the shape correction factor for the foundation, and β is the foundation embedment factor.

The stiffness coefficients for various degrees of freedom of matrix K_0 can be determined using the following relationships:

$$\left.\begin{aligned} K_{11} &= K_{22} = 8GR / (2-\nu) \\ K_{33} &= 4GR / (1-\nu) \\ K_{44} &= K_{55} = 8GR^3 / 3(1-\nu) \\ K_{66} &= 16GR^3 / 3 \end{aligned}\right\} \qquad (2.2)$$

Where K_{11} and K_{22} are for horizontal translations, K_{33} is for vertical translation, K_{44} and K_{55} are for rocking rotations and K_{66} is for torsional rotation. G and ν are the shear modulus and Poisson's ratio for the elastic half-space, respectively. R is the radius for circular footings.

The application of these equations to rectangular footings involves two steps. First the radius of an equivalent circular footing must be determined as shown in Figure 2-8. The next step requires determination of the shape factor, α, which depends on aspect ratio (Length, L / Width, B) and mode of displacement. FHWA (1986) provides graphical relationships for this factor, which is in the range of 1.0 to 1.2 for typical L/B values between 1.0 and 4.

The typical value for α, based on the geometry of the bridges is around 1.1. Similarly, the embedment factor, β, for various modes of displacements is given in a graphical format. The embedment factor depends on the embedment ratio, which for the typical situation encountered in highway bridges is equal to the ratio of footing depth (D) to footing radius (R). For D/R in the range of 0.0 to 2.5, for translational degrees of freedom the value of β is in the range of 1.0 to 2.75, and for torsional and rotational modes it varies from 1.0 to as high as 8. For the bridges considered in this study, the value of β is around 1.1 for translational degrees of freedom and about 1.4 for rotational/torsional degrees of freedom.

In the analyzed bridges, abutment footings are U-shaped, continuous and skewed. In order to use the FHWA's procedure, the U shaped and skewed footings are idealized into equivalent rectangular segments and then the above procedure is applied to each of them. Tables 2-8 to 2-13 presents the footing's calculated stiffnesses.

In the FHWA procedure the flexibility of the footings was not considered in calculating the stiffness coefficients. This leads particularly to unreasonable rotational stiffnesses for long rectangular footings (as in pier footings). To include footing flexibility in rotational stiffnesses, a separate model of foundation with a uniform distribution of vertical springs and short-side-rotation springs is considered. In these models, half of the uncracked cross sectional moment of inertia and torsional constant are assigned for the footings. Table 2.14 presents the bridge footing stiffnesses that also include the obtained rotational stiffnesses by this method and Figure 2.9 shows the local axis of the footings in which these stiffnesses are presented. For the pier columns, transnational and rotational soil springs are placed at the base of the columns and their load-deformation behavior is assumed to be linear and elastic.

2.9) ABUTMENT WALL STIFFNESS

In the previous section development of stiffness coefficients for soil-foundation system were discussed. In this section the stiffness of the system consisting of the abutment wall and backfill soil will be evaluated. In the next section the procedure to combine all abutment foundation and wall stiffnesses into a simple longitudinal spring is discussed. In abutment stiffness calculation, it is assumed that the abutment wall is always in contact with back fill soil and always contributes to overall abutment stiffness. In determination of the stiffness of the abutment wall-backfill system, the FHWA's procedure considers the nature of pressure/displacement distribution when the wall is displaced (pushed) into the backfill by longitudinal seismic forces from the bridge deck (FHWA,1986). Employing the appropriate pressure diagrams for translational and rotational cases, the resultant stiffnesses for longitudinal translational and rotational (tilting) modes can be obtained using the following equations.

For translational stiffness (longitudinal):

$$K_w = 0.425*E_s*B \tag{2.3}$$

For rotational stiffness:

$$K_{Rw} = 0.072*E_s*B*H^2 \tag{2.4}$$

Where

E_s = Young's modulus of soil = $2*(1+\nu_{soil})*$ Gs, $\nu_{soil} = 0.4$ (2.5)

G_s = shear modulus of soil.

B = width of the abutment wall.

H = height of the wall.

These two springs is located at 0.37 of the height of the wall as shown in Figure 2.10. Table 2.15 presents the calculated abutment wall stiffnesses for the studied bridges.

2.10) EQUIVALENT ABUTMENT SPRING IN BRIDGE LONGITUDINAL DIRECTION

Figure 2-11 shows schematic diagrams of various foundation springs at an abutment including the final simplified model. In arriving at the final simple model, it is assumed that the abutment deforms as a rigid body and translational stiffness of the system at the location of impact between the abutment and bridge deck is determined. It should be noted that experimental investigation (Maroney et al. ,1994) has shown that the abutment movement is indeed rigid body movement.

As shown in Figure 2.11b, the rotational and translational stiffness springs from various components (abutment footings and the back wall) are moved to the center of stiffness located at height x above the base of the footing. The resultant translational stiffness is equal to the simple algebraic sum of all translational stiffnesses, that is:

$$K_T = K_{f1} + K_{f2} + K_w \qquad (2.6)$$

Where K_{f1} is the stiffness for the backwall footing, K_{f2} is the stiffness for the wing wall footings (sum of the two), and K_w is the stiffness of the backwall. The resultant rotational stiffness is equal to:

$$K_R = K_{rw} + K_{r1} + K_{r2} + K_W*(0.37H_w + t_f - x)^2 + (K_{f1} + K_{f2})*x^2 \qquad (2.7)$$

Where K_{rw} is rotational stiffness for the backwall, K_{r1} rotational stiffness for the backwall footing, K_{r2} rotational stiffness for the wing wall footings (sum of the two), H_w is height of the backwall, and t_f is the depth of the footing, x is the center of stiffness from the base of the footing and is equal to:

$$x = (K_W / K_T) * (0.37H_w + t_f \ ) \quad (2.8)$$

Continuing on the assumption of rigid body movement of the abutment, the model of Figure 2-5b is simplified further into an equivalent translational stiffness, Kh, equal to:

$$K_h = (K_R * K_T) / (K_T * h^2 + K_R) \quad (2.9)$$

As an example, using the above procedure the final value of translational springs at the abutments for Bridge-1 (one of the three case studies) are 1875G k/in and 1930G k/in, where G the shear modulus of soil is in ksi. For a typical value of G = 4 ksi the abutment longitudinal stiffness is 7,600 k/in. For the same bridge, CALTRANS' simplified procedure, which only depends on the width of the bridge in this case, will result in a value of 17,200 k/in. The factor of two differences is consistent with the results reported by Goel et al. (1997).

Similarly, the mobilized abutment mass is lumped at the point of impact between the deck and abutment forming a simple spring-mass system as shown in Figure 2-11c. Note that the point of impact is assumed to be at the centroid of the deck. Table 2-9 presents the calculated stiffnesses for the bridge abutments.

2.11) ABUTMENT TRANSVERSE AND VERTICAL STIFFNESSES

Transverse and vertical translational springs were calculated based on the methodology presented by Wilson and Tan (1990). It is notable FHWA does not provide any guidelines with regard to transverse and vertical directions. The Wilson method is used because it is more compatible with FHWA's procedure as it relates to consideration of soil properties in calculating these stiffnesses. Based on Wilson's method transverse and vertical stiffnesses are dependent on soil embankment dimensions and soil elastic and shear modulus. Following are the equations that were used for this purpose.

Transverse stiffness of the soil embankment for unit length:

$$K_h = \frac{2SE}{Ln\{\ 1 + 2S\dfrac{H}{W}\ \}} \qquad (2.10)$$

Vertical stiffness of the soil embankment for unit length:

$$K_t = \frac{2SG}{Ln\{\ 1 + 2S\dfrac{H}{W}\ \}} \qquad (2.11)$$

Where,

E = Elastic modulus of the embankment soil

G = Shear modulus of the embankment soil

S = Side slope of the embankment soil

W = Wedge top width of the embankment soil

H = Height of the embankment soil

The length (L) for the embankment soils were assumed equal to the abutment's wing wall length. Figure 2-12 shows the dimensions of an embankment used in calculating transverse and vertical stiffnesses as shown in Table 2-17.

2.12) ABUTMENT STRENGTH

It is assumed that abutment behavior in transverse and vertical directions are elastic. A nonlinear load-deformation characteristic is employed for the translational springs that model abutment in the longitudinal direction. The nonlinearity includes yielding of the spring as well as an unequal strength under compressive and tensile loads on the abutments.

Under the longitudinal compressive load, the established Mononobe-Okabe pseudostatic approach for passive force is employed to determine the yield strength in compression. Under the assumptions of full mobilization of soil strength, cohesionless back-fill soil, and lack of liquefaction, the suggested formula for compressive yield force, Cy, is FHWA (1986):

$$Cy = (½) * \ * H^{2} * (1 - K_{v}) * K_{PE} * B \qquad (2.12)$$

Where

$$K_{PE}=\frac{\cos^{2}(\varphi-\theta+\beta)}{\cos\theta * \cos^{2}\beta * \cos(\delta-\beta+\theta) * \left|1-\sqrt{\frac{\sin(\varphi-\delta) * \sin(\varphi-\theta+i)}{\cos(\delta-\beta+\theta) * \cos(i-\beta)}}\right|^{2}} \qquad (2.13)$$

H = Height of backfill soil (here, from bottom of back wall footing)

B = Abutment width

γ = Unit weight of soil

φ= Angle of friction of soil

θ= Arc tan [k_h / (1 - k_v)]

δ = Angle of friction between soil and abutment, assumed equal to (φ/ 2)

k_h = Horizontal acceleration coefficient, 0.18

k_v = Vertical acceleration coefficient.

i = Backfill slope angle.

β = Slope of backfill soil.

Table 2-18 presents K_{PE} values for different soil angle of frictions and Table 2-19 shows the calculated C_y for different bridges.

Tensile yield strength at the abutment, T_y, is assumed to be equal to frictional sliding capacity. That is:

$$T_y = N * \tan\delta \qquad (2.14)$$

Where, δ is the frictional angle between abutment footing and foundation soil, and it is assumed to be equal to φ/2.

N is the total normal force at the interface, which is equal to the sum of the supported dead load plus the entire abutment weight (including wing walls, back wall, footings and soil over the footings) and listed in Table 2.20.

2.13) BACKWALL

The geometry of abutment backwall consists of two segments. One portion, which is narrower, is the back of the seat normally slightly longer than the depth of the superstructure and referred to as the backwall.
The second segment, which extends from the seat to the top of the footing, is called the breast wall. It is quite possible for inertia forces in the longitudinal direction to cause shear failure of the abutment at the junction of these two segments, normally called backwall failure (Figure 2.13). It is even recommended

in seismic design to use this mode of damage as a fuse, since fixing the upper portion of the abutment is much easier. As a parametric study in this investigation,special attention is devoted to this possible mode of failure. For damaged backwall situation the stiffness of the abutment in the longitudinal direction is determined based on mobilizing only an amount of soil equal to the depth of the superstructure (Table 2.21)

.

Two different load transfer mechanisms control the capacity of a section at the junction of the backwall and breast wall, namely:

i) Shear resistance provided by the concrete, and

ii) Shear friction, which is a post failure behavior and follows the first mode.

The strength of the latter mode is actually larger and it is used. In accordance with AASHTO LRFD (1994) the following equation can be used to determine the nominal shear capacity, V_n:

$$V_n = \mu * Avf * Fy \tag{2.15}$$

Where μ is the friction coefficient between two sliding surfaces and here is assumed equal to one for concrete placed against hardened concrete, A_{vf} is the sum of areas of vertical rebars at the juncture, and F_y is the yield strength of the rebar's. Table 2.22 presents the calculated values for the bridges.
If time history analysis indicates that this shear capacity is exceeded, the model is modified such that the backwall stiffness and compressive strength are determined using only the height of the back wall (i.e. total abutment height minus breast wall height). The strength of the abutment in tension is also

reduced since only the weight of the back wall is used in calculating the frictional resistance when the abutment is under tensile load.

2.14) SUMMARY

Detailed descriptions of the different parts of three model bridges are presented including their schematic description. Soil spring stiffnesses of pier and abutment footings have been calculated and presented in tabular form for all three bridges in horizontal and vertical direction. Equivalent soil spring stiffnesses for the three bridges in terms of G in three orthogonal directions are also calculated and shown in tables. Finally simplification of the abutment and pier footings are done and shown diagrammatically.

Table 2.8 Bridge-1 soil spring stiffnesses for pier footings:

Bridge Name	Footing of	2L (ft)	2B (ft)	Stiffness component	R (ft)	K_o	α	K
Bridge-I	Pier #1	47.5	14	Vertical	14.55	1163.9*G	1.11	1291.9*G
				Horizontal-X		872.9*G	1.16	1012.6*G
				Horizontal-Y			1.04	907.8*G
				Rocking-X	19.97	61209000*G	1.13	69166000*G
				Rocking-Y	10.84	9794000*G		11067000*G
	Pier#2	47	18	Vertical	16.41	1313*G	1.07	1404.9*G
				Horizontal-X		984.6*G	1.11	1092.9*G
				Horizontal-Y			1.03	1014.1*G
				Rocking-X	21.10	72166000*G	1.09	78661000*G
				Rocking-Y	13.06	17104000*G		18643000*G

Table 2.9 Bridge-1 soil spring stiffnesses for abutment footings.

Bridge Name	Footing of	2L (ft)	2B (ft)	Stiffness component	R (ft)	K
Bridge-1	Abutment #1 Back wall	86	13.25	Vertical	19.05	1523*G
				Horizontal-X		1143*G
				Horizontal-Y		
				Rocking-X	19.97	223327000*G
				Rocking-Y	10.84	13506000*G
	Abutment #1 Wing wall	23	13.1	Vertical	9.79	578.6*G
				Horizontal-X		587.6*G
				Horizontal-Y		
				Rocking-X	11.40	11389000*G
				Rocking-Y	8.61	4896000*G
	Abutment #2 Back wall	86	16.25	Vertical	21.09	1687*G
				Horizontal-X		1265*G
				Horizontal-Y		
				Rocking-X	32.96	260267000*G
				Rocking-Y	14.07	21377000*G
	Abutment #2 Wing wall	36	17.75	Vertical	14.26	11.41*G
				Horizontal-X		855.7*G
				Horizontal-Y		
				Rocking-X	17.22	39196000*G
				Rocking-Y	12.09	13570000*G

Notes:

1) For wing walls that have different footing dimensions, the average dimensions were used for calculating equivalent soil spring constants.
2) For U-shaped abutment footings no shape correction factor (α) is used.

Table 2.10 **Bridge-2 soil spring stiffnesses for pier footings.**

Bridge Name	Footing of	2L (ft)	2B (ft)	Stiffness component	R (ft)	K_o	β	K
Bridge 2	Pier #1	115	14	Vertical	22.64	1881.0G	1.25	2263.8G
				Horizontal-X		1358.3G	1.25	1697.9G
				Horizontal-Y			1.15	1562.0G
				Rocking-X	38.77	447532000G	1.45	648921000G
				Rocking-Y	13.53	19009000G	1.3	24711700G

Table 2-11 Bridge-2 Bridge soil spring stiffnesses for abutment footings.

Bridge Name	Footing of	2L (ft)	2B (ft)	Stiffness component	R (ft)	K
Bridge 2	Abutment #1 Back wall	111.7	13	Vertical	21.50	1719.9G
				Horizontal-X		1290.G
				Horizontal-Y		
				Rocking-X	37.24	396634000G
				Rocking-Y	12.70	15742000G
	Abutment #1 Wing wall	11.85	15.75	Vertical	7.71	616.6G
				Horizontal-X		462.5G
				Horizontal-Y		
				Rocking-X	7.26	2941000G
				Rocking-Y	8.37	4506000G
	Abutment #2 Back wall	111.7	13	Vertical	21.50	1719.9G
				Horizontal-X		1290.G
				Horizontal-Y		
				Rocking-X	37.24	396634000G
				Rocking-Y	12.70	15742000G
	Abutment #2 Wing wall	7.67	13.75	Vertical	5.79	463.5G
				Horizontal-X		347.6G
				Horizontal-Y		
				Rocking-X	5.07	998000G
				Rocking-Y	6.78	2396000G

Notes:

1) For wing walls that have different footing dimensions, the average dimensions were used for calculating equivalent soil spring constants.
2) For U-shaped abutment footings no shape correction factor (α) is used.

Table 2.12 Bridge-3 soil spring stiffnesses for pier footings.

Bridge Name	Footing of	2L (ft)	2B (ft)	Stiffness component	R (ft)	K_o	β	K
Bridge 3	Pier #1,2,3	71	8	Vertical	13.45	1075.7G	1.35	1452G
				Horizontal-X		806.77G	1.25	1008GG
				Horizontal-Y			1.2	968
				Rocking-X	23.48	99381752G	1.5	149073000G
				Rocking-Y	7.88	37588420G	1.35	5074000G

Table 2-13 Bridge-3 soil spring stiffnesses for abutment footings.

Bridge Name	Footing of	2L (ft)	2B (ft)	Stiffness component	R (ft)	K
Bridge 3	Abutment #1 south Back wall	55	7	Vertical	11.070	885.6G
				Horizontal-X		664.2G
				Horizontal-Y		
				Rocking-X	18.749	50617000G
				Rocking-Y	6.689	2298000G
	Abutment #1 south Wing wall	28.65	9	Vertical	9.060	724.8G
				Horizontal-X		543.6G
				Horizontal-Y		
				Rocking-X	12.242	14089000G
				Rocking-Y	6.861	2481000G
	Abutment #2 North Back wall	46.7	8.5	Vertical	11.241	899.3G
				Horizontal-X		674.4G
				Horizontal-Y		
				Rocking-X	17.409	40521000G
				Rocking-Y	7.427	3147000G
	Abutment #2 North Wing wall	26.75	11	Vertical	9.678	774.2G
				Horizontal-X		580.7G
				Horizontal-Y		
				Rocking-X	12.226	14034000G
				Rocking-Y	7.840	3701000G

Notes:

1) For wing walls that have different footing dimensions, the average dimensions were used for calculating equivalent soil spring constants.
2) For U-shaped abutment footings no shape correction factor (α) is used.

Table 2-14 Soil spring stiffnesses at the base of pier columns considering pier footing flexibility.

A) Bridge-1

Pier	Translational (kips/inch)			Rotational (kips-in/ rad)			
	Kx	Ky	Kz	Kr(x-x)		Kr(y-y)	
Left(#1)	506G	454G	646G	G=0.4ksi G=4.0ksi G=40 ksi	$5.8*10^6$ $23*10^6$ $51*10^6$	G=0.4ksi G=4.0ksi G=40 ksi	$3.6*10^6$ $19*10^6$ $82*10^6$
Right (#2)	546G	507G	702G	G=0.4ksi G=4.0ksi G=40 ksi	$6.1*10^6$ $24*10^6$ $54*10^6$	G=0.4ksi G=4.0ksi G=40 ksi	$5.7*10^6$ $29*10^6$ $10*10^6$

B) Bridge-3

Pier	Translational (kips/inch)			Rotational (kips-in/ rad)		
	Kx	Ky	Kz	Kr(x-x)		Kr(y-y)
1,2 and 3	202*G	194*G	290*G	G=0.4ksi G=4.0ksi G=40 ksi	$5.3*10^6$ $30*10^6$ $46*10^6$	$1.0*10^6$

Notes:

1) For Bridge-3, Kr (x-x) is calculated at the second pier column base. This value is considered as an average and typical value.
2) Since no.3-D model is developed for Bridge-2, stiffness values presented in Table-2.10 are sufficient.
3) G is in ksi

Table 2-15 Abutment wall stiffnesses

Bridge Name	Abutment No.	H(ft)	B(ft)	K_w (kips/in)	K_{rw} (kips-in-rad)
Bridge 1	1	14	86	1228G	5872000G
	2	21	86	1228G	13212000G
Bridge 2	1	17	86	1595G	11246000G
	2	13.9	111.7	1595G	7518000G
Bridge 3	1	13.1	55	785G	13805000G
	2	16.2	46.7	667G	12308000G

Notes:

1) B is the width of the abutment wall.
2) For notations used in the table refer to Figure 2-9.

Table 2-16 Equivalent spring stiffnesses of the abutment soil system.

Bridge #	abutm- -ent #	K_t (kips /in)	K_r (kips-in/rad)	H_w (ft)	t_f (ft)	c (ft)	t_d (in)	e (ft)	x (ft)	h (in)	K_h kips/in
Bridge 1	1	(1228+1143+2*587.6)*G =3546*G	48146105	14.05	2.0	7.5	74.8	4.4	2.5	110	1875*G
	2	(1228+1265+2*855.7)G =4204*G	124750450	20.8	2	7.5	74.8	4.4	2.8	187	1930*G
Bridge 2	1	(1595+1290+2*462.5)G =3810G	44394068G	17	3	5.9	54.6	3.6	3.9	150	1300*G
	2	(1595+1290+2*347.6)G =3580G	33701190G	13.9	3	5.7	54.6	3.4	3.6	118.8	1432*G
Bridge 3	1	(785+664.2+2*543.6)G =2536G	48494142G	13.1	2.5	7.5	~70	4.6	2.3	104.4	1615*G
	2	(667+674.4+2*580.7)G =2503G	48605901G	16.2	2.5	6.7	~70	3.8	2.3	151.2	1150*G

Notes:

1) In CALTRANS method the abutment longitudinal stiffness for bridge-1 is equal to 200(k/in)/ft*B=200*86=17200k/in.
2) In CALTRANS method the abutment longitudinal stiffness for bridge-2 is equal to 200(k/in)/ft*B=200*11.7'=22340 k/in.
3) In CALTRANS method the abutment longitudinal stiffness for bridge-3 is equal to 200(k/in)/ft*B_{ave}~200*50=10000k/in.
4) For notations used in the table refer to Figure 2.10.

Table 2-17 Abutment spring stiffnesses in transverse and vertical directions

Bridge no.	Abutment	Transverse (kips/inch)	Vertical (kips/inch)
Bridge-1 (Whole width)	Left (# 1)	883.5G	2473.7G
	Right (# 2)	1382.8G	3871.8G
Bridge-3	Left (# 1)	422*G	1183*G
	Right (# 2)	426*G	1191*G

Table 2-18 K_{PE} coefficient for different soil frictional angle (Φ)

(Deg)	K_{PE}
20	1.554
30	2.096
35	2.440
40	2.859
45	3.384
50	4.071

Note:
In this study it is assumed that for soils with G = 0.4 ksi, φ=is equal to 20^0 and for soils with G = 40 ksi, φ = is equal to 45^0

Table 2-19 Compression yield capacity (C_Y) of the abutments in longitudinal direction

Bridge	Abutment No.	Height (ft.)	Width B (ft.)	C_y (kips)
Bridge-1	1	14+2 =16	45	661*K_{PE}
	2	20.8 + 2 =22.8	45	1341*K_{PE}
Bridge-2	1	20	111.7	2681*K_{PE}
	2	16.9	111.7	1914*K_{PE}
Bridge-3	1	15.6	50	730*K_{PE}
	2	18.7	50	730*K_{PE}

Table 2.20 Total normal weight (N) on the abutment footings

Bridge	Abutment No.	P_D (kips)	W_m (kips)	W_w (kips)	W_s (kips)	N (kips)
Bridge-1 (Whole width)	1	1381.4	992.8	363.8	1014	3752
	2	1381.4	1466.8	924.4	3212	6985
Bridge-2	1	1055.2	1498.7	335	715.3	3604
	2	1055.2	1213	183.2	382.2	2936
Bridge-3	1	3400	578.2	509.9	531	5319
	2	4900	678.9	536.4	1144	7259

Notes :

1) P_D is the dead load of superstructure carried by abutment.
2) W_m is the weight of abutment main wall and it's footing.
3) W_w is the weight of abutment wing-walls and their footings.
4) W_s is the weight of soil over the abutment footings.

Table 2.21 Back-wall geometry and its soil spring properties

Bridge	L (ft.)	c (ft)	t_w (ft)	Weight (kips)	Stiffness K_s (kips/in)	Compression Yield limit C_Y (kips)
Bridge-1	102.5	7.5	1.5	173	1228.1*G	290.25* K_{PE}
Bridge-2	111.8	5.9 5.7	1.5	148 143	1595.1G	225.46* K_{PE} average
Bridge-3	77.3 66.5	7.5 6.7	1.5	130.5 100.2	785.4G 666.9G	156.25* K_{PE} average

Table 2-22 Shear friction capacity (Vn) of the abutment back-wall cross section.

Bridge Name	Rebar I			Rebar II			A_{vf} in	F_y ksi	V_n kips
	size	No.	Area	Size	No.	Area			
Bridge-1	5	131	131*.31	4	76	76*.2	55.81	60	3349
Bridge-2	5	112	122*.31	5	112	112*.31	69.44	60	4166
Bridge-3	6	~70	70*.44	6	~70	70*.44	61.6	40	2464

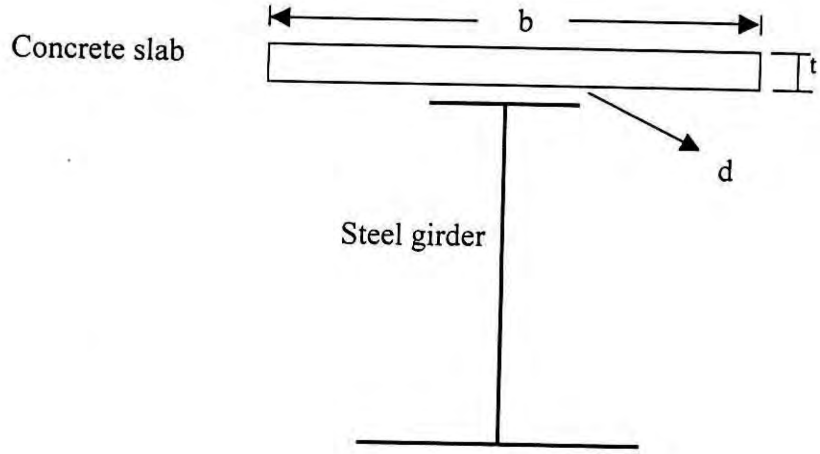

Bridge Name	b (inch)	t (inch)	d (inch)
Bridge-1	89.0	9.5	3
Bridge-2	95.5	8.75	1.625
Bridge-3	86.0	8.0	2.0

Figure 2.1 Typical girder with pertinent slab dimensions

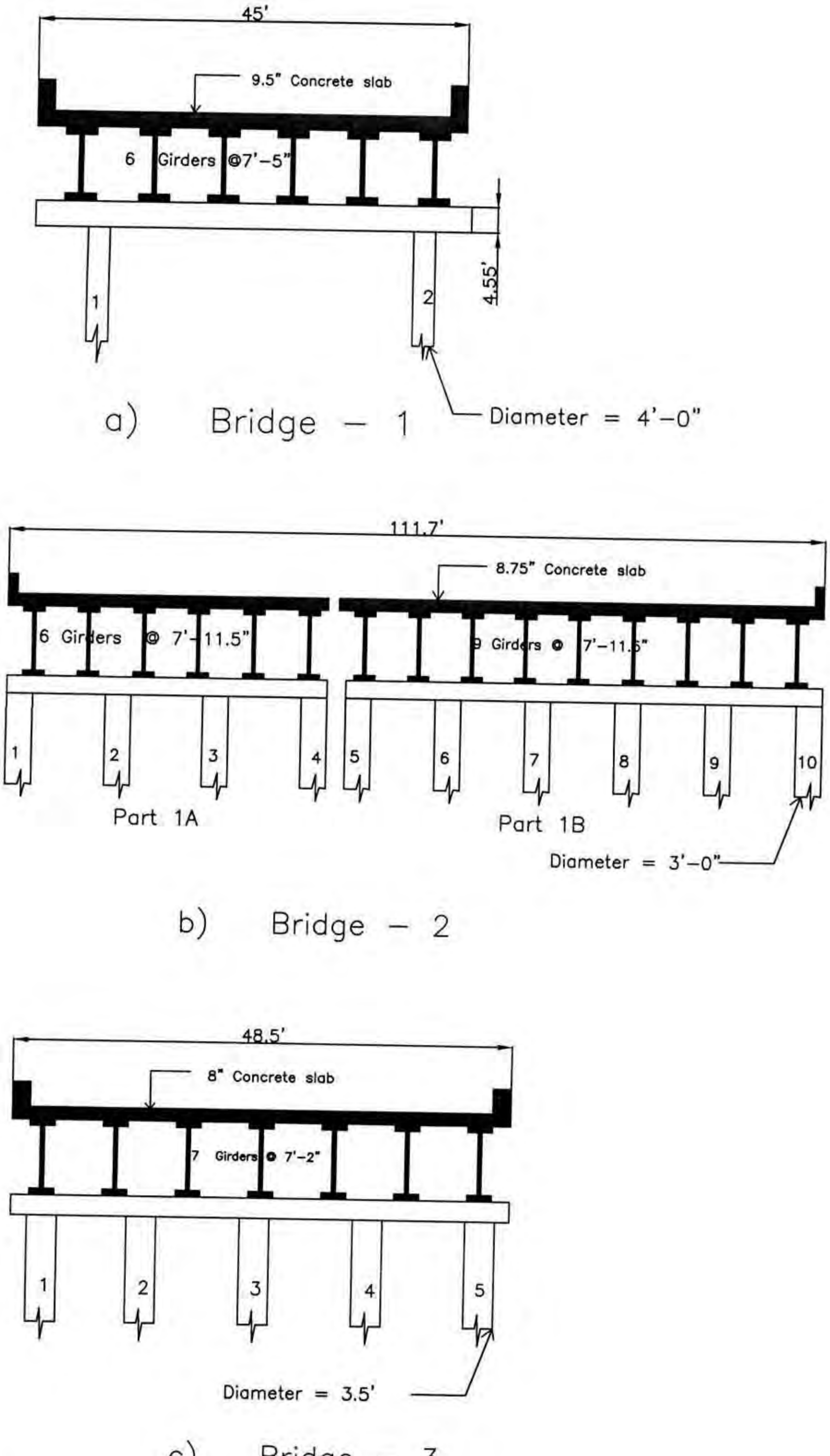

Figure 2.2 Cross section of the bridge decks

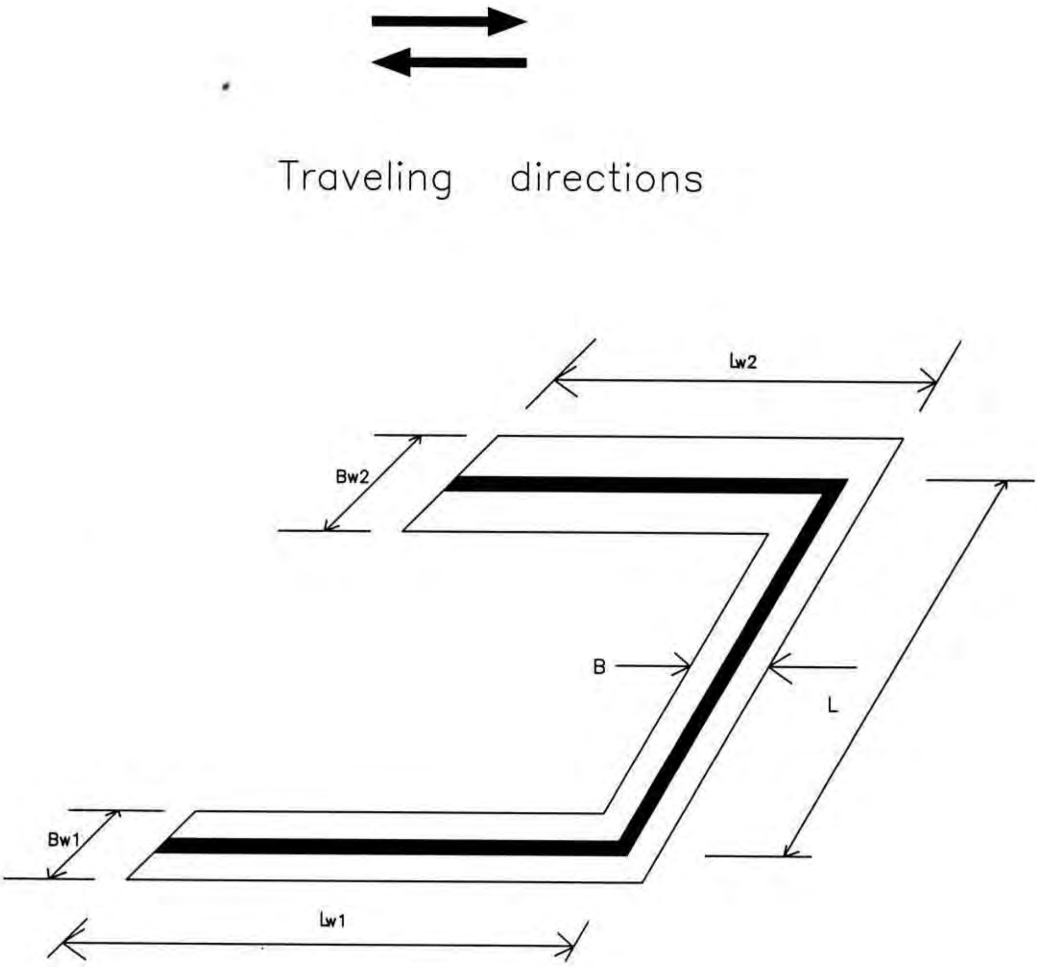

Bridge Name	**Left Abutment(#1)**						**Right Abutment (#2)**						α
	L	B	Lw 1	Bw1	Lw 2	Lw 2	L	B	Lw1	Bw1	Lw 2	Lw 2	
Bridge –1	45	13.3	23	13.8	23	12.5	45	16.3	36.5	17.8	36	17.8	33°
Bridge –2	111.7	13	12.7	17	11	14.5	111.7	13	6.0	13.0	9.3	14.5	3°
Bridge -3	50	7	31.5	9	25.8	9	50	8.5	30.5	11	23	11	45°

Figure : 2.3 Abutment footings

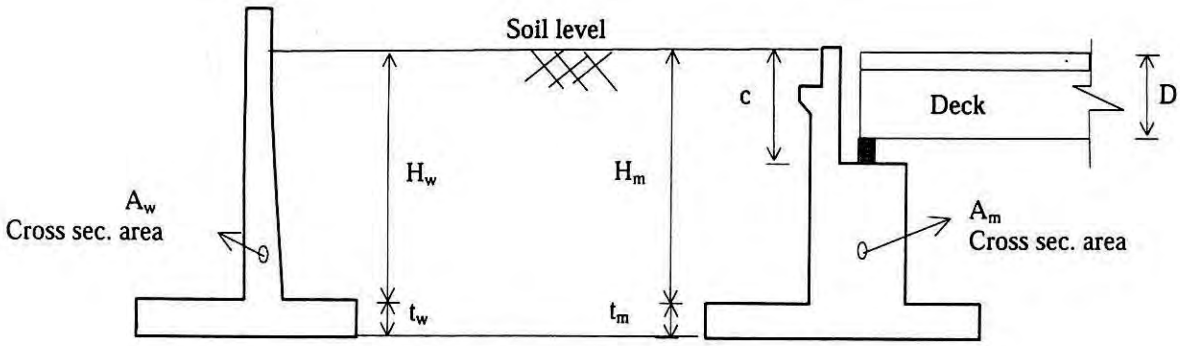

a) Typical wing wall section

b) Typical main wall section

Figure 2.4 Cross sections of abutment walls.

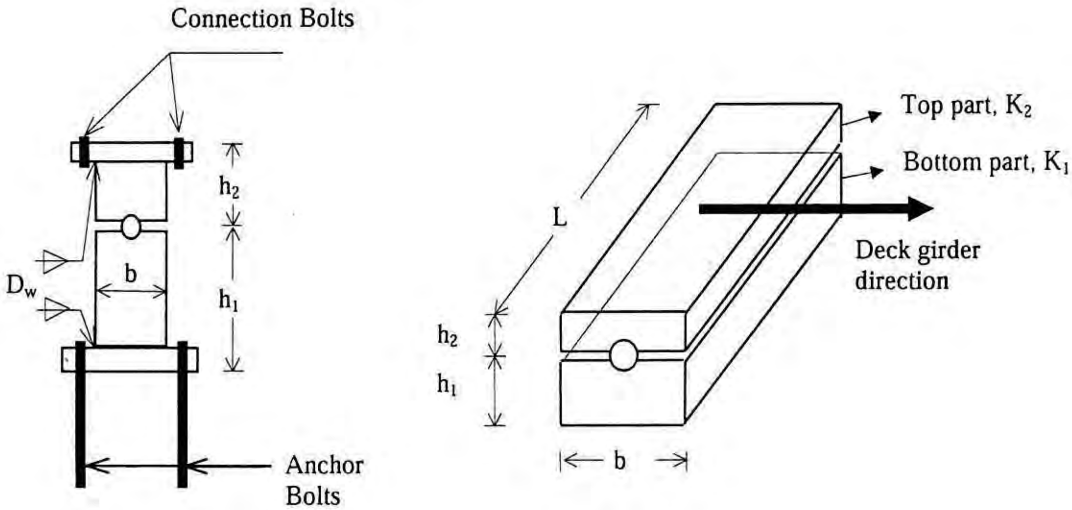

Figure 2.5 Fixed bearing general shape and components

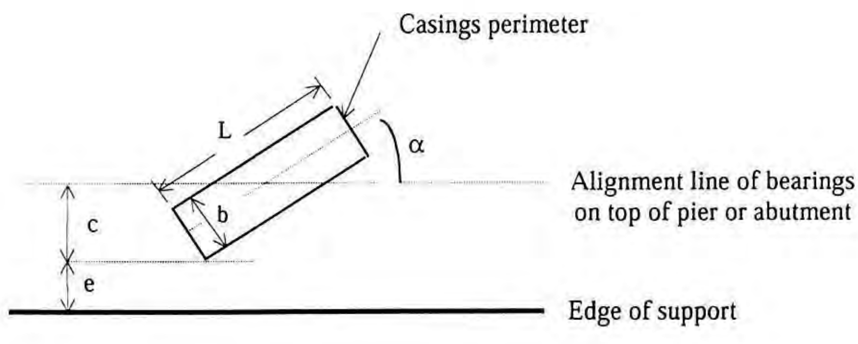

Figure 2.6 Edge distance of bearings

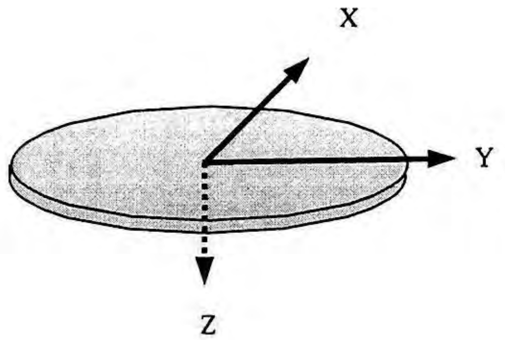

$$
\begin{array}{c}
\begin{array}{cccccc} \quad\delta_X & \quad\delta_Y & \quad\delta_Z & \quad\theta_X & \quad\theta_Y & \quad\theta_Z \end{array} \\
\begin{bmatrix}
K_{11} & 0 & 0 & 0 & -K_{15} & 0 \\
0 & K_{22} & 0 & K_{24} & 0 & 0 \\
0 & 0 & K_{33} & 0 & 0 & 0 \\
0 & K_{42} & 0 & K_{44} & 0 & 0 \\
-K_{51} & 0 & 0 & 0 & K_{55} & 0 \\
0 & 0 & 0 & 0 & 0 & K_{66}
\end{bmatrix}
\end{array}
$$

Figure 2.7 Stiffness matrix of an equivalent circular footing(K_0).

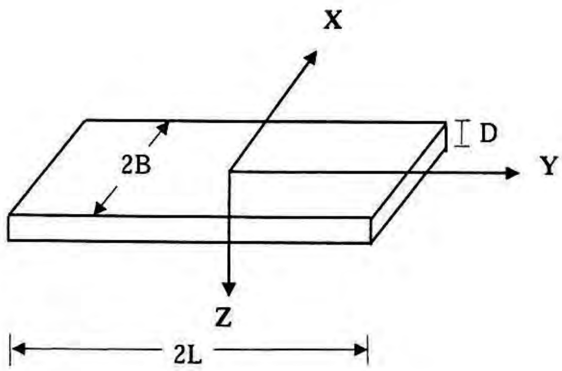

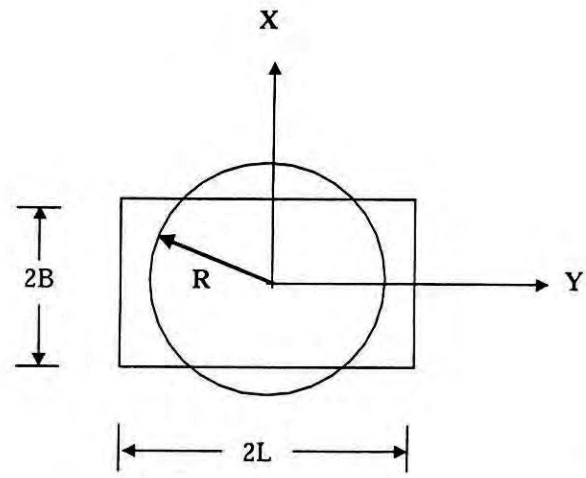

Translation:

$$R = \sqrt{(4BL)/\pi}$$

Rotation:

$$R = \left[(2B)*(2L)^3/3\pi\right]^{\frac{1}{4}} \quad \text{(X-axis Rocking)}$$

$$R = \left[(2B)^3*(2L)/3\pi\right]^{\frac{1}{4}} \quad \text{(Y-axis Rocking)}$$

$$R = \left[(4BL)*(4B^2+4L^2)/6\pi\right]^{\frac{1}{4}} \quad \text{(Z-axis Torsion)}$$

Figure 2.8 Equivalent radius for rectangular footing.

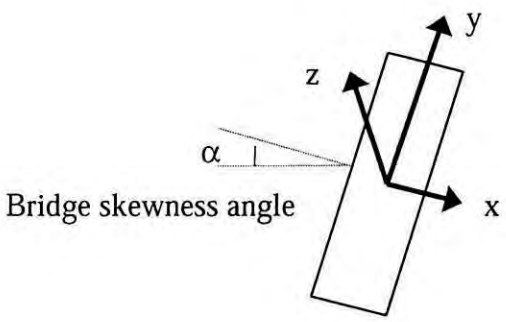

Figure 2.9 Footing Local axes

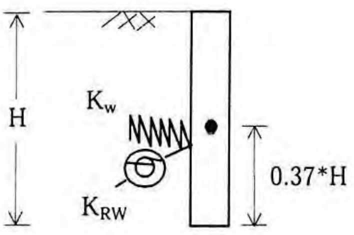

Figure 2.10 Abutment back wall and equivalent soil springs.

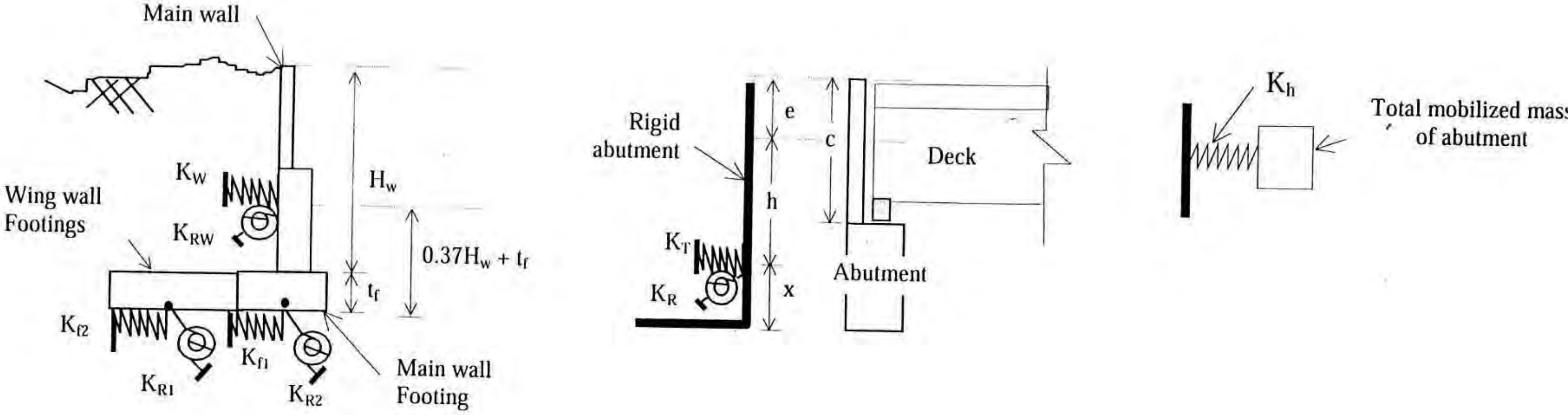

a) Abutment main wall and footings soil springs (Step1)

b) Equivalent spring set at the center of stiffness (Step2)

c) Simplified abutment model (Step3)

K_{f1} = Equivalent horizontal spring stiffness for main wall footing.
K_W = Equivalent horizontal spring stiffness for main wall.
K_{R2} = Equivalent rotational spring stiffness for wing wall footings.
$K_R = K_{RW}+K_{R1}+K_{R2}+K_W*(0.37H_w+t_f-x)^2+(K_{f1}+K_{f2})*x^2$
$x = (K_W/K_{tot})*(0.37H_w+t_f)$ locates the center of stiffness.

K_{f2} = Equivalent horizontal spring stiffness for wing wall footings.
K_{R1} = Equivalent rotational spring stiffness for back wall footing.
K_{RW} = Equivalent rotational spring stiffness for back wall.
$K_T = K_{f1}+K_{f2}+K_w$
$h = (H_w+t_f)-x-e$

e = Distance from top of the back wall to the application point of the resultant impact force, which assumed to be equal to {c-(Deck-Thickness)/2}.
K_h = Equivalent translational stiffness at distance " e " below top of the abutment back wall = $(K_R*K_T)/(K_T*h^2+K_R)$

Figure 2.11 Graphical illustration of determination of equivalent abutment model.

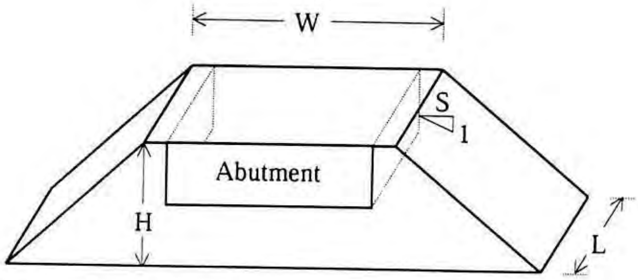

Figure 2.12 Abutment embankment dimensions used in calculating transverse and vertical stiffnesses.

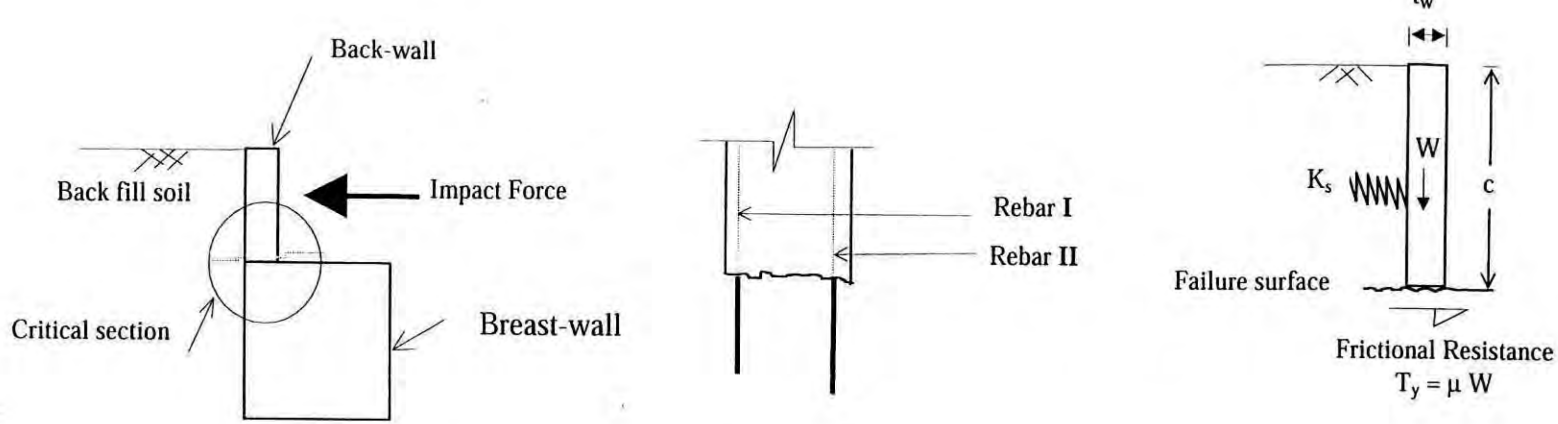

a) Typical abutment main wall

b) Critical section

c) Failed back wall

T_y = Abutment back wall frictional resistance force, assumed equal to μ*W with μ = 1
K_s = Back fill equivalent translational spring stiffness =0.425 E_s B
W = L*c*t_w*$\gamma_{concrete}$, $\gamma_{concrete}$ = 0.15 kips/ft^3
E_s = Soil modulus of elasticity = $2(1+\nu)$*G, (ν=0.4)
L = B / cos α, α is the angle between deck centerline and an axis perpendicular to the abutments back wall. B is the width of abutment.

Figure 2.13 Typical abutment wall and damaged back wall

CHAPTER 3

COMPUTER MODELS FOR 2- DIMENSIONAL AND 3- DIMENSIONAL ANALYSIS

3.1) GENERAL

The bridges were analyzed using DRAIN-2DX (Prokash et al., 1994) and DRAIN-3DX (Powell and Campbell, 1994) computer programs, where beam-column elements are used to model the columns and simple connection elements are employed in modeling bearings and soil-structure springs. The link elements are used to model the gap and impact between adjacent spans and between an end-span and the abutment.

In this study a 5% damping has been considered in the bridge models. This is consistent with AASHTO's response spectra and it is a commonly used value in time history analyses. This level of damping can be looked upon as radiation damping at the foundations. Since, there is no other source of viscous damping due to high rigidity of the deck cross-section. It is notable, as mentioned before, that energy dissipation due to nonlinear phenomena such as plasticity in the columns and friction at the bearings are modeled explicitly. It is assumed that the abutment back-wall is always in contact with the back-fill soil and contributes to the abutment stiffness. Abutment geometry, cap beam and deck widths are modeled with relatively rigid elements.

Several parameters are investigated for each bridge. These are types of soils (shear modulus of 400 psi, 4000 psi and 40,000 psi), backwall condition (intact and broken) bearing performance (intact and failed with two different coefficient of frictions equal to 0.2 and 0.6).

Three earthquake records along with their orthogonal components, as described in section 3-4, are considered for the analyses. Following are the description of the 2-D and 3-D models of the bridges.

3.2) 2-D MODELS

Drain-2DX (Prokash et al. 1994) was employed for modeling bridges in the longitudinal direction. For multi span simply supported bridges it is reported that longitudinal seismic response is more important (Zimmerman and Brittain, 1979). Figures 3.1 to 3.3 show the analytical models and loadings for the bridge models. Table 3.1 presents the summary of soil spring stiffnesses at abutments and pier column bases for the analyzed bridges. For Bridge-1 because of symmetry with regard to center of the deck only half of the bridge was modeled. For Bridge-2, although unsymmetrical, the dynamic characteristics of the segments are similar, and they are lumped together. Two-dimensional models are not able to represent the bridge skewness, for which one of the consequences is having a negligible axial force variation at pier columns from earthquake analyses. Cap beams and deck elements are assumed to remain elastic. A rigid-end-zone equal to the height of a bridge cap beam was placed at the top of pier columns. Rayleigh's damping proportional to both stiffness and mass matrices is used. The coefficients of proportionality are determined so that the damping matrix will correspond to 5% damping in the first and second modes. Under Peak Ground Acceleration (PGA) of 0.18g for each bridge, fifteen basic models as shown in Table 3.2 were analyzed under three different earthquake records (Park field, El-Centro and Nahanni). This results in a total of 135 computer runs. Additionally, for further study with PGA of 0.4g were also analyzed.

Following is a brief description of the DRAIN-2DX (Prokash et al., 1994) element types used to model bridges in longitudinal direction.

Beam-Column Element (Type 02)

This is a one-dimensional element that can be oriented arbitrarily in XY plane. Nonlinear behavior is limited to the concentric plastic hinges at the element ends. Plastic hinges are capable of considering P-M interaction curves for steel and reinforced concrete column sections. This element was used for modeling decks, piers and cap beams. Figure 3.4 shown stress-strain curves for steel and concrete.

Simple Connection Element (Type 04)

This is a zero-length element that connects two coincident nodes. It has either rotational or translational stiffness. Element behavior is nonlinear with the ability to have elastic or inelastic unloading with or without gap. Complex behaviors can be obtained by placing two or more elements in parallel positions. Bearings, abutment back-fill soils (with inelastic unloading) and soil springs at the pier column footings were modeled by this element.

Link Element (Type 09)

The link element is a uniaxial element with finite length and arbitrary orientation. An element can be specified to act in tension (tension force and extension are positive) or in compression (compression force and shortening are positive). A tension element has finite stiffness in tension and goes slack in compression. A compression element has finite stiffness in compression and a gap opens in tension. This element was used between decks and also between an end-span and abutment for modeling the impact.

3.3) 3-D MODELS

DRAIN-3DX (Powell and Campbell, 1994) is used for 3-D nonlinear time history analysis. Figures 3.5 and 3.6 show the analytical 3-D models for Bridge-1 and Bridge-3, respectively.

Because of the lack of symmetry with regard to deck center (Figure 2.2b), a 3-D model of Bridge-2 would require modeling two bridges along side each other with link elements in between and common abutments. Therefore, due to time limitations the 3-D analysis of this bridge was not performed. For Bridge-1, similar to 2-D model, due to symmetry only half of the bridge is modeled. For major mode shapes in the three translational directions (i.e., longitudinal, transverse and vertical) corresponding mass proportional damping was assigned to the bridge models. For cap beams half of the gross moment of inertia (I_g) and torsional constant (J) are used to account for concrete cracking. However, for the composite decks due to the presence of steel girders, 75% of I_g for transverse bending and 75% of the torsional constant (J) are used. In vertical direction due to low amplitude response the gross moment of inertia is assumed for the composite deck sections. For major mode shapes 5% damping proportional to the mass matrix is assumed (i.e., 5% damping for dominant modes in longitudinal, transverse and vertical directions). A brief description of different element types that used in the 3-D models follows.

Fiber Hinge Beam-Column Element (Type 08)

This is an inelastic element for modeling steel, reinforced concrete or composite beam-columns. Three hinge types, namely P-M hinges, Shear hinges, and connection hinges (Fig.3.7a, b,c) are available with this element type. Due to the aspect ratio of the bridge columns flexural mode is dominant, therefore only P-M plastic hinges were used. These are placed at the ends of the pier columns. The fiber arrangements and its property at each P-M hinge were defined such that the ultimate strength of the cross section is properly represented.

Elastic Beam-Column Element (Type 17)

This is a linear elastic beam-column element. This element is used to model decks, cap beams and abutments.

Simple Connection Element (Type 04)

This is a zero-length element that connects two coincident nodes. It has either rotational or translational stiffness. Element behavior is nonlinear with the ability to have elastic or inelastic unloading with or without gap. Complex behaviors can be obtained by placing two or more elements in parallel positions. Bearings, abutment back-fill soils (with inelastic unloading) and soil springs at the pier column footings were modeled by this element.

Link Element (Type 09)

The link element is a uniaxial element with finite length and arbitrary orientation. An element can be specified to act in tension (tension force and extension are positive) or in compression (compression force and shortening are positive). A tension element has finite stiffness in tension and goes slack in compression. A compression element has finite stiffness in compression and gap opens in tension. This element was used between decks and also between an end-span and abutment for modeling the impact.

As a part of the parametric study the following parameters and earthquake records were considered:

a) Post failure frictional coefficient μ was assumed to be equal to 0.2, 0.6 and infinity (i.e., no failure of the bearings)

b) Soil shear modulus was assumed to be equal to 0.4, 4 and 40 ksi.

c) Two earthquake records, Parkfield and El Centro, along with their orthogonal components were considered. These earthquake records are described in the following section.

d) Two alternative sets for each set of earthquake records are considered.

Alternate 1 (alt-1) has component-1 in longitudinal direction and component-2 in transverse direction of the bridge, and Alternate 2 (alt-2) has reverse component arrangement.

e) The strength and stiffness of the whole abutments are used.

3.4) Input Earthquake Motions

Two peak ground accelerations of 0.18g and 0.4g are considered. The former is the maximum acceleration coefficient. The latter is for higher seismic regions.
Two horizontal earthquake components were considered simultaneously to excite the 3-D models of the bridges in longitudinal and transverse directions. For each set of components two possible alternatives are considered.

Alternative 1 (alt-1) refers to the earthquake record when component-1 is in the longitudinal direction and component-2 in the transverse direction of the bridge. Alternative 2 (alt-2) is the reverse of this. For 2-D models only the first component of the earthquake records, which is the strongest one of two, was considered. The following are earthquake records that after being scaled to PGA of 0.18g or 0.4g are used in analyzing the bridges:

Parkfield, California earthquake June 27, 1966

Component-1

N65E
Cholame, Shandon, California array N0. 2
PGA = -479.64 cm/sec^2 at 3.74 sec

Component-2

N05W
Cholame, Shandon, California array N0. 5
PGA = -347.82 cm/sec^2 at 7.40 sec

Imperial Valley earthquake May 18, 1940

Component-1

S00E
El Centro site Imperial Valley irrigation district
PGA = 341.70 cm/sec^2 at 2.12 sec

Component-2

S90W
El Centro site Imperial Valley irrigation district
PGA = 210.14 cm/sec^2 at 11.44 sec

Nahanni aftershock, Dec. 23, 1985, Canada *(only used for 2-D models)*

Component-1

Site-2, Slide Mountain, Component 240
PGA=534.4 cm/sec^2

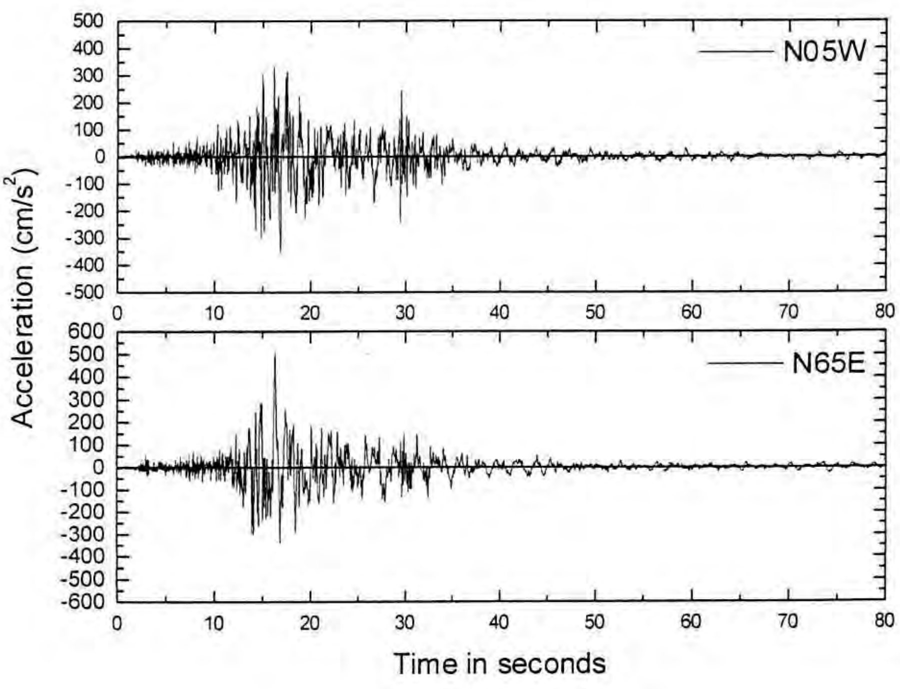

Figure 3.8(a) Time History data for 1966 Parkfield earthquake at Cholane

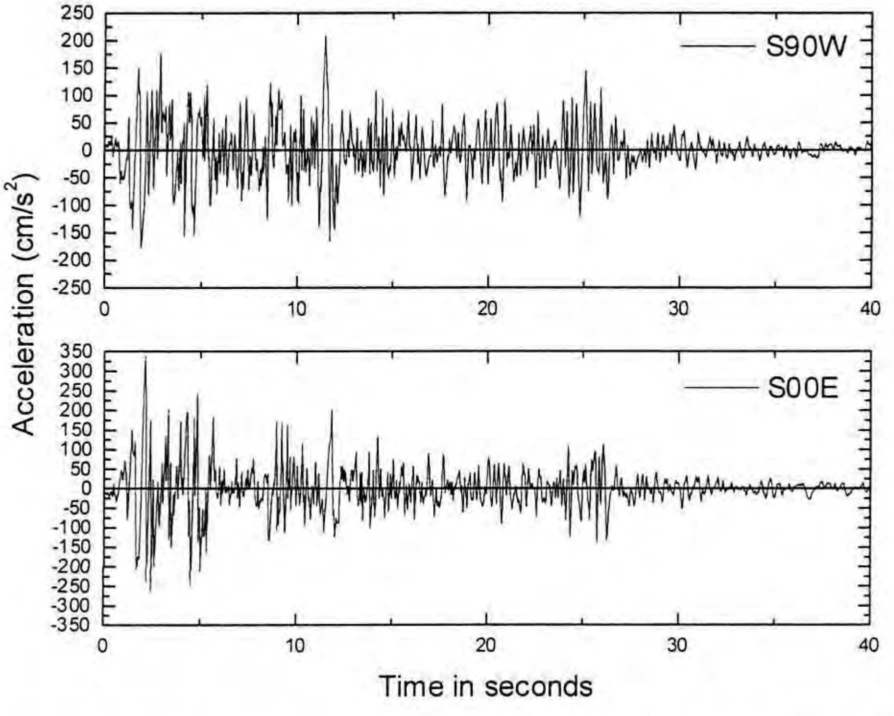

Figure 3.9(b) Time History data for 1940 Imperial Valley earthquake at El-Centro

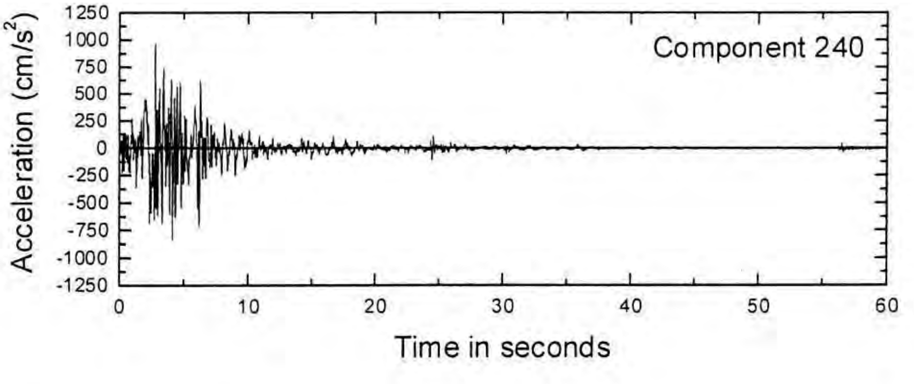

Figure 3.8(c) Time History data for 1985 Nahanni aftershock at Slide Mountain

In the time history analyses only the first 10 seconds of the above records and cut off acceleration of 0.025g has been used. Figure 3.9 presents the response spectrum of Parkfield and El Centro records (scaled to 0.18g) and AASHTO response spectrum for PGA of 0.18 and site coefficient (S) equal to 1.2. This site coefficient (S=1.2) is an average value based on the AASHTO specifications.

3.5) SUMMARY

Approaches to develop computer models of the super structure (bridge), substructure (foundation) by equivalent springs both rotational and transnational are discussed. Both 2-dimensional and 3-Dimensional model of the bridges have been outlined and shown diagrammatically 5% damping has been considered in the bridge models which is consistent with AASHTO response spectra. Radiation damping at foundation has been considered.

Different values of soil shear modulus (G=0.4, 4.0 and 40 ksi) and bearing performances (μ =0.2, 0.6, $\propto$) are considered for parametric study. Three earthquake records along with their orthogonal components are considered in the analysis.

Table 3-1 Soil spring stiffness coefficients in 2-D Computer models

Bridge-1

Abutments		Piers			
No. 1	**No. 2**	**No.1**		**No.2**	
Ka_1 (kips/in)	Ka_1 (kips/in)	Kh_1 (kips/in)	kr_2 (kips-in/rad)	Kh_2 (kips/in)	Kr_2 (kips-in/rad)
½ 1,875*G Top portion : ½ 1,228*G	½ 1,930*G Top portion : ½ 1,228*G	1,012.6*G	11,067,000*G	1,092*G	18,643,000*G

Bridge-2

Abutments		Pier	
No.1	**No.2**		
Ka_1 (kips/in)	Ka_2 (kips/in)	Kh (kips/in)	Kr (kips-in/rad)
1,300*G Top portion : 1,595*G	1,432*G Top portion : 1,595*G	1,698*G	24,711,700*G

Bridge-3

Abutments		Piers #1, #2 and # 3	
No.1	**No.2**		
Ka_1 (Kips/in)	Ka_2 (Kips/in)	K_h (Kips/in)	K_r (Kips-in/rad)
1,615*G Top portion: 785.4*G	1,150*G Top portion: 666.9*G	1,000*G	9,944,484*G

Note : G is in ksi.

Table 3-2 Different 2-D models with associated modeling parameters

Model No.	Description
1	At bearings μ= 0.6, G_{-soil}=0.4ksi, Damaged abutment
2	At bearings μ= 0.6, G-soil=0.4ksi
3	At bearings μ= 0.6, G-soil=0.4ksi
4	At bearings μ= 0.6, G-soil=40.0 ksi
5	At bearings μ= 0.6, G-soil=40.0 ksi, Damaged abutment
6	At bearings μ= 0.2, G-soil=0.4ksi, Damaged abutment
7	At bearings μ= 0.2, G-soil=0.4ksi
8	At bearings μ= 0.2, G-soil=4.0ksi
9	At bearings μ= 0.2, G-soil=40.0 ksi
10	At bearings μ= 0.2, G-soil=40.0 ksi, Damaged abutment
11	Elastic bearings, G-soil=0.4 ksi, Damaged abutment
12	Elastic bearings, G-soil=0.4 ksi
13	Elastic bearings, G-soil=4.0 ksi
14	Elastic bearings, G-soil=40.0 ksi
15	Elastic bearings, G-soil=40.0 ksi, Damaged abutment

Notes:

1) μ is the coefficient of friction at failed bearings.
2) G-Soil soil shear modulus.
3) Damaged-abutment model is a case of shear failure at the junction of back wall and breast wall

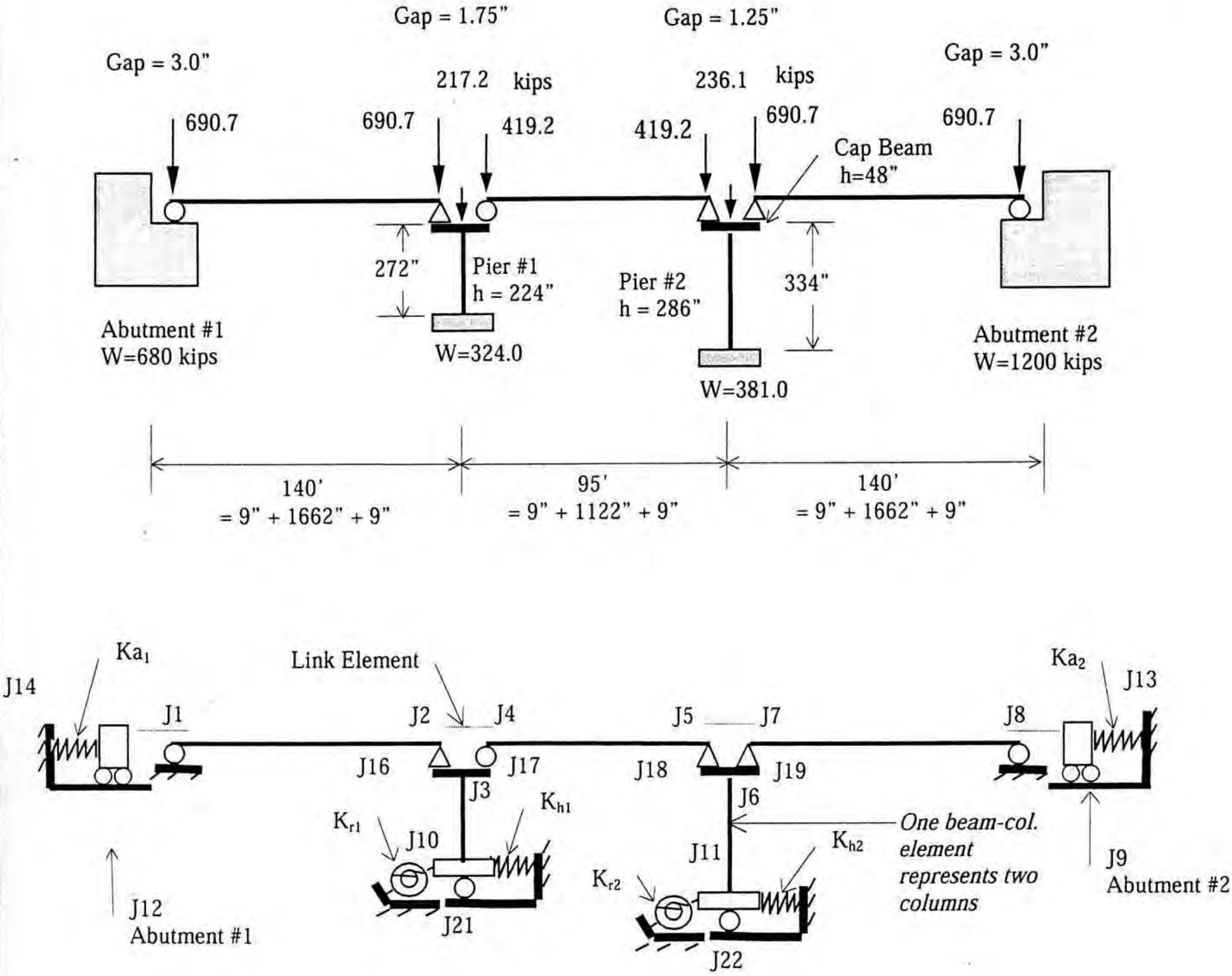

Figure 3-1 2 Dimensional Computer model of Bridge-1

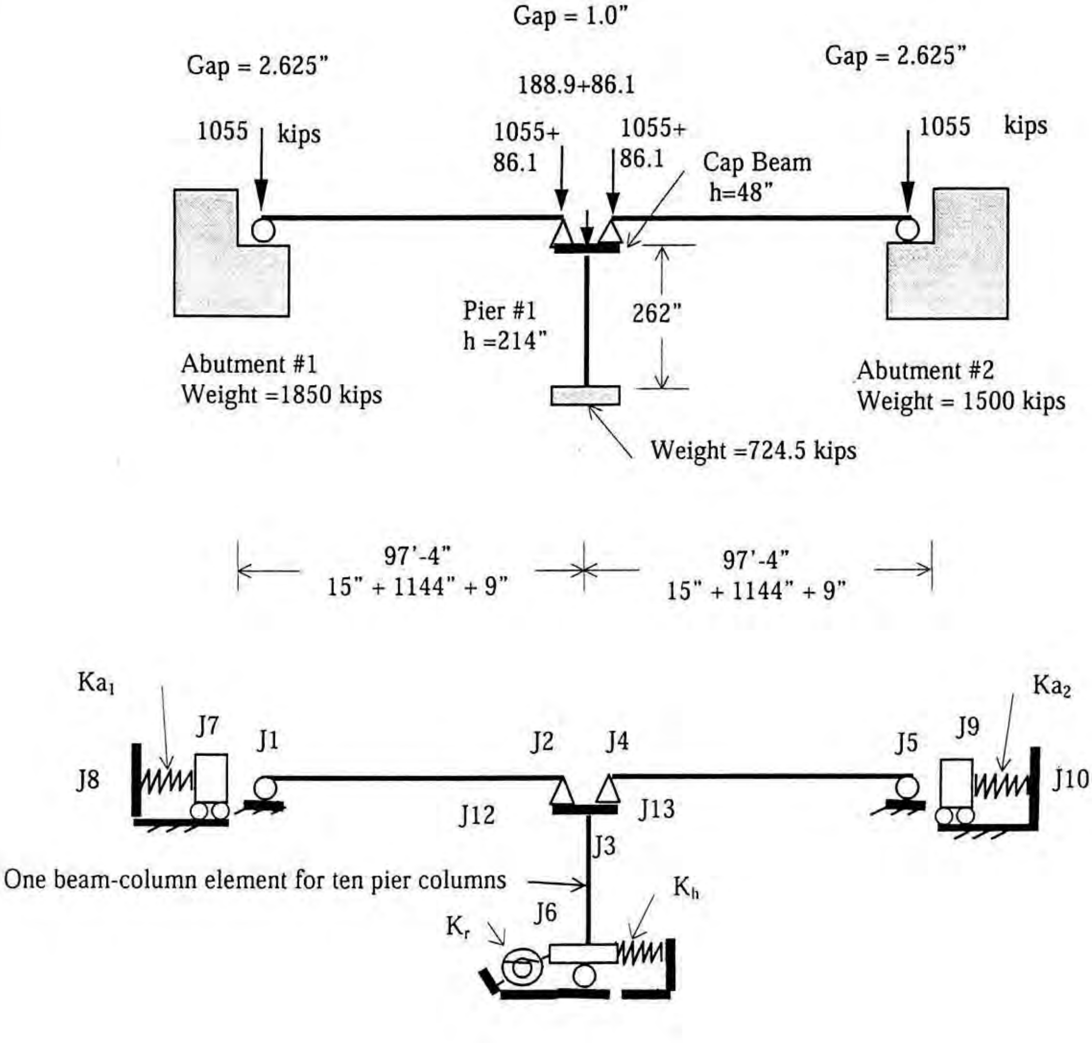

Figure 3-2 2 Dimensional Computer model of Bridge-2

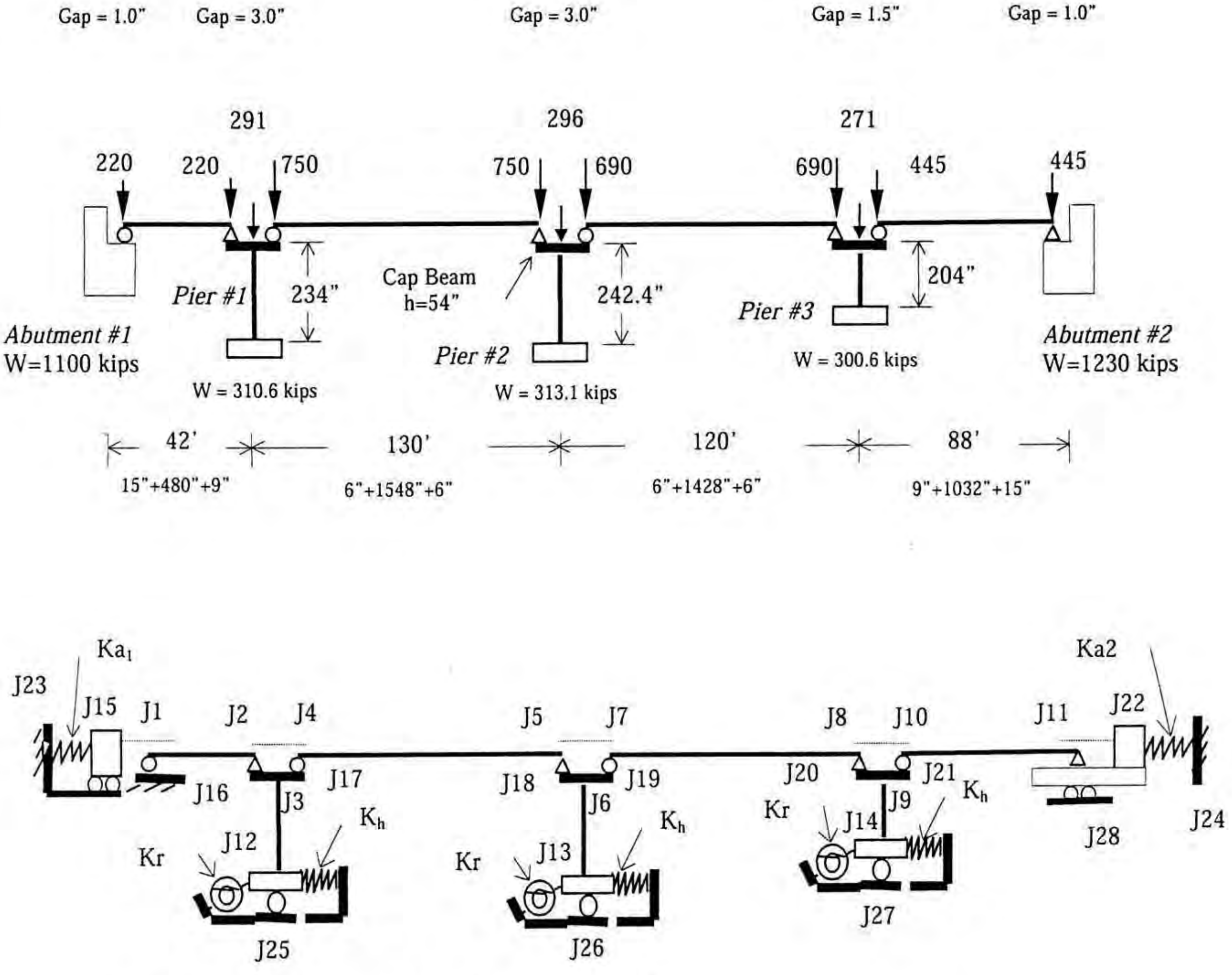

At each pier, five beam-column elements were used.
For col. type #1 the minimum flexural yield moment under the min. axial load at pier #3 is used as the yield limit at all pier locations.

Figure 3-3 2 Dimensional Computer model of the Bridge-3

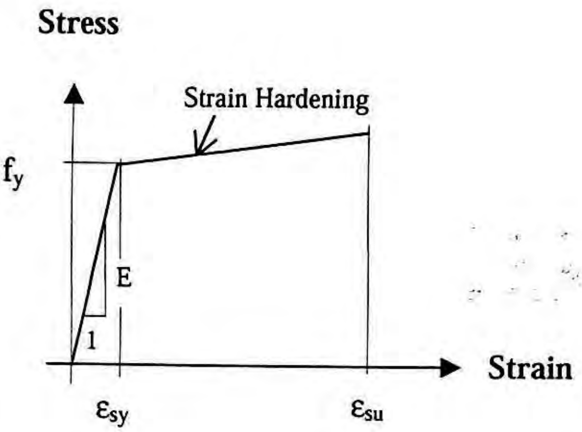

a) Steel stress-strain curve

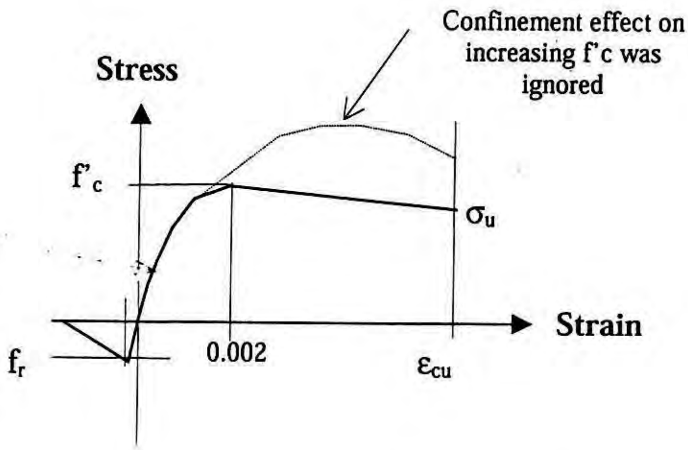

b) Concrete stress-strain curve

Figure 3.4 Stress strain curve for steel and concrete.

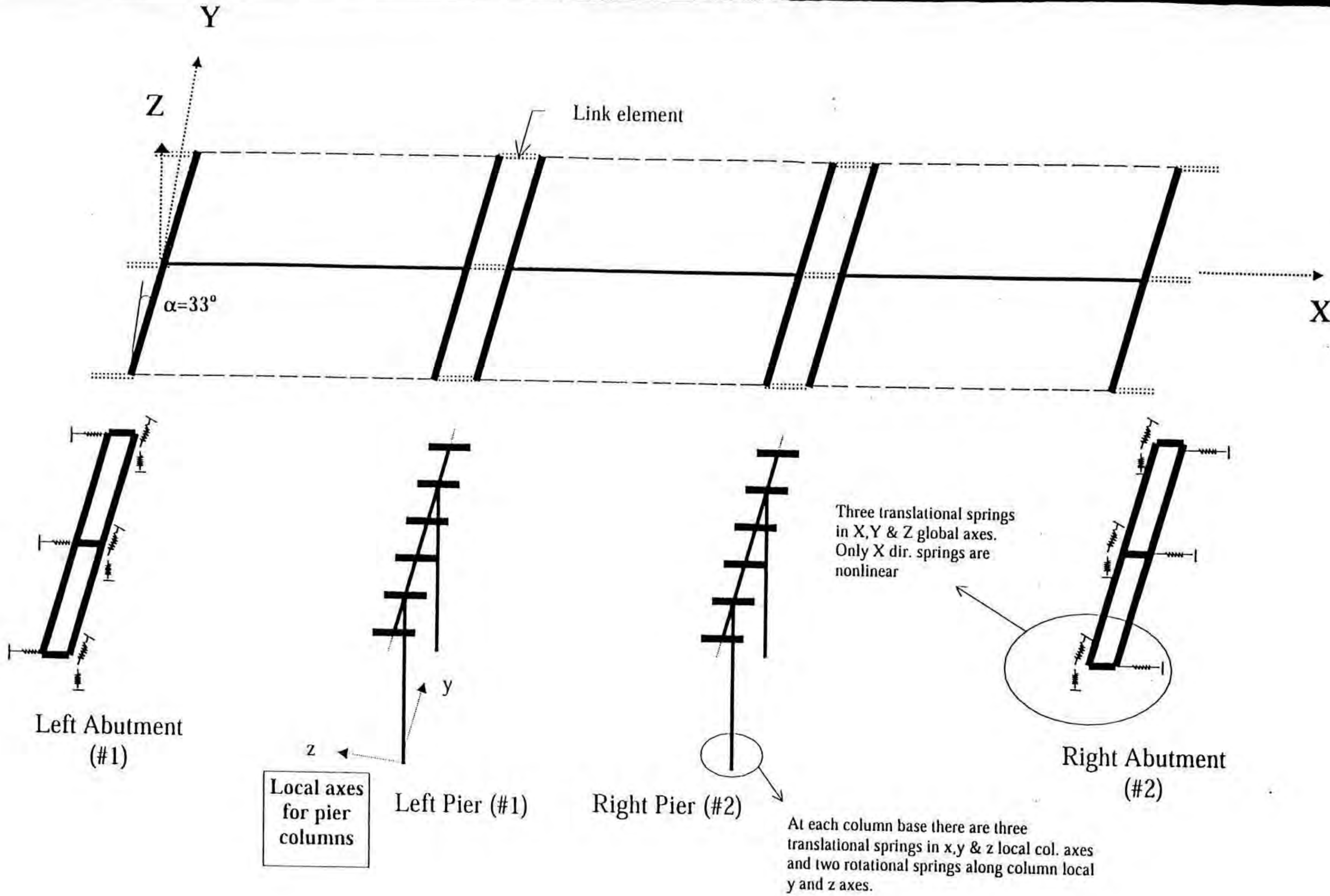

Figure 3.5 3 Dimensional model of Bridge-1.

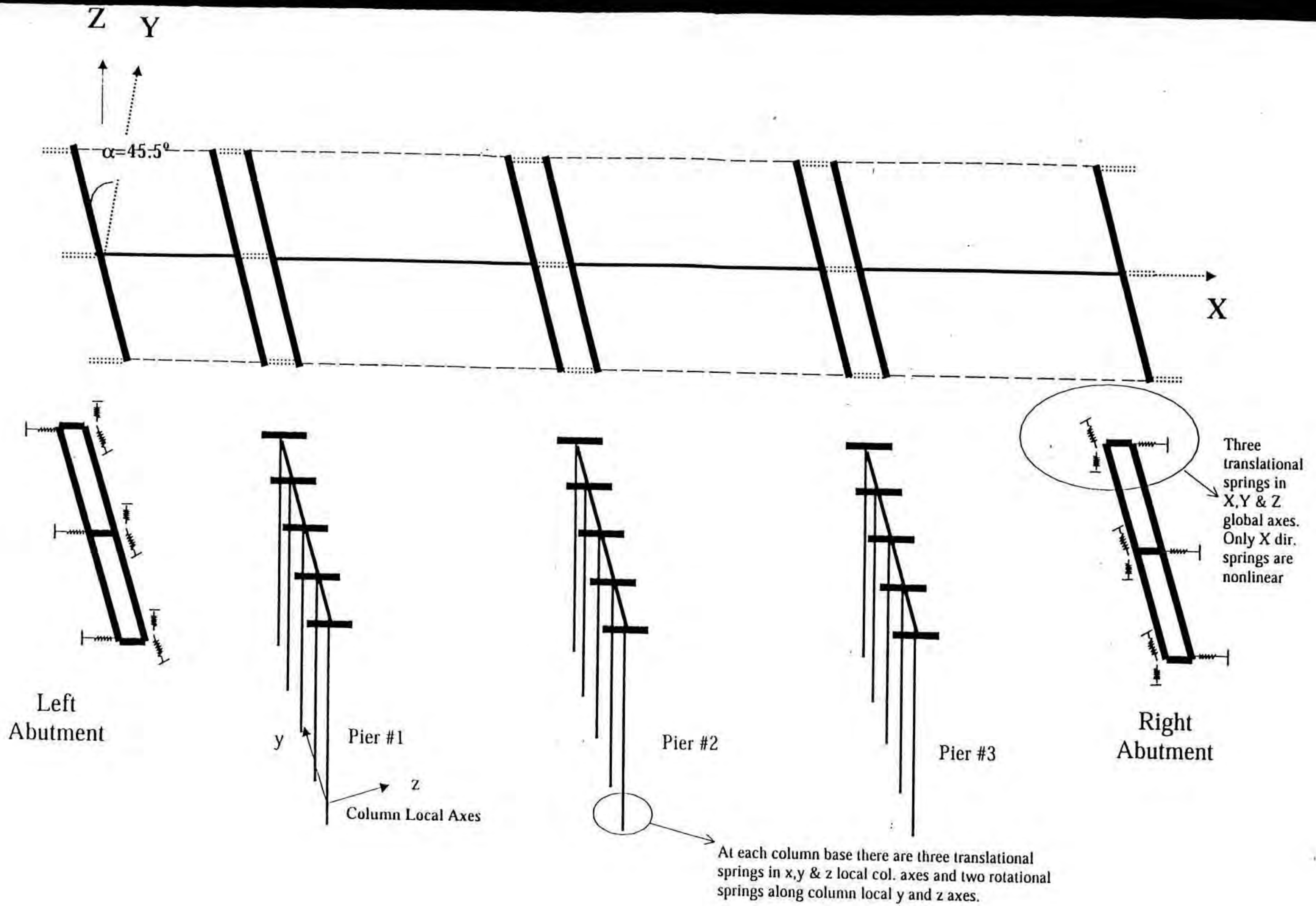

Figure 3.6 3 Dimensional model of Bridge-3.

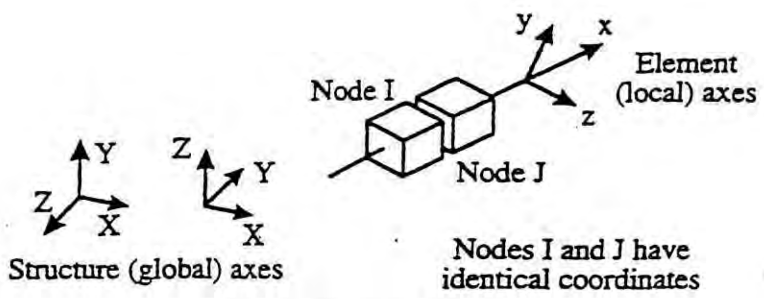

(a) Nodes and Axes

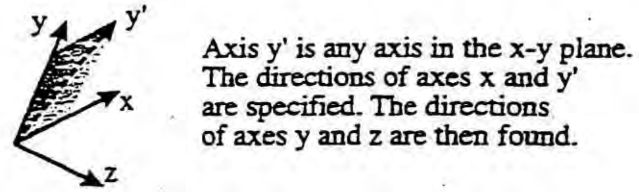

(b) Procedure for Orienting Axes

Figure 3-7 a Element Geometry

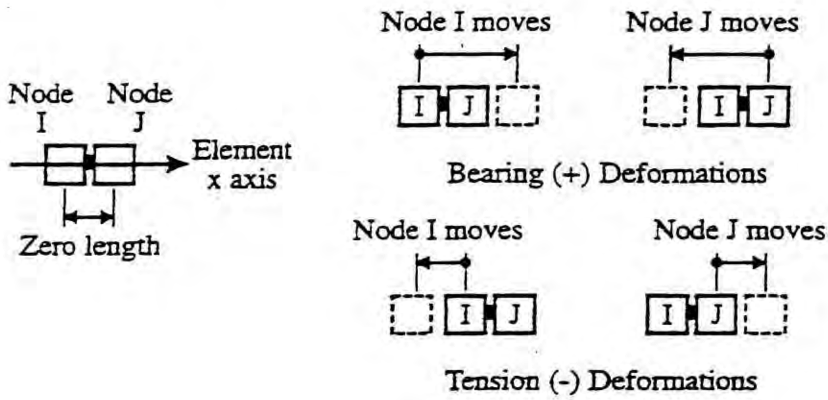

(a) Bearing Component

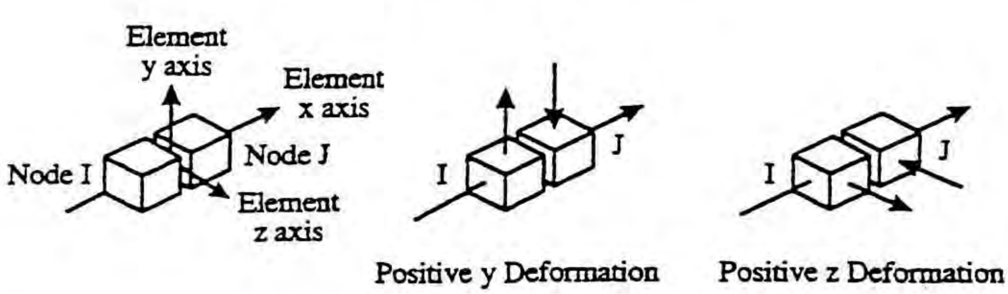

(b) Friction Component

Figure 3-7 b Sign Conventions

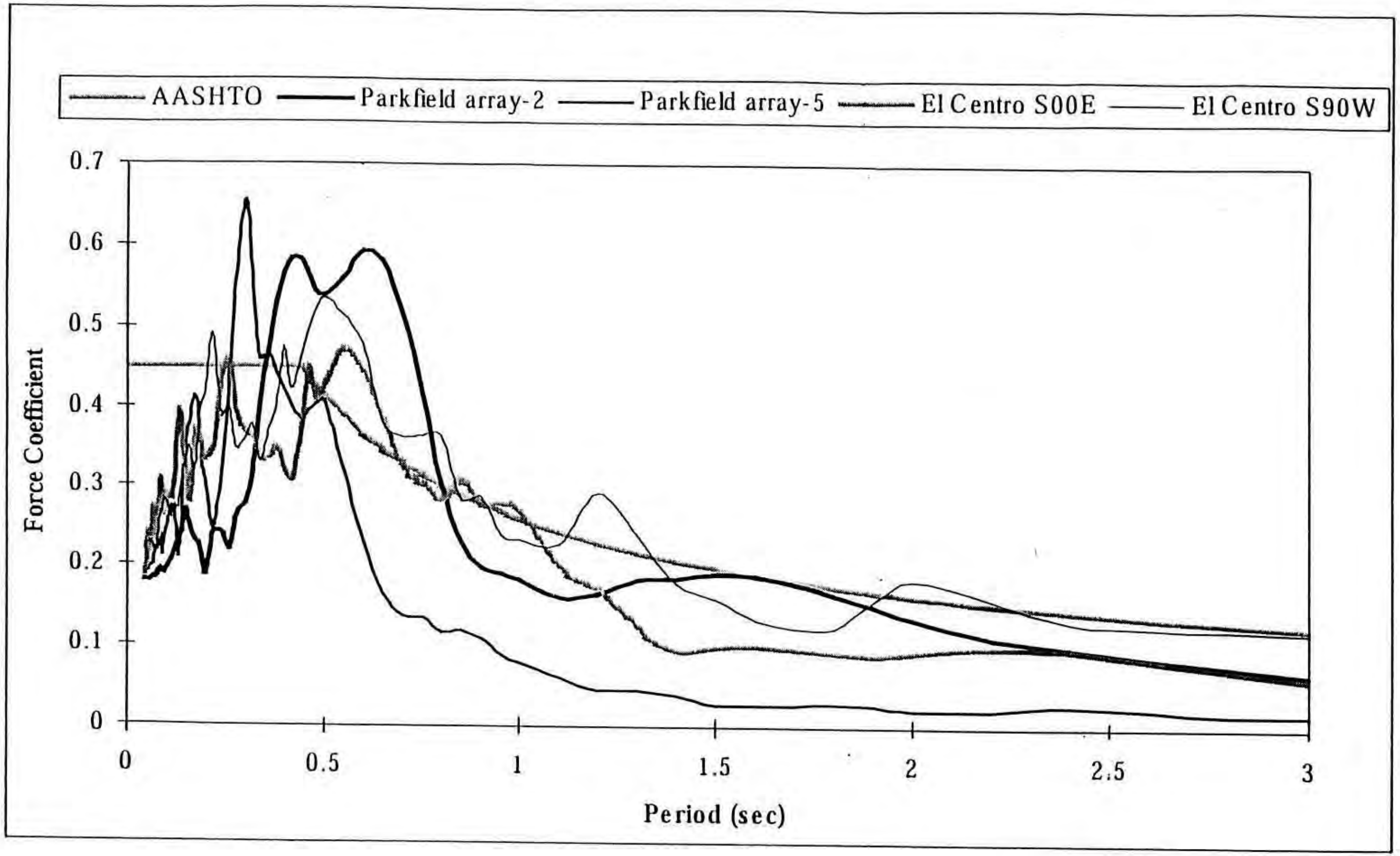

Figure 3.9 Response spectrum graphs (PGA=0.18g).

CHAPTER 4

RESULTS OF 2-DIMENSIONAL ANALYSIS

4.1) GENERAL

In this chapter the results of the nonlinear time history analyses are presented. Primarily the PGA of 0.18g was considered in the bridge analyses and the effects of the higher PGA of 0.4g are investigated only for the Bridge-1, which had the poorest seismic response under 0.18g PGA. Also a nonlinear static analysis based on the AASHTO specifications is performed for the Bridge-1 and its nonlinear response characteristics, which can be generalized for other bridges, are explained by a simplified graphical approach. It should be noted that this method is commonly known as pushover analysis and is described first in the next section.

4.2) PUSH-OVER ANALYSIS

Although pushover analysis was not among the initial objectives of this study, it is instructive to compare the relationship between the pseudo static response and demand based on design guidelines. A graphically useful method for such comparison is to plot the push-over load-deformation behavior of the bridge. This is shown in Figure 4-1 for seismic coefficient equal to 0.18g and 0.4g and site coefficient (S) equal to 1.2 as an average value. It is assumed that stiffness is equal to load divided by displacement and then using the weight of the bridge the response spectrum is transferred from period vs. acceleration space to displacement vs. load. Thus, on this diagram, lines radiating from the origin will show systems with different periods (e.g., x-axis is a system with infinite period and y-axis a system with zero period).

The load-deformation for the bridge is obtained by applying an increasing force at the level of the deck in the longitudinal direction. The load-deformation relationship, in general, is highly nonlinear and originally of a stiffening nature as the gaps close and other elements of the bridge system get involved.

As seen from these curves, the stiffness and strength of the foundations significantly influence the load-deformation behavior of the system. It appears that the abutment strength would have more effect on the seismic response of the system than the abutment stiffness and also more than the soil-structure interaction at the base of the columns. Shown in this figure is also the bridge response using CALTRANS approximate approach, where the maximum strength is based on the maximum soil strength of 7.7 ksf and stiffness is equal to 200 k/in per unit width of the deck. Based on CALTRANS approach the displacement of the Bridge-1 in the longitudinal direction is limited due to high stiffness and strength at the abutment. Actually, using this method there is not much difference in the longitudinal deck displacement between the two seismic coefficients (0.18 and 0.4). There will be yielding in only one of the columns, in this case in the right pier columns since the push over analysis was initiated by pushing the span next to the right abutment towards the left abutment. The maximum displacement is limited by the sum of the gap openings at the left pier and the left abutment plus deformation in the left abutment. In this example the maximum displacement is 4.75" plus the slight elastic deformation in the abutment. The abutment deformation is small due to high stiffness, and this is the reason for a minimal difference between seismic coefficient of 0.18 and 0.4. As seen from Figure 4-2, at this level of deformation (i.e., about 5") the plastic rotation in the columns of pier #2 (right pier) is well below the plastic rotation capacity.

Comparison of the design spectra to the load-deformation curves for the bridge where the soil-structure interaction is considered using the procedures outlined before, indicate that the bridge response will involve a significant nonlinear response at the abutments. As it can be seen from Figure 4-1, there is a significant difference between the effects of the two levels of motion. Similarly, bridges that may have failure in their abutment backwall will need a much large hystersis energy capacity and ductility demand at various components. Since the spectra are for 5% damping and linear system, the actual displacement demand can not be determined using the curves of Figure 4-1. This will require a time history analysis, which is described in the next section.

4-3) RESULTS OF THE NONLINEAR 2-D TIME HISTORY ANALYSIS

In this report first general observations for all three bridges under 0.18g PGA are described and along with that, the results of selected cases of Bridge-1 under 0.4g PGA are also presented. Then the response of each bridge is individually described.

4-3-1) General response of bridges

Among the three earthquake records used, almost always the Nahanni record caused the lowest response in all three bridges regardless of PGA and soil-structure interaction. Although, a similar conclusion cannot be made about the other two records (both from California Earthquakes) responses were higher more often for the Parkfield record. This can be seen in Figures 4-3, 4-9 and 4-10, which show different responses of bridges under these earthquake records.For an input motions with PGA of 0.18g the overall seismic response in the longitudinal direction is marginal with the lowest capacity / demand ratio (aside from bearing performance) of 1.04 for the seat length for Bridge-1.

Except for fixed bearings, other components of the bridges have enough capacity to withstand the demands under earthquakes with PGAs of 0.18g.

The level of impact force depends on the soil-type and abutment condition (intact vs. damaged back wall). When the abutment is assumed intact the impact forces are increasing as the soil stiffness decreases. In the case of damaged back wall the trend is reversed. For the same soil type there is less impact force in a damaged back wall case compared to an undamaged (or intact) abutment. These variations have to do with the relative value of the abutment stiffness with respect to its mobilized mass. Depending on these two parameters the amplitude of abutment response will change resulting in a different interaction with the bridge deck indicating the importance of modeling soil-structure interaction. The higher the input ground motion the more significant is the effect of soil-structure and abutments interaction on the response of the bridge.

Impact forces between two adjacent spans or between an end-span and the abutment are large enough to cause damage to the bridge in the form of bearing failure. Upon failure of the bearings the coefficient of friction has also an effect on the level of impact forces, where a higher coefficient of friction causes larger impact forces. This is probably due to the fact that under a lower coefficient of friction there is more energy dissipation through friction. Thus, the equal displacement concept does not necessarily hold.

Figure 4-17 shows various time histories of Bridge-1 for the Parkfield record with 0.4g peak ground acceleration. The time histories are for deck sliding at the right abutment for Bridge-1 for various SSI models. Note that the shear modulus, G, of 4 ksi is assumed to be, in an average sense, representative of typical fill and embankment soils used for bridges in Bangladesh. Furthermore, the case of 0.4 ksi shear modulus is taken as the extreme lower end of the spectrum, and may not represent actual cases. The compressive strength of abutments with this type of soil is assumed equal to that for $G = 4$ ksi (proportional to frictional angle $\varphi = 20$ degree). However, the stiffnesses are different. This will enable comparison of results with respect to both strength and stiffness.

As it can be seen from Figure 4-17, for the case of the damaged back wall, deck displacement exceeds the seat length. The maximum horizontal deck displacements of Bridge-1 for different SSI models are given in Table 4-1. A lower strength for the case of damaged back wall, as it will be discussed later, is the main cause of higher deck displacements for all three-soil types. However, comparison of two cases of $G = 0.4$ ksi and 4 ksi indicates that abutment stiffness also has an important effect (e.g., 7.3" vs.

9.7" or 33 percent increase) on the seismic response. Bridge displacement in the longitudinal direction is limited by abutment deformation and stiffer soils tend to act more like the fixed abutment.

The only difference between two cases of undamaged back wall and reduced compressive strength is in their strength. For the latter case the strength is reduced to that for a damaged abutment with G = 4 ksi. Comparison of these two curves indicates that abutment strength has a more dominant effect on the response.

Time histories of plastic rotation at the base of the columns in both Piers 1 and 2 of Bridge-1 are shown in Figure 4-16. Again, SSI plays a significant role on the ductility demand at the base of the columns. However, the trend is not directly proportional to soil property. Note that consideration of soil type and its interaction with the bridge includes boundary springs and masses at the base of the piers too. In general, bridges supported on softer soil will have larger displacements, mostly due to deformation of the abutment.

For the same bridge deck displacement, flexibility at the base of the columns for softer soils will mean lower plastic rotation. Increasing the soil stiffness, one expects, should further increase the plastic rotation demand. But, as the results show, the plastic rotation demand at the base of the columns may even be less for stiffer soils (Table 4-2). This is due to a limiting effect of abutment for stiffer soils because of its higher strength and stiffness.

This nonlinear effect on the substructures interaction with the superstructure causes the highest plastic rotation demands in the columns for moderately stiff soils and not in the stiffest soil. Once again demonstrating the need for explicit consideration to SSI. It should be mentioned that for lower PGAs where abutments are not significantly involved, the plastic rotation is higher for stiffer soils as expected. In the following sections a brief description of the analyses results for each bridge under PGA of 0.18g is given.

4.3.2) 2-D Response of Bridge-1 under PGA of 0.18g

The maximum displacements, plastic rotations and shear forces at selected locations are presented in Tables 4-3, 4-4, and 4-5, respectively. Table 4-6 presents minimum Capacity/Demand (C/D) ratios for different components of Bridge. As it is seen, the most critical C/D ratio belongs to the deck relative displacement over abutment #2, which for the softest considered soil (G = 0.4 ksi) under the Parkfield earthquake reaches a value of 1.04. Under the Parkfield earthquake the deck sliding C/D ratios for different models are also presented in Table 4-7 and as seen, this ratio ranges from 1.04 to 2.14 for different models.

Based on the results of different 2-D analyses of Bridge-1, following are the observed nonlinear response behavior in longitudinal direction under 0.18g PGA.

1) The maximum demand for plastic rotation, shear and moment forces at the pier columns tends to decrease with softer soils. Figure 4-4 shows the shear time history of pier #1 for different soil shear moduli. As it appears from the graph, for very soft soil (G-soil = .4 ksi) the maximum shear response has decreased about 40% compared to the stiffer soils (G=40 and 4 ksi). Softer soil also causes a larger gap opening/closure and bridge longitudinal displacements. Figure 4-18 shows the gap width of abutment #2 for different soil stiffnesses and as seen, a larger gap opening/closure has occurred in very soft soils with G=0.4 ksi.

2) A lower frictional coefficient at failed bearings does not always result in a lower demand on the pier columns. This can be seen in Figure 4-5, which shows the shear time histories of pier #2 for different frictional coefficients at the bearings.

3) Impact forces at pier column are higher for softer soils.

4) Higher impact forces occur with higher frictional coefficients at failed bearings.

5) In most cases the impact force between abutment and the end-span deck is much higher than the shear capacity of the top portion of the abutments. This requires consideration of back wall failure in modeling the bridge.

6) Stiffer soil causes higher seismic demand in the abutments backfill soil.

7) At abutment #1 impact forces and the number of impacts are small. This abutment has almost no effect on the response of the bridge. At abutment #2, where the number and level of impact forces are higher, a larger frictional coefficient at failed bearings will cause higher abutment forces.

8) The influence of the abutment modeling parameters including mass, back fill soil stiffness and yield limits on the response of the bridge tends to decrease with stiffer soils. This observation can be seen by considering Figure 4-19, which shows the gap opening over abutment #2 for three different abutment models with two different soil conditions.

9) The influence of the abutment parameters on the rest of the bridge tends to decrease as the soil stiffness increases. This can be seen by comparing Figures 4-19a and 4-19b, which show the gap opening over abutment #2 for three different abutment models and two different soil types.

10) For points farther from abutments the effect of abutment modeling parameters tends to decrease. Figure 4-11 shows the time histories of pier#1 top displacement for different abutment conditions for a very soft soil (G=0.4 ksi), which a negligible effect from abutments can be seen.

11) Lower frictional coefficients at failed bearings cause higher deck sliding.

4.3.3) 2-D Response of Bridge-2 Under PGA of 0.18g

The maximum displacements, plastic rotations and shear forces at selected locations are presented in Tables 4-8, 4-9, and 4-10, respectively. Considering C/D ratios, the most critical values belong to deck relative displacement over the abutments. Table 4-11 presents C/D ratios for different bridge components. The most critical C/D ratio belongs to deck relative displacement over abutment #1, which for very soft soils (G = 0.4 ksi) reaches its minimum value of 1.1 under the Parkfield earthquake.

Based on the results of different 2-D analyses performed for Bridge-2, following are the observed nonlinear response behavior in longitudinal direction under 0.18g PGA.

1) Regarding the overall bridge response, softer soils cause larger displacements (Figure 4-12), larger gaps opening over the pier and abutments (Figure 4-20), less moment and shear force demands for pier columns, and more impact between the decks and also between the abutments and end spans.

2) No plastic rotation at pier columns has occurred and stiffer soils result in larger shear and moment demands.

3) A lower frictional coefficient at failed bearings does not always result in lower demand on pier columns. This can be seen in Figure 4-6, where it shows the shear time histories of the central pier for different frictional coefficients at failed bearings.

4) Impact forces at pier column are higher for softer soils.

5) Higher impact forces occur with higher frictional coefficients at failed bearings.

6) Stiffer soil causes higher seismic demand in the abutments.

7) The influence of the abutment modeling on the rest of the bridge tends to decrease as the soil stiffness increases. This can be seen by comparing Figures 4-21a and 4-21b, which show the gap opening over abutment #1 for three different abutment models and two different soil conditions.

8) As a 2-span bridge, abutments parameters show considerable influence on the overall bridge responses. Figure 4-13 shows the influence of different abutment models on the top displacement response of the pier. As it can be seen, the responses (amplitude and frequency contents) are considerably different for different abutment models.

9) A lower frictional coefficient at failed bearing along with stiffer soils cause higher sliding at fixed bearings (upon their failure).

4.3.4) 2-D Response of Bridge-3 Under PGA of 0.18g

The maximum displacements, plastic rotations and shear forces at selected locations are presented in Tables 4-12, 4-13 and 4-14 respectively. Table 4-15 shows different C/D ratios for different bridge components. As it is seen, the most critical values belong to deck relative displacements. This ratio could be as low as 1.2 for very soft soils.

Based on the results of different 2-D analyses performed for Bridge-3, following are the nonlinear response behavior in longitudinal direction under 0.18g PGA.

1) Regarding the overall bridge response, softer soils cause larger displacements, larger gap opening/closure over piers and abutments (4-18), less force and plastic rotation demands for pier columns (Figure 4-7), and more impact between decks and also between abutments and the end spans.

2) A higher frictional coefficient at failed bearings causes larger plastic rotation (if there is any occurrence), shear, and moment demands at the base of pier columns. This can be seen in Figure 4-8, which shows the shear time histories of column type 3 at pier #1 for different frictional coefficients at failed bearings.

3) ..Abutment strength has more effect on longitudinal seismic response than stiffness and mass.

4)..Soil-structure interaction has an effect on seismic response in the longitudinal direction and dynamic analysis of this class of bridge system should explicitly consider the SSI.

4.4) SUMMARY

Based on a comprehensive study on three multi-span simply supported bridges the following conclusions can be made with regard to their 2-D seismic response in the longitudinal direction:

1). Seismic response of bridges is complicated by the impact between adjacent spans,

2) Due to impact forces, bearing failure and backwall damage are quite possible even under low levels of peak ground accelerations,

3) Except for fixed bearings failure and marginal C/D ratios for deck sliding in very soft soils, other components of the bridges have enough capacity to withstand the demands of earthquakes with PGA of 0.18g. Thus, it is unlikely for

an earthquake with 0.18g PGA to cause bridge collapse. This is the maximum acceleration coefficient required by AASHTO specifications,

4). Abutment strength has more effect on longitudinal seismic response than stiffness and mass.

Table 4-1 Bridge-1 maximum deck displacements for different SSI models. (2-D model, Parkfield record, PGA=0.4g)

Abutment Model	G-Soil (ksi)		
	0.4	4.0	40.0
Intact	9.7"	7.3"	6.7"
Damaged	13.5"	10.8"	9.4"

Table 4-2 Bridge-1 pier column plastic rotation (rad) for different SSI models. (2-D model, Parkfield record, PGA = 0.4g)

Abutment Model	G-Soil (ksi)		
	0.4	4.0	40
Intact	0.00"	0.015"	0.014"
Damaged	0.015"	0.021"	0.016"

Table 4-3 Bridge-1 maximum displacements (2-D model, PGA=0.18g).

Location	Displacement (inch.)	Model Description
Top of pier # 1	4.63 -4.42	G=.4 ksi, Elastic bearing, PF EQ G=0.4 ksi, μ =0.6 or elastic bearing, PF EQ, Damaged-abut.
Top of pier # 2	5.00 -6.16	G=0.4 ksi, μ=0.2, PF EQ, Damaged-abut. G = .4 ksi, μ =.6, EC EQ.
Gap width over pier # 1	+.0045 -6.75	G=.4 ksi, Elastic bearing, PF EQ G=0.4 ksi, μ =0.6, PF EQ, Damaged-abut.
Gap width over pier # 2	+.0025 -1.27	G = .4 ksi, μ =.6, EC EQ G=.4 ksi, Elastic bearing, EC EQ
Gap width over pier # 1	+.0061 -8.21	G=.4 ksi, Elastic bearing, PF EQ
Gap width over pier # 2	+.0067 -10.70	G =.4 ksi, μ =.6, PF EQ G= .4 ksi, μ=.2, PF EQ
Abutment # 1	+1.00 -1.43	G=.4 ksi, Elastic bearing, EC EQ G=0.4 ksi, μ=0.6 or elastic bearing, PF EQ, Damaged-abut.
Abutment # 2	+1.69 -2.00	G=.4 ksi, μ =.2, .6 & Elastic bearings, PF EQ

Notes :

1) PF = Parkfield , EC =El-Centro

Table 4-4 Bridge-1 maximum plastic rotation demand at the base of pier columns . (2-D model, PGA = 0.18g)

Location	Plastic Rotation (rad)	2-D Model Description
Base of pier # 1	+0.00287 -0.0	G=40 ksi, Elastic bearing, PF EQ, Whole or Damaged abut. All models
Base of pier # 2	+0.00480 -0.00264	G = 40 ksi, μ = .2 , PF EQ G = 40 ksi, μ =.2, PF EQ, Whole or Damaged abut.

Note : PF = Parkfield

Table 4-5 Bridge-1 maximum shear force at pier columns (2-D model, PGA = 0.18g)

Location	Shear Force (kips)	2-D Model Description
Column of pier # 1	238.3/2 = 119.2	G = 40 ksi, Elastic bearing, PF EQ, Whole or Damaged abut.
Column of pier # 2	194.1/2 = 97.1	G = 40 ksi, μ =.2, PF EQ, Whole or Damaged abut.

Table 4-6 Bridge-1 minimum Capacity/ Demand ratios (2-D model, PGA = 0.18g)

Response	Demand	Capacity	C/D Ratio
PlasticRotation			
φ_P(rad)			
at the base of pier # 1	1.00287	0.015	5.2
at the base of pier # 2	0.0264	0.0173	6.6
Curvature Ductility			
$\mu = \varphi_u / \varphi_p = 1 + \varphi_p / \varphi_y$			
(1/inch)			
at the base of pier # 1	1+.00009/.00008= 2.12	.00055/.00008 = 6.88	3.2
at the base of pier # 2	1+.000072/.00008=1.9	.00055/.00008 = 6.88	3.6
Shear			
(kips)			
at the base of pier # 1	238.3/2 = 119.2	315- .12*91 =304	2.6
at the base of pier # 2	194.1/2 = 97.1	315	3.2
Deck Relative			
Displacement (inch.)			
over pier # 1	(6.75-1) $\pm$ 1.02=5 $\pm$ 1.02	10	2.5-1.7
over pier # 2	1.27	10	7.9
over abutment # 1	8.21-3 = 5.21	8	1.5
over abutment # 2	10.70-3 = 7.70	8	1.04

NOTES:

1) Deck relative displacement is obtained from link element deformation
2) C/D ration of the deck relative displacement over pier # 1 is given in a range. This range is calculated by considering the fixed bearing maximum displacement and gap opening over the pier.
3) The maximum fixed bearing displacements are equal to 1.02" at pier # 1 and pier # 2.

Table 4-7 Bridge-1 Capacity/Demand ratios for deck relative displacement over abutment # 2 under Parkfield earthquake. (2-D model, PGA = 0.18g)

2-D model Description	Demand	Capacity/Demand
At bearing μ= 0.6, G-soil =. 4 ksi Damaged abutment	8.52-3 = 5.52	8/5.52 = 1.45
At bearings μ= 0.6, G-soil =. 4ksi	10.54-3 = 7.54	1.06
At bearingsμ = 0.6, G-soil =. 4ksi	7.51 = 4.51	1.77
At bearings μ= 0.6, G-soil =.4ksi	7.04-3 = 4.04	1.98
At bearing μ= 0.6, G-soil =.4 ksi Damaged abutment	7.14 –3 =4.04	1.98
At bearing μ= 0.2, G-soil =. 4 ksi Damaged abutment	8.78-3 = 5.78	1.38
At bearingsμ = 0.2, G-soil =. 4ksi	10.70-3 = 7.70	1.04
At bearingsμ = 0.2, G-soil =40ksi	8.13 –3 = 5.13	1.56
At bearingsμ= 0.2, G-soil = 40 ksi	7.96-3 = 4.96	1.61
At bearingμ = 0.2, G-soil =40 ksi Damaged abutment	7.96-3 = 4.96	1.61
Elastic bearing, G-soil=.4ksi, Demaged abutment	8.79-3 = 5.49	1.46
Elastic bearing, G-soil=.4ksi	9.71-3 = 6.71	1.19
Elastic bearing, G-soil= 4ksi	7.29-3 = 4.29	1.86
Elastic bearing, G-soil= 40ksi	6.74-3 = 3.74	2.14
Elastic bearing, G-soil=40ksi, Damaged abutment	6.74 –3 = 3.74	2.14

Table 4-8 Bridge-2 maximum displacements (2-D model, PGA = 0.18g)

Location	Displacement (inch.)	2-D Model Description
Top of pier # 1	4.73 -4.69	G=.4 ksi, PF EQ Damaged-abut. G=.4 ksi, elastic bearing, PF EQ, Damaged-abut.
Gap width over pier # 1	+.0042 -1.011	G=.4 ksi, μ =.6 at bearing, PF EQ G= 4 ksi, elastic bearing, PF EQ
Gap width over pier # 1	+. 0082 - 8.90	G = .4 ksi, μ =.6, bearing, EC EQ G=.4 ksi, μ=.6, PF EQ, Elastic bearing, EC EQ Damaged-abut.
Gap width over abut. # 2	+.0129 - 7.95	G=.4 ksi, Elastic bearing, PF EQ G = .4 ksi, μ = .2, PF EQ, Damaged-abut
Abutment # 1	+2.51 - 2.06	G=.4 ksi, Elastic bearing, PF EQ G=.4 ksi, elastic bearing, PF EQ, Damaged abut.
Abutment # 2	+2.47 - 2.09	G=.4 ksi, μ =.6 at bearings, PF EQ G=.4 ksi, μ =.6, PF EQ, Damaged-abut.

Notes :

1) PF= Parkfield, EC = El – Centro
2) Positive gap width is for gap closure.

Table 4-9 Bridge-2 maximum plastic rotation demands at the base of pier columns(2- D model, PGA = 0.18g)

Location	Shear Force	2-D Model Description
Base of pier # 1	652.0/10=65.2	All Models

Table 4-10 Bridge-2 maximum shear force demand at the pier columns (2-D model, PGA = 0.18g)

Location	**Shearforce (kips)**	**2-D Model Description**
Column of pier # 1	652.0/10 = 65.2	G = 4 ksi, μ = .6 at bearings, PE EQ

Table 4-11 Bridge-2 Capacity/Demand ratios (2-D model, PGA = 0.18g)

Response	Demand	Capacity	C/D Ratio
Plastic Rotation, θ_p(rad) at the base of pier	0.00	0.126	No Demand
Curvature Ductility $\mu = \varphi_u / \varphi_p = 1 + \varphi_p / \varphi_y$ (1/inch) at the base of pier	~ 1	.0045/.0001 = 45	45
Shear(kips) at the base of pier	65.2	442.1	6.8
Deck Relative Displacement (inch.) over the pier over abutment # 1 over abutment # 2	 2.64 8.896- 2.625 = 6.3 7.952 – 2.625 = 5.3	 7 7 7	 2.7 1.1 1.3

Notes:
1) At abutments the deck relative displacement is obtained from the link deformation.
2) The maximum fixed bearing displacement over the pier is equal to 2.64".

Table 4-12 Bridge-3 maximum displacements (2-D model, PGA = 0.18g)

Location	Displacement (inch.)	2-D Model Description
Top of pier # 1	+2.93 -1.96	G=.4 ksi, μ=.6 at bearing, PF EQ G= .4 ksi, =0.2, EC EQ
Top of pier # 2	+4.82 -4.15	G=.4 ksi, Elastic bearing PF EQ, Damaged abut. G = .4 ksi, μ=.2, PF EQ, Damaged abutment.
Top of pier # 3	+3.53 -3.37	G = .4 ksi, Elastic bearing PF EQ
Gap width over pier # 1	+.0035 -7.42	G=.4 ksi, Elastic bearing, PF EQ ,Damaged-abutment G=. 4 ksi, μ=0.6, PF EQ, Damaged-abut.
Gap width pier # 2	+. 0084 -6.51	G = .4 ksi, Elastic bearing PF EQ G=. 4 ksi, Elastic bearing, EC EQ
Gap width over pier # 3	+ .0056 -6.23	G =.4 ksi, Elastic bearing PF EQ
Gap width over abut. # 1	+. 0049 -4.82	G=. 4 ksi, Elastic bearing, PF EQ G =. 4 ksi, μ= .2,PF EQ.
Gap width over abut # 2	+. 0075 -6.82	G =.4 ksi, μ =.6, PF EQ G= .4 ksi, μ=.2, PF EQ
Abutment # 1	+. 72 -1.12	G =. 4 ksi, μ =. 6, PF EQ G= .4 ksi, μ =.2, PF EQ
Abutment # 2	+3.59 -3.06	G=.4 ksi, μ=.2, PF EQ Damaged- abut. G=.4 ksi, Elastic bearings, PF EQ

Notes :
PF = Parkfield, EC = El-Centro
Positive gap width is for gap closure.

Table 4-13 Bridge -3 maximum pier column plastic rotation (2-D model, PGA= 0.18g)

Location	Plastic Rotation (rad)	2-D model Description
Base of pier # 1	col.Type 1 + .00015 -0.0 col.Type 3 +0.0 -0.0	G= 40 ksi, Elastic bearing, EC EQ, Damaged-abut. All Models All Models
Base of pier # 2	col.Type 1 + .0015 -0.0017 col.Type 2 +0.00 -0.0	G=4 ksi,μ =.6, EC EQ. G=40 ksi, Elastic bearings, EC EQ, Damaged-abut. G=4 ksi, μ=.6, EC EQ. G=40 ksi, Elastic bearings, EC EQ, Damaged-abut.
Base of pier # 3	col.Type 1 + .0011 -0.0038 col.Type 4 +0.0017 -0.0044	G=40 ksi, Elastic bearings, EC EQ, Damaged-abut. G= 40 ksi, μ=.6, PF EQ, Damaged-abut. G=40 ksi, Elastic bearings, EC EQ, Damaged-abut. G= 40 ksi, μ=.6, PF EQ, Damaged-abut.

Notes:
PF = Parkfield, EC = El-Centro

Table 4-14 Bridge-3 maximum pier column shear force. (2-D model, PGA = 0.18g)

Location	Shear Force (kips)	2-D Model Description
Columns of pier # 1	col.Type 1 54.8	G= 40 ksi, Elastic bearing, EC EQ, Whole or Damaged abutment
	col.Type 3 72.6	G= 40 ksi, Elastic bearing, EC EQ, Damaged-abutment
Columns of pier # 2	col.Type 1 78.8	G=40 ksi, μ=.6, EC EQ, Whole or Damaged-abutment
	col.Type 2 58.0	G=40 ksi, μ=. 6, EC EQ.
Columns of pier # 3	col.Type 1 124.0	G=40 ksi, Elastic bearings, EC EQ, Damaged-abutment
	col.Type 4 71.7	G= 40 ksi, μ=.6, PF EQ, Damaged-abutment

Table 4-15 Bridge-3 Capacity/Demand ratios (2-D model, PGA= 0.18g).

Response	Demand	Capacity	C/D Ratio
Plastic Rotation, θ_p (rad)			
at the base of pier # 1			
col. type-1	0.000152	0.124	815.8
col. type-3	0.00	0.124	ND
at the base of pier # 2			
col. type-1	0.00220	0.124	56.4
col. type-2	0.00167	0.124	74.3
at the base of pier # 1			
col. type-1	0.00441	0.098	22.2
col.type-4	.00383	0.098	25.7
Curvature Ductility			
$\mu = \varphi_u / \varphi_p = 1 + \varphi_p / \varphi_y$ (1/inch)			
at the base of pier # 1			
col. type-1	1+.0000048/.00006 = 1.08	.004/.00006 = 66.7	61.8
col. type-3	~1	66.7	66.7
at the base of pier # 2			
col. type-1	1+.000017/.00006 = 2.16	66.7	30.9
col. type-2	1+.000053/.00006 = 1.88	66.7	35.5
at the base of pier # 3			
col. type-1	1+.000178/.00006 = 3.96	66.7	16.8
col. type-4	1+.00154/.00006 = 3.57	66.7	18.7
Shear (kips)			
at the base of pier # 1			
col. type-1	72.6	421.8	5.8
col. type-3	54.8	421.8	7.7
at the base of pier # 2			
col. type-1	78.8	421.8-16*69.8 =410.6	5.2
col. type-2	58.0	421.8	7.3
at the base of pier # 3			
col. type-1	124.0	421.8-1.96*69.8=285.0	2.3
col. type-4	71.7	421.8-1.57*69.8=312.2	4.4
Deck Relative Displacement (inch)			
over pier # 1	3.47to(7.42 – 3) + 3.47 = 7.42	9.3	2.7-1.3
over pier # 2	(6.51 – 3) 1.32 = 3.51 1.32	9.5	4.3 -2.0
over pier # 3	3.59 to (6.23-1.5) + 3.59 = 8.3	10.2	2.8 – 1.2
over abutment # 1	4.82 - 1= 3.82	9.3	2.4
over abutment # 2	6.82-1 = 5.82	9.3	1.6

Notes:

a) At abutments and piers the deck relative displacements are obtained from link element deformation.

b) Capacity/Demand ratios for the deck relative displacement of piers are given in a range. This range is calculated by considering the fixed bearing maximum displacement and gap opening over the piers.

c) The maximum displacements at fixed bearings are 3.47" at pier # 1, 1.32" at pier # 2, and 3.59" at pier # 3

d) ND = No Demand.

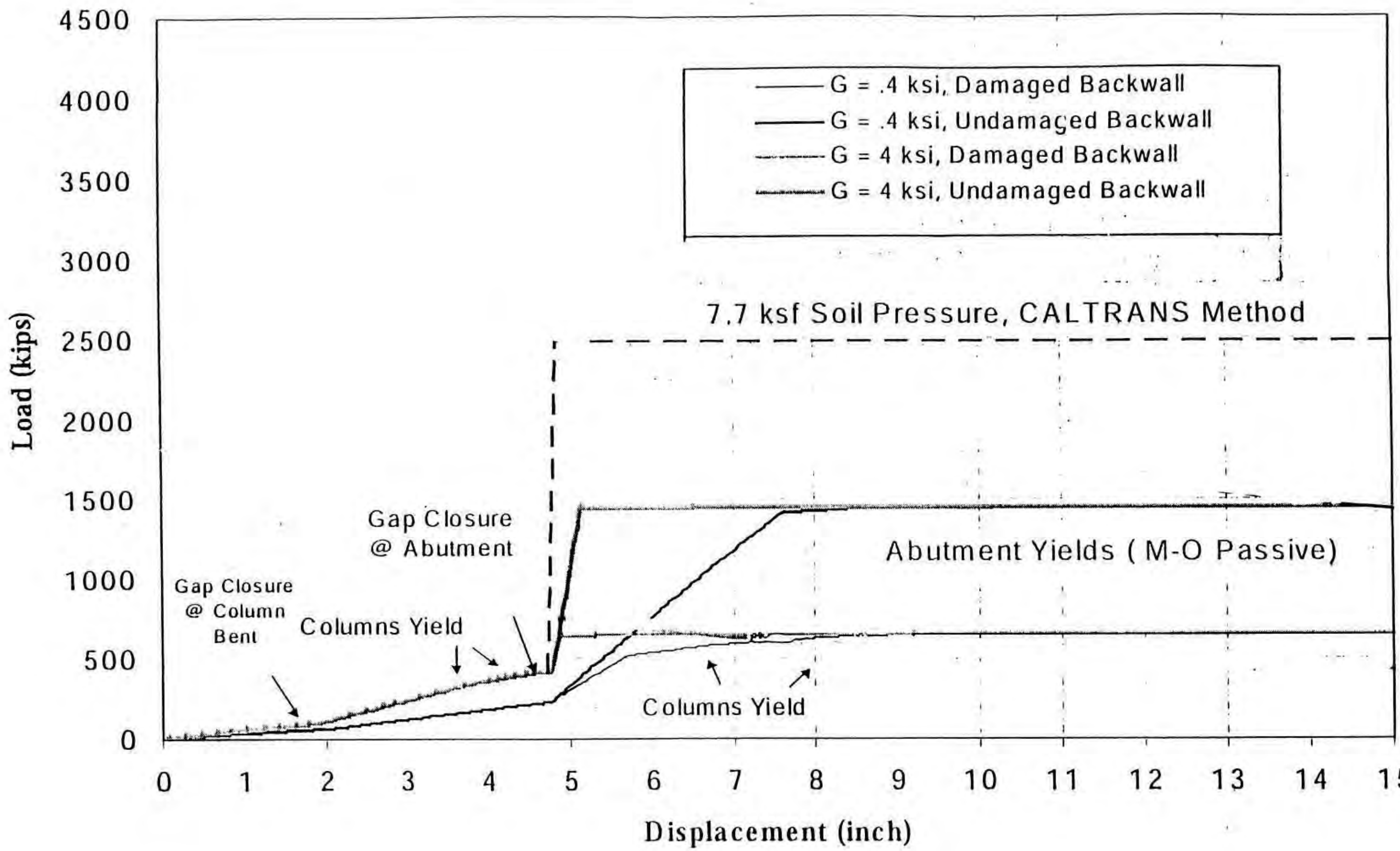

Figure 4-1 Pushover analysis of Bridge-1 (2-D model).

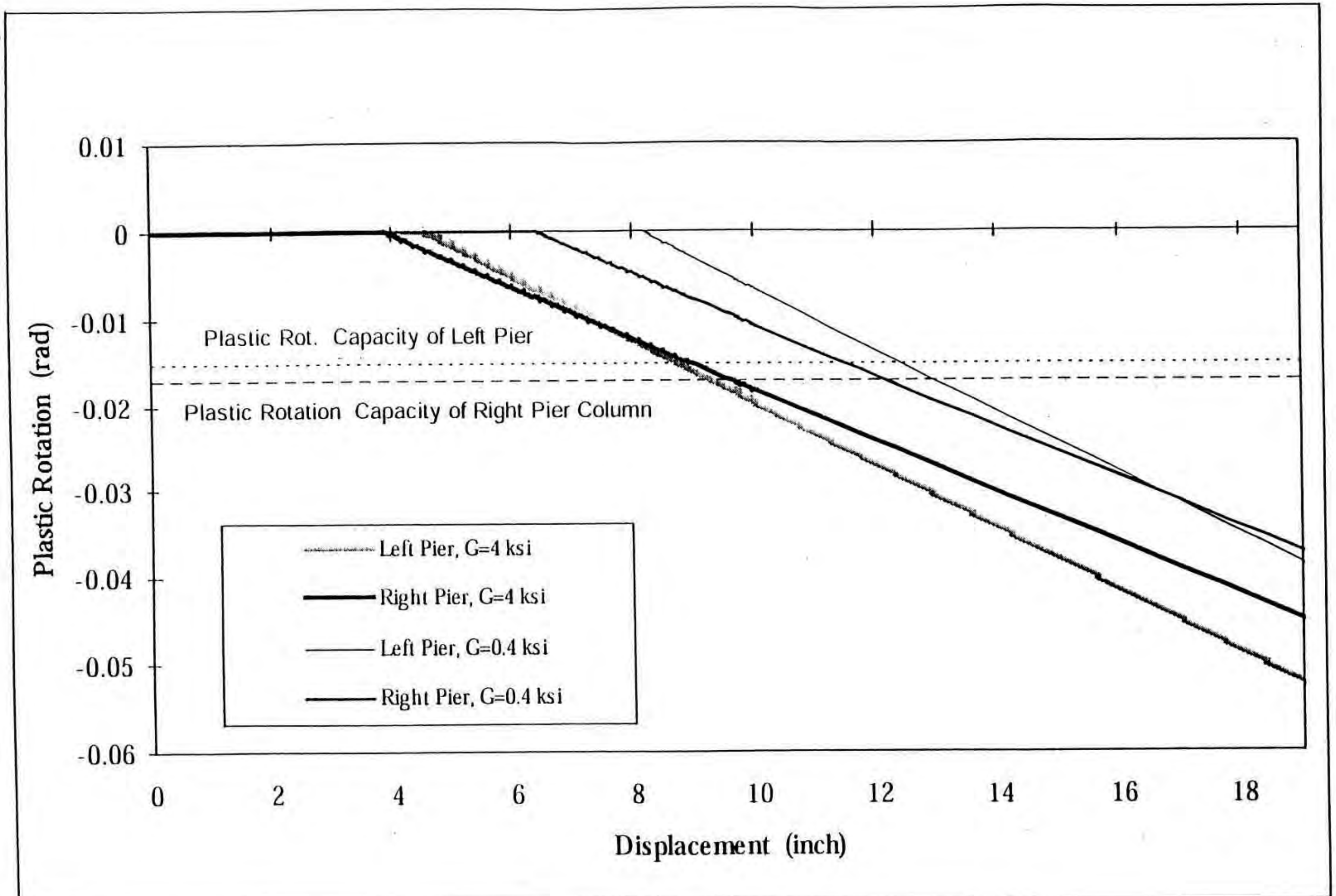

Figure 4.2 Plastic rotation at the base of Bridge Pier columns from 2-D Pushover analysis

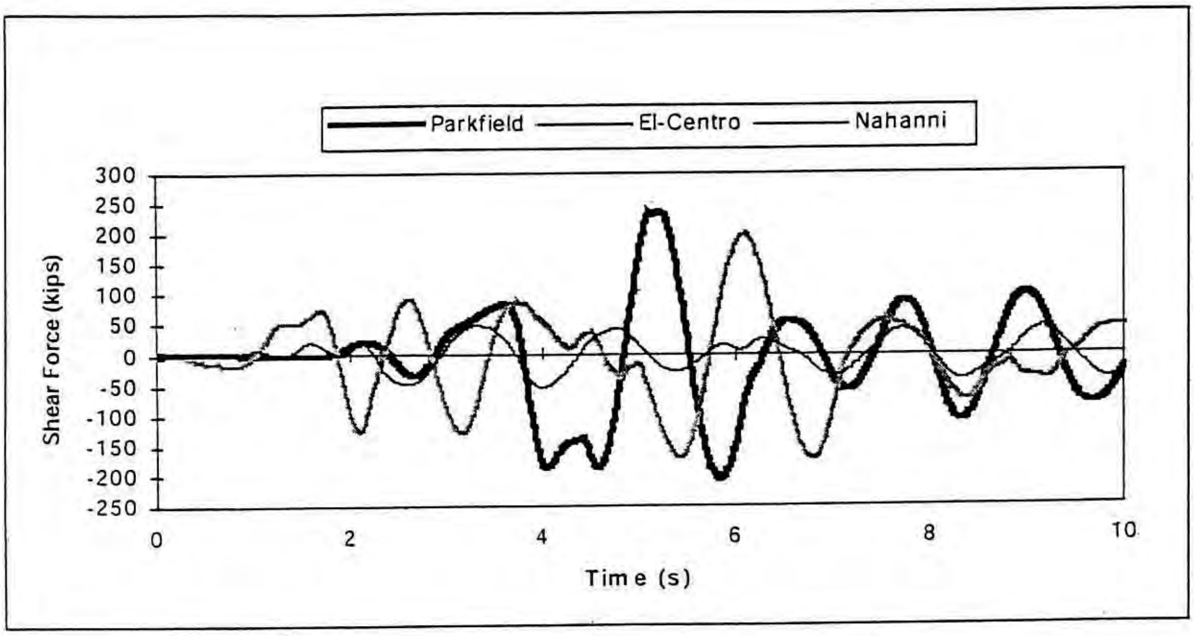

Figure 4-3 Shear force time histories of Pier#1 columns (2 columns) of Bridge-1 for thre earthquake records with PGA of 0.18g . (2-D model, μ =0.6 at bearings G-soil=4.0 ksi)

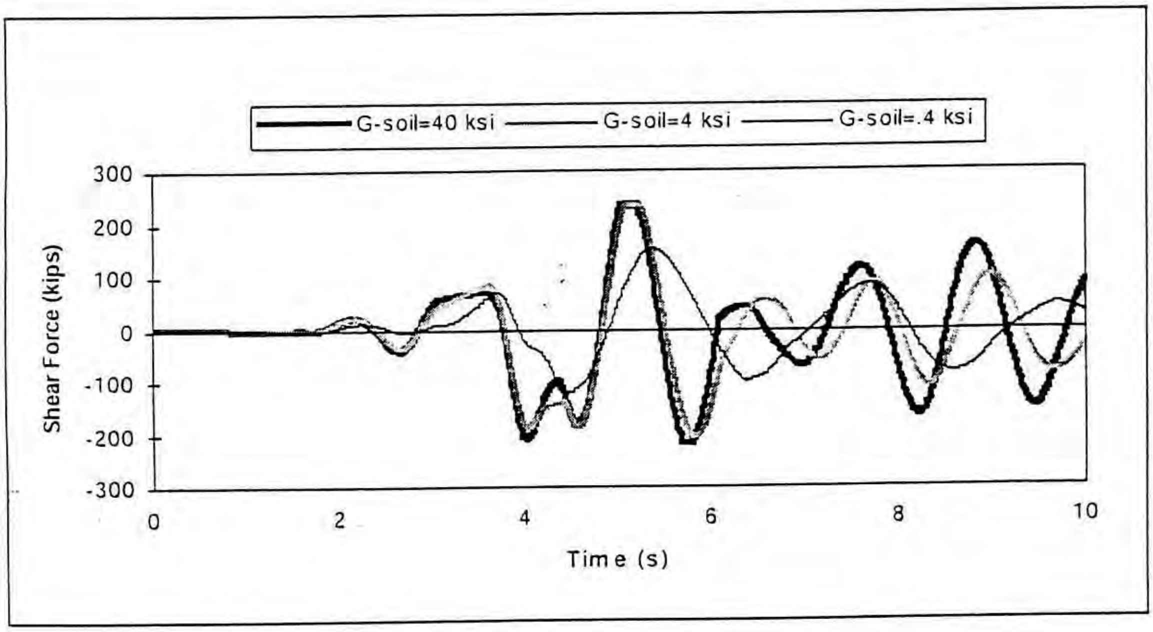

Figure 4-4 Shear force time histories for Bridge-1 pier#1. Different soil shear modulus under Parkfield earthquake. (2-D model, μ =0.6 at bearings PGA=0.18g)

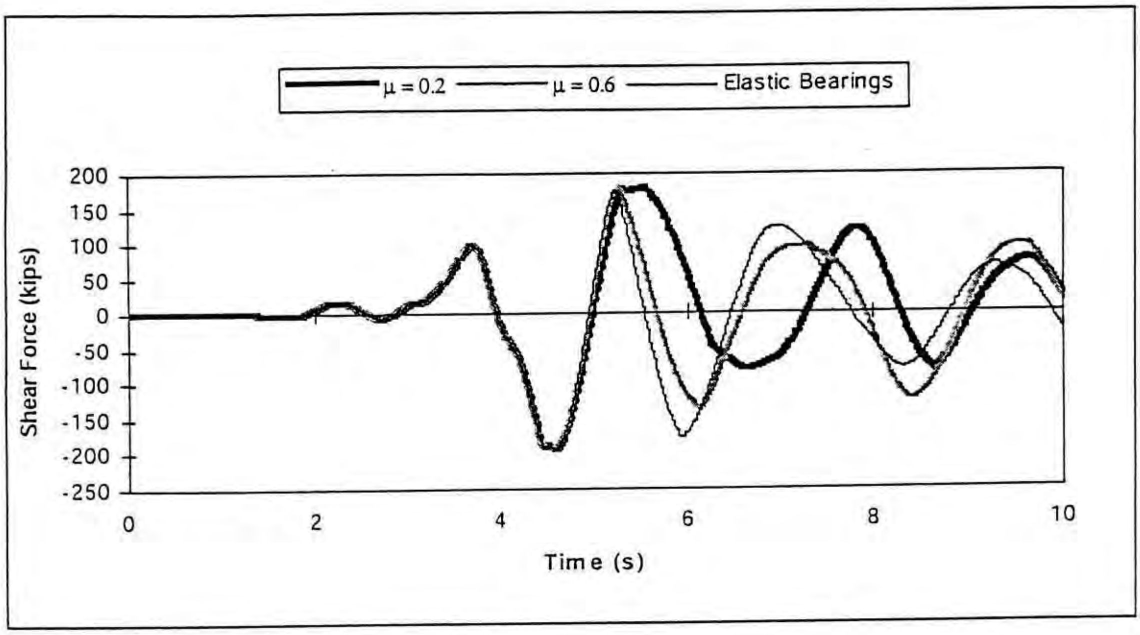

Figure 4-5 Shear force time histories for Bridge-1 pier#2.
Different bearing frictional coefficients under Parkfield earthquake.
(2-D model, μ =0.6 at bearings PGA=0.18g)

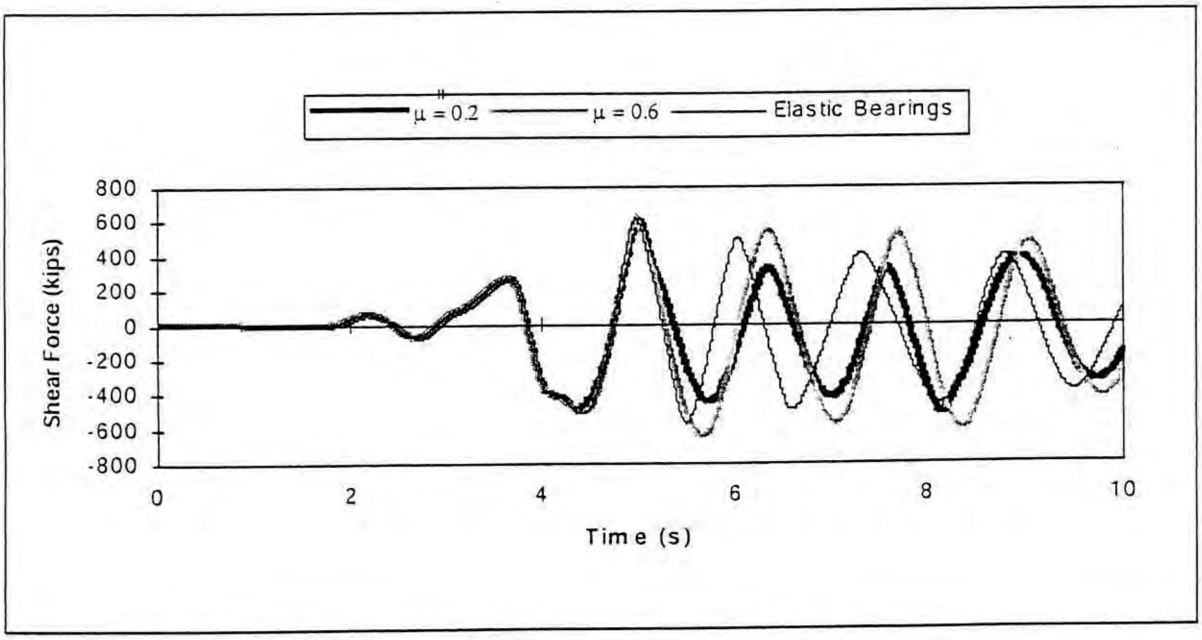

Figure 4-6 Shear force time histories for Bridge-2 Pier.
Different bearing frictional coefficients under Parkfield earthquake
(2-D model, G-soil=0.4 ksi, PGA=0.18g)

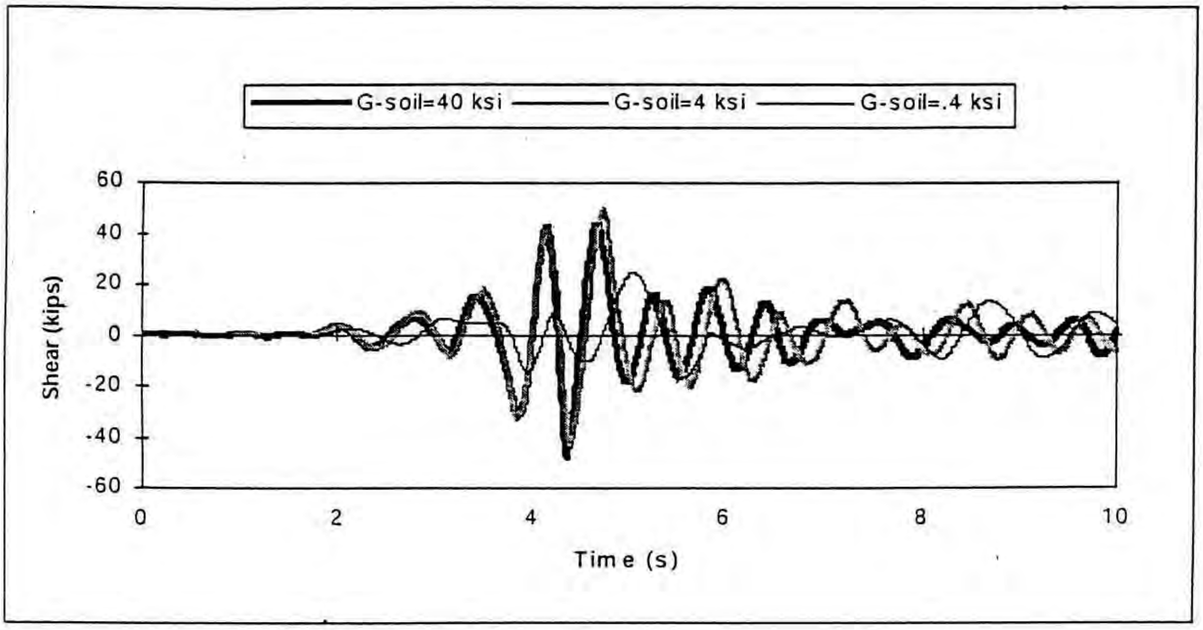

Figure 4-7 Shear force time histories for Bridge-3, pier#1column type-1. Different soil shear moduli under Parkfield earthquake. (2-D model, μ =0.6 at bearings PGA=0.18g)

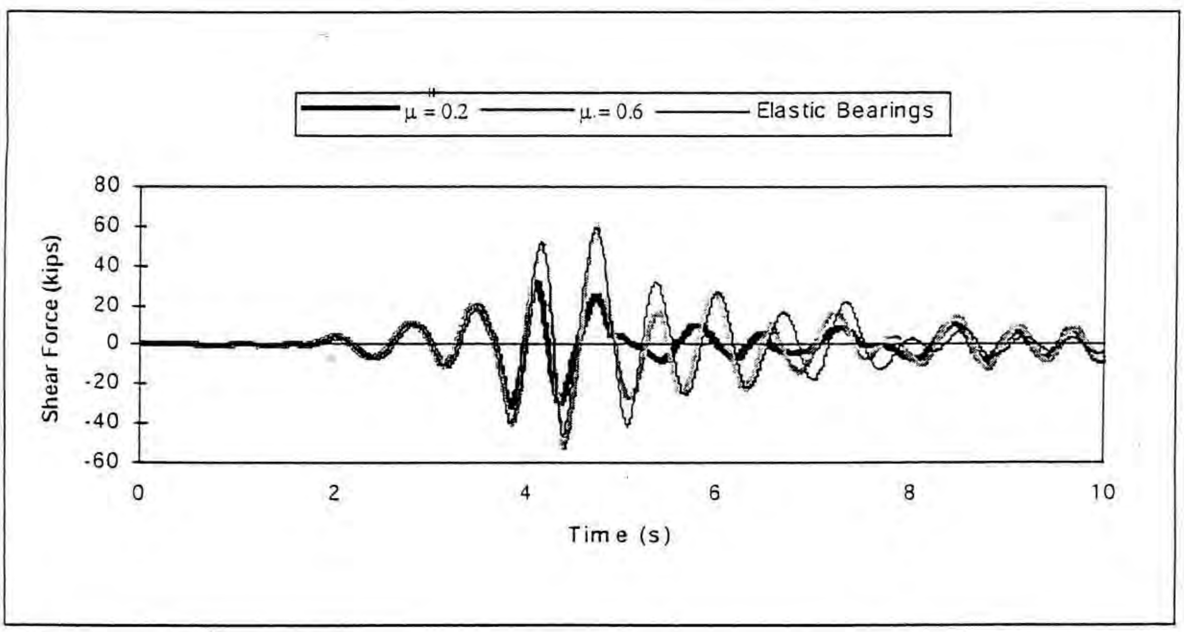

Figure 4-8 Shear force time histories for Bridge-3 ,pier#1column type-3. Different bearing frictional coefficients under Parkfield earthquake. (2-D model, G-soil=0.4 ksi , PGA=0.18g)

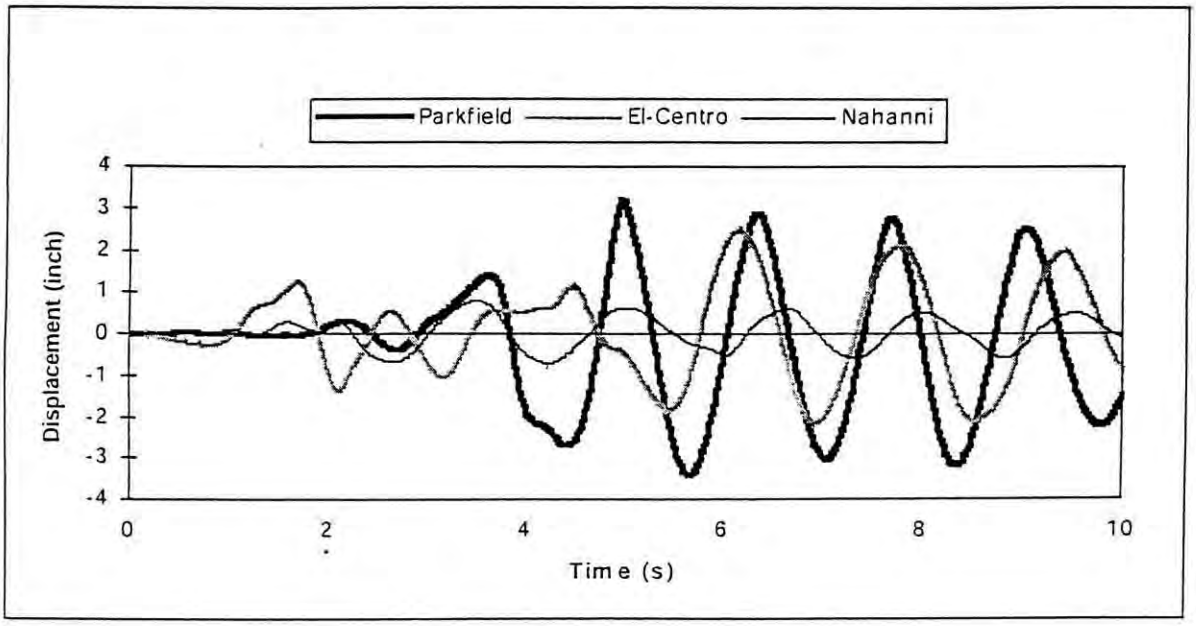

Figure 4-9 Bridge-2 pier top displacement time histories for three earthquake records with PGA of 0.18g. (2-D model , μ =0.6 at bearings G-soil=4.0 ksi)

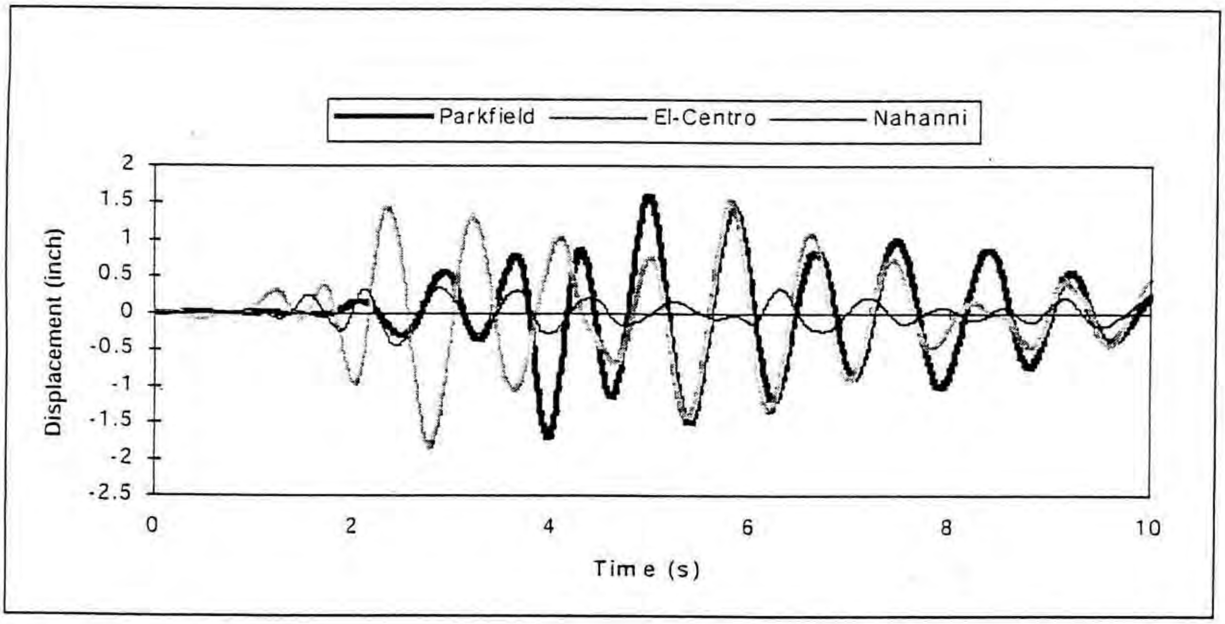

Figure 4-10 Top displacement time histories of Brudge-3 pier-3 for three earthquake records with PGA of 0.18g. (2-D model, μ =0.6 at bearings ,G-soil=4.0 ksi)

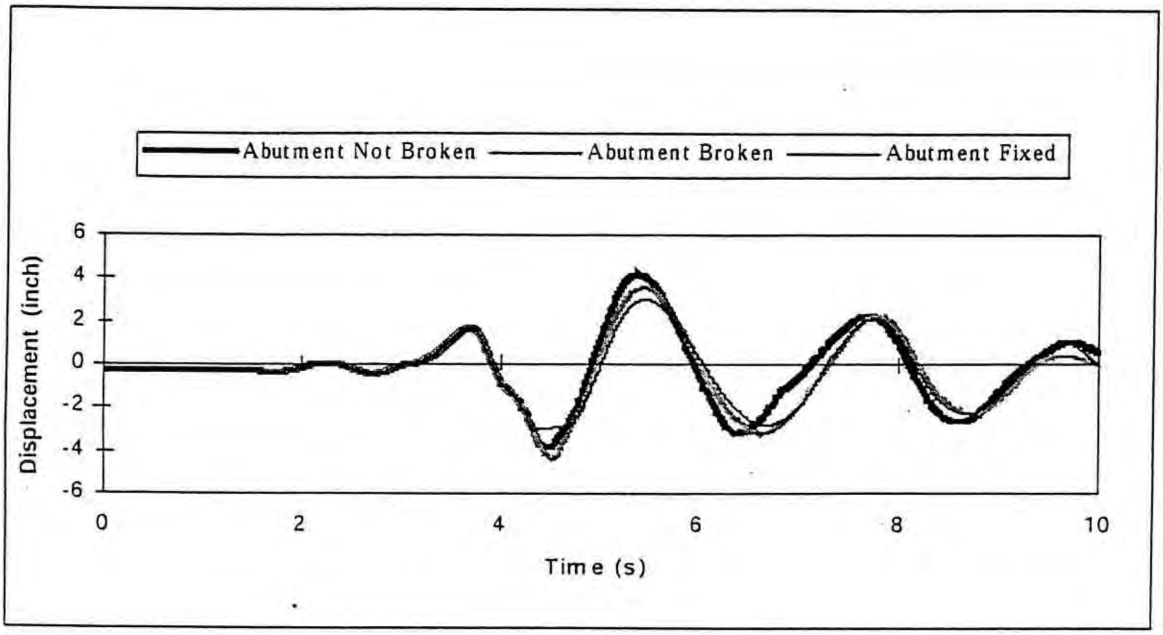

Figure 4-11 Top displacement time histories for Bridge-1 pier#1. Different abutment model under Parkfield earthquake. (2-D model, μ =0.6 at bearings ,PGA=0.18g)

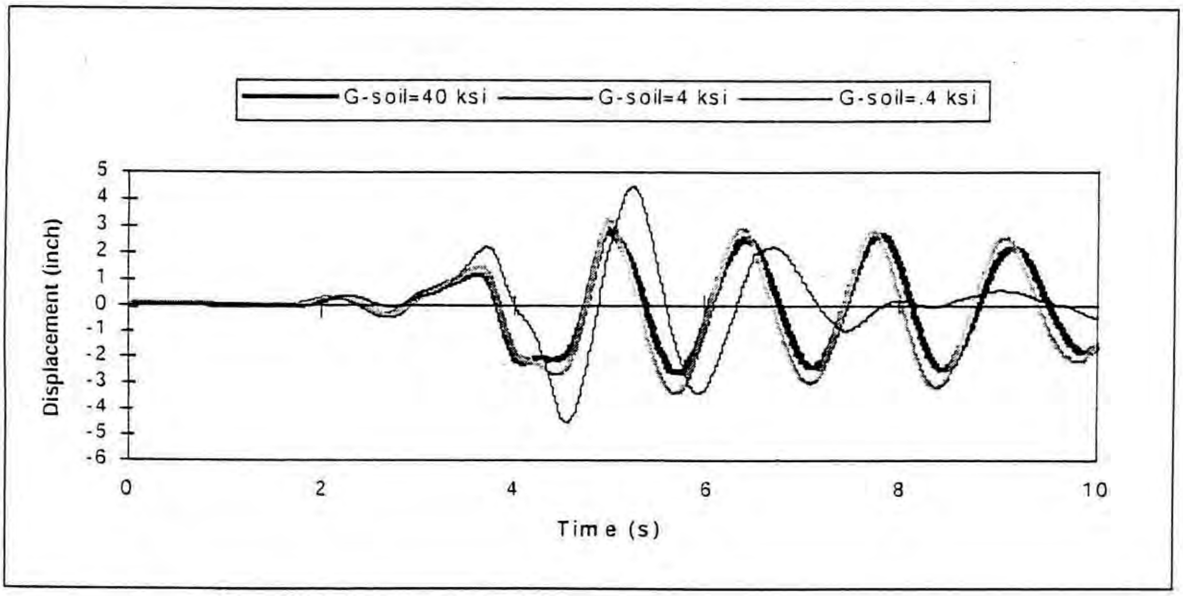

Figure 4-12 Top displacement time histories for Bridge-2 pier#1. Different soil shear modulus under Parkfield earthquake. (2-D model, μ =0.6 at bearings ,PGA=0.18g)

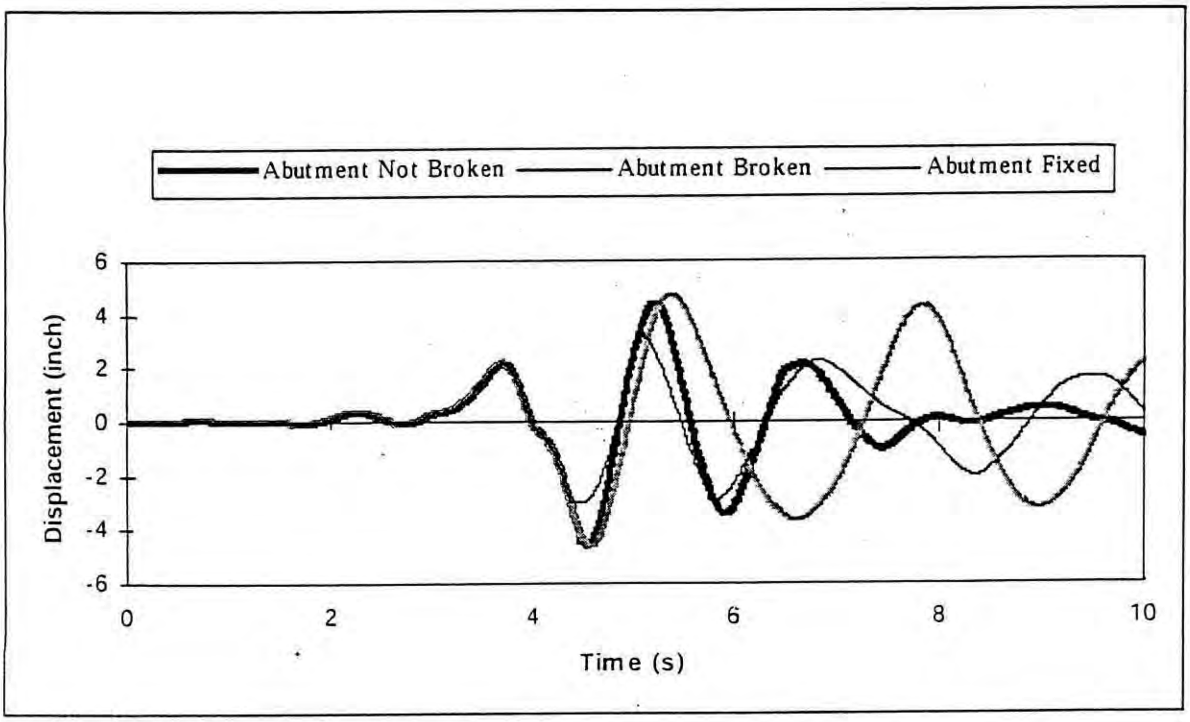

Figure 4-13 Top displacement time histories for Bridge-2 pier. Different abutment models under Parkfield earthquake. (2-D model, μ =0.6 at bearings ,PGA=0.18g)

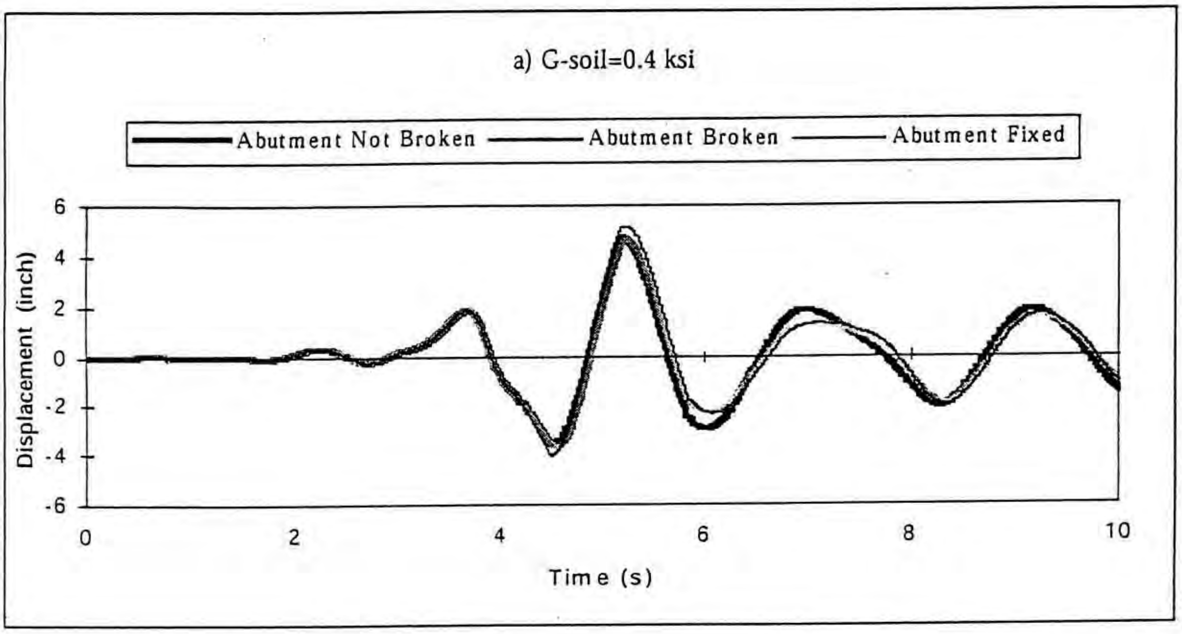

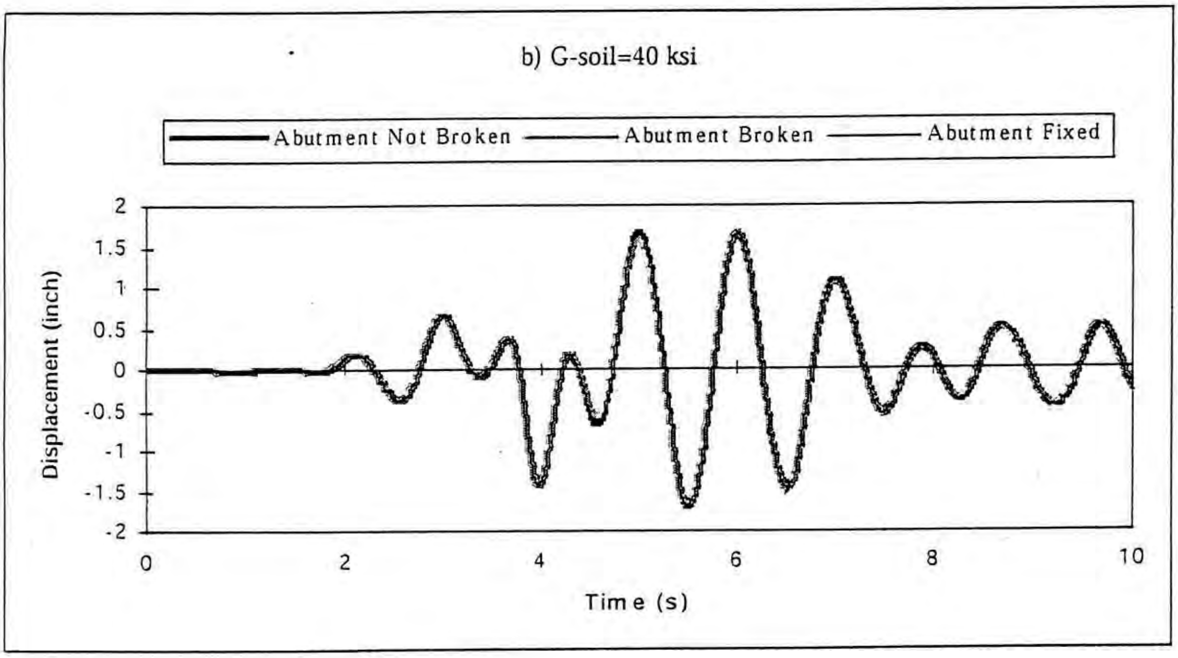

Figure 4-14 Top displacement time histories for Bridge-3 pier#2. Different SSI models under Parkfield earthquake. (2-D model, μ =0.6 at bearings, PGA=0.18g)

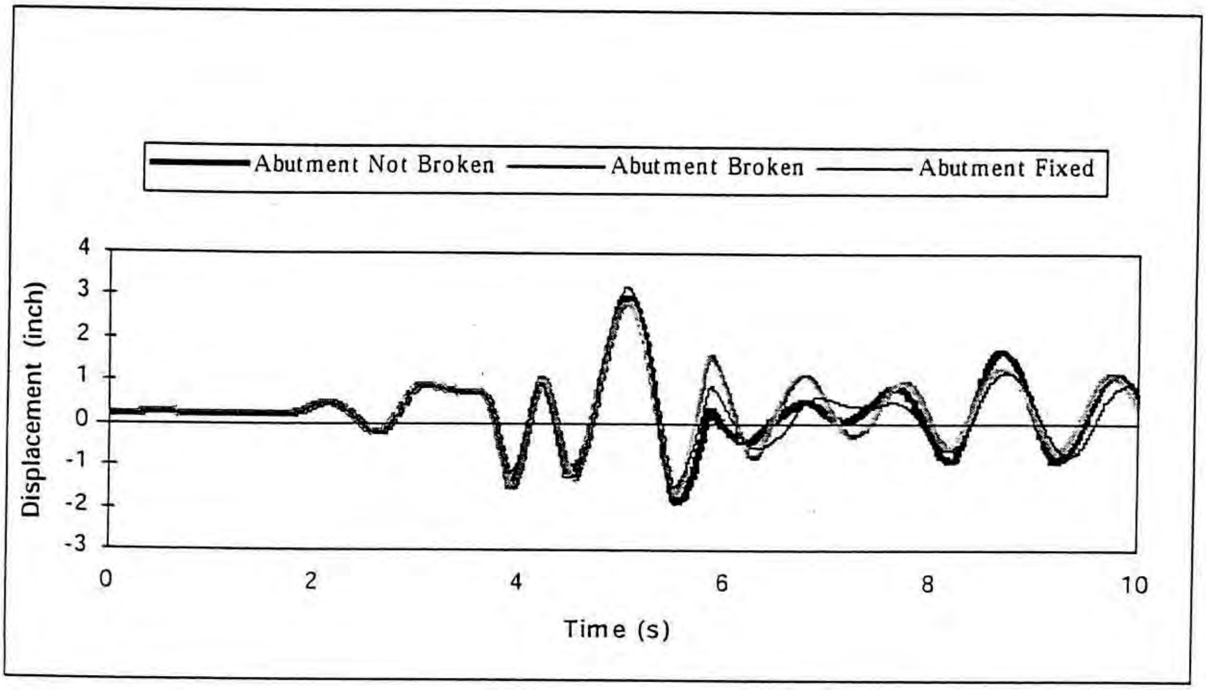

Figure 4-15 Top displacement time histories for Bridge-3 pier#2. Different abutment models under Parkfield earthquake. (2-D model, μ =0.6 at bearings, PGA=0.18g)

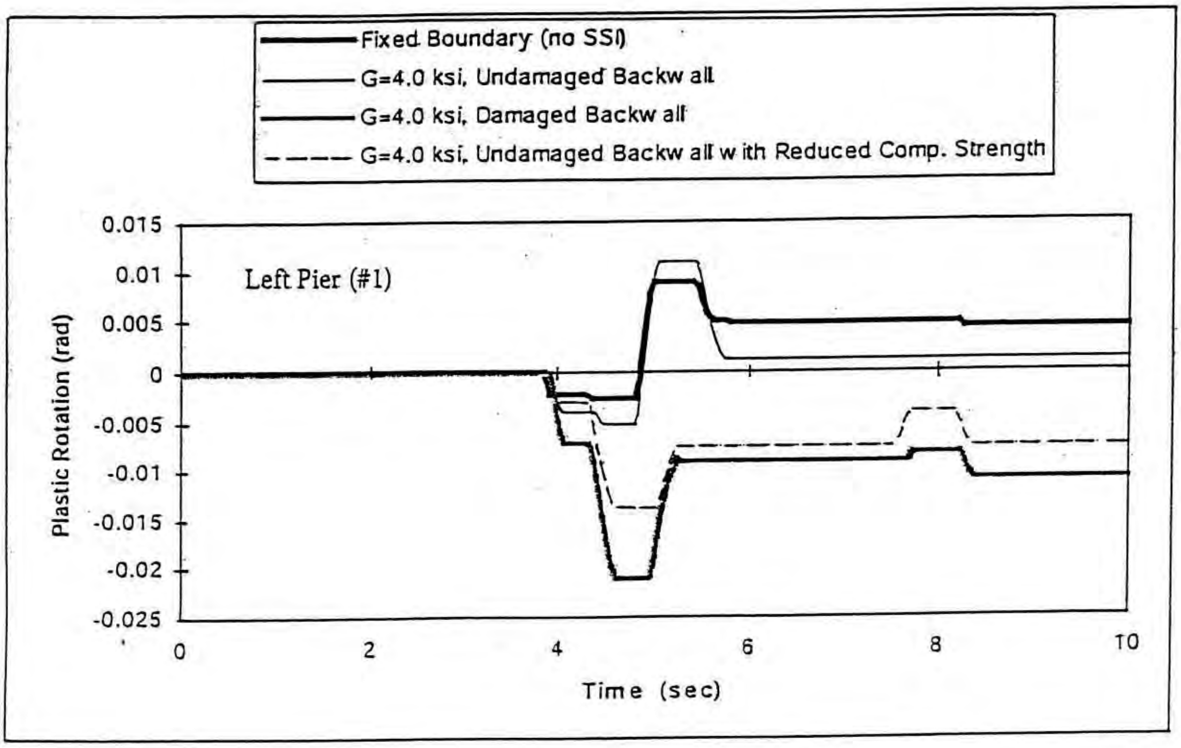

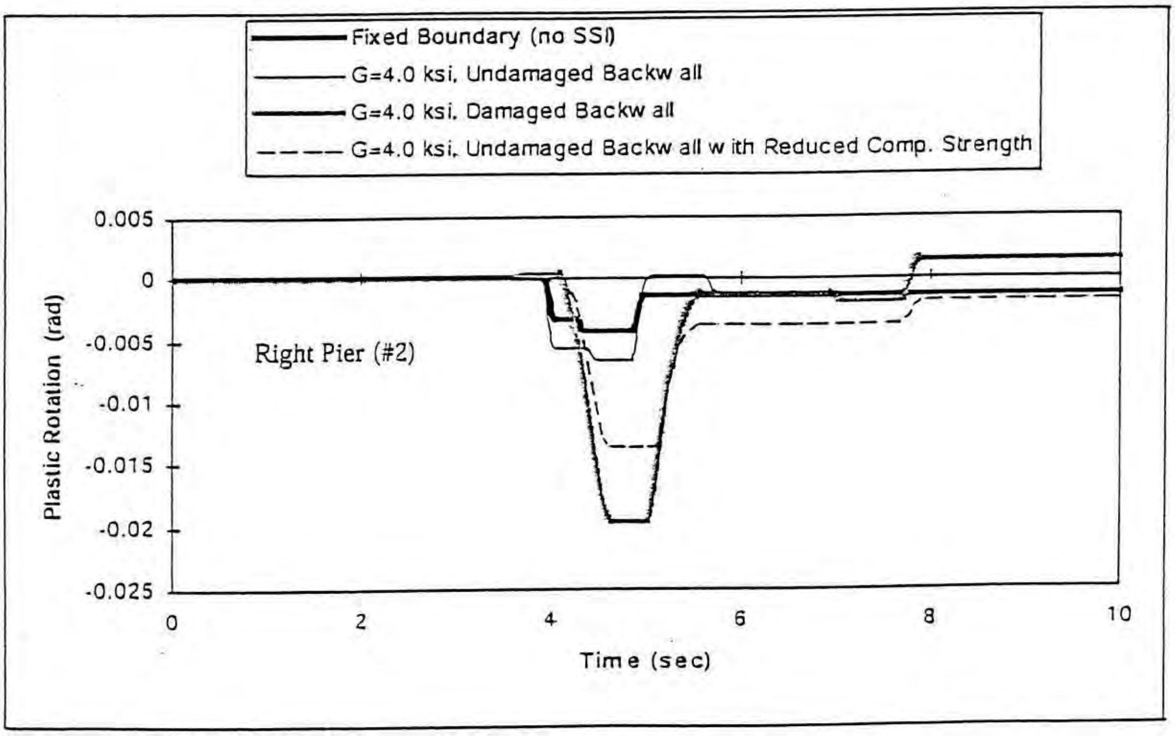

Figure 4-16 Time histories of plastic rotation at the base pier columns in Bridge-1. Bridge abutment for various SSI models Parkfield record scaled to 0.4g PGA. (2-D model,elastic bearings)

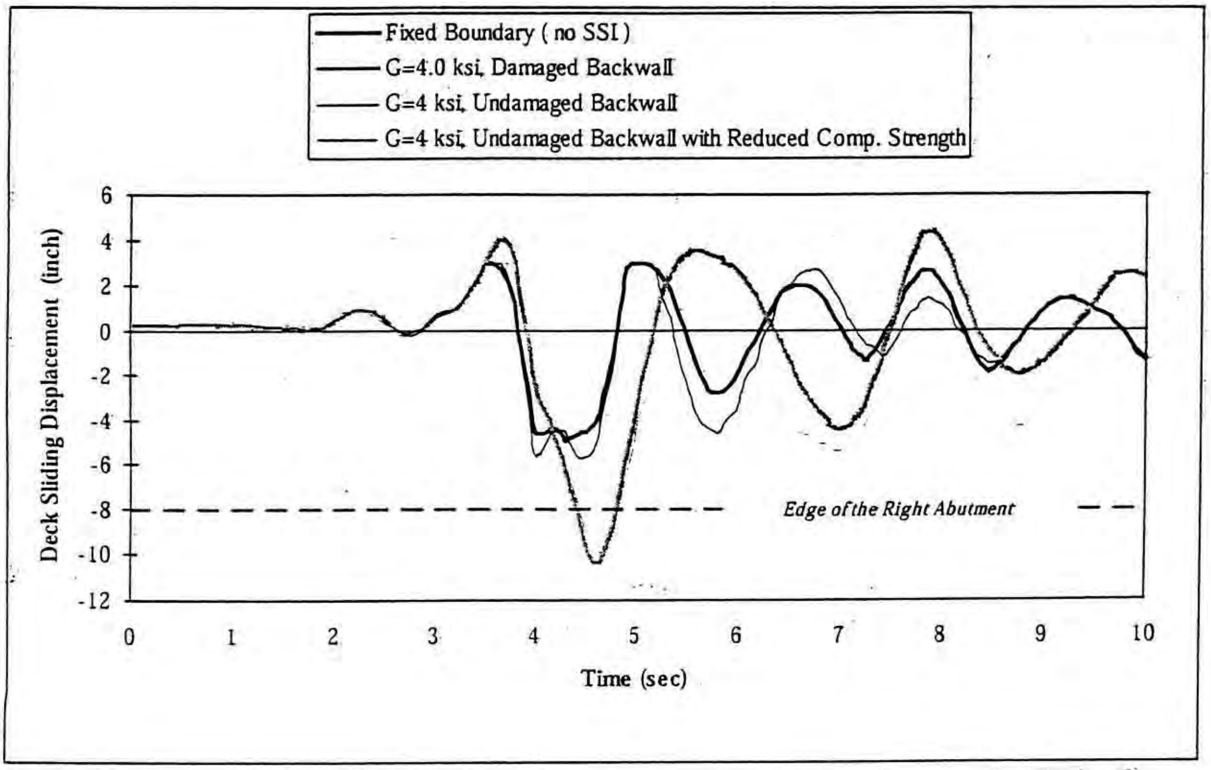

Figure 4-17 Time histories of deck sliding at Bridge-1 abutment#2 for various SSI models under Parkfield record scaled to 0.4g PGA. (2-D model, elastic bearings)

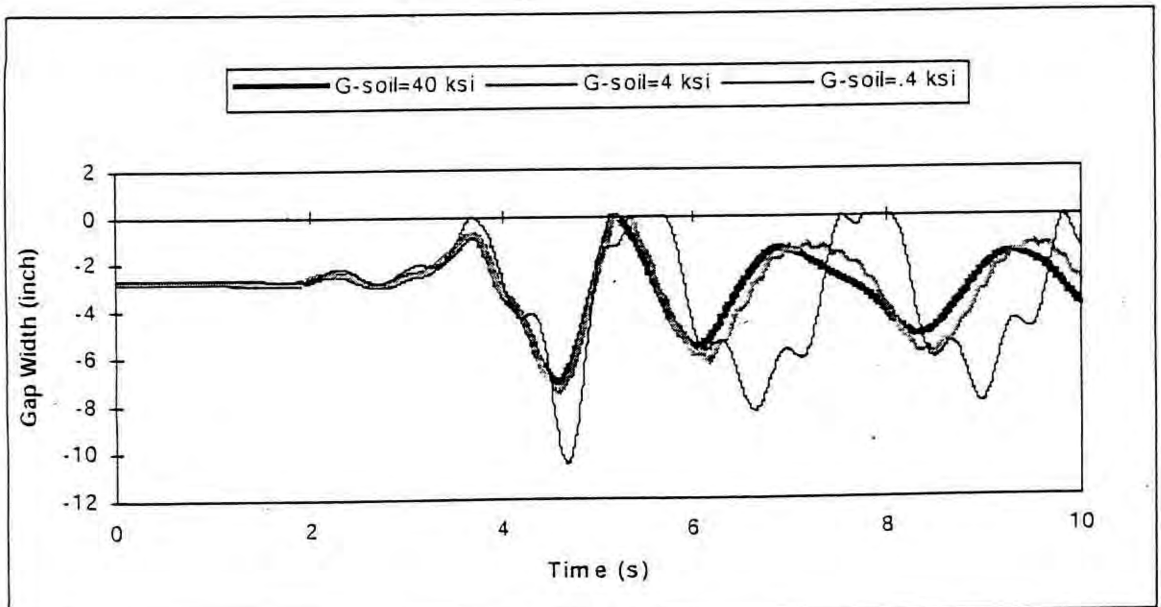

Figure 4-18 Gap width time histories for Bridge-1 abutment#2. Different soil shear modulus under Parkfield earthquake. (2-D model, μ =0.6 at bearings PGA=0.18g)

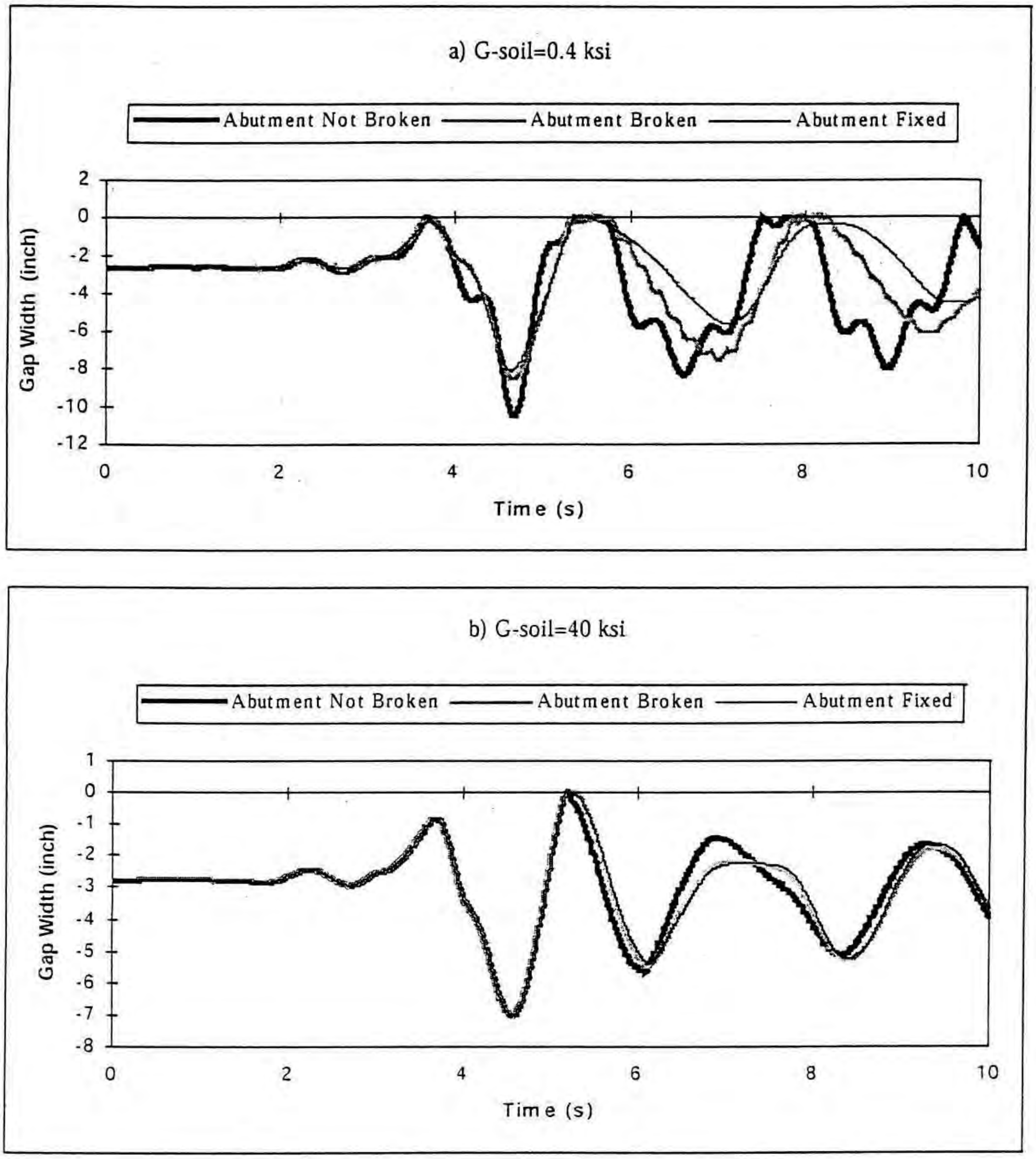

Figure 4-19 Gap width time histories for Bridge-1 abutment#2. Different SSI model under Parkfield earthquake (2-D model, μ =0.6 at bearings PGA=0.18g)

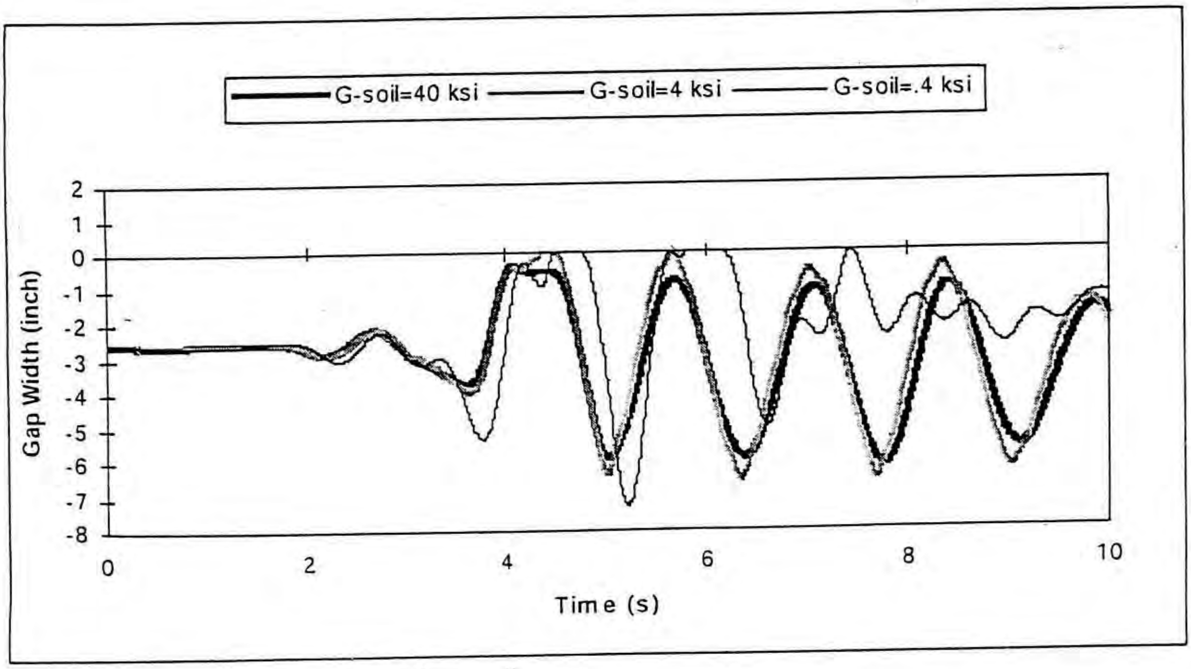

Figure 4-20 Gap width time histories for Bridge-2 abutment#1. Different soil shear modulus under Parkfield earthquake. (2-D model, μ =0.6 at bearings PGA=0.18g)

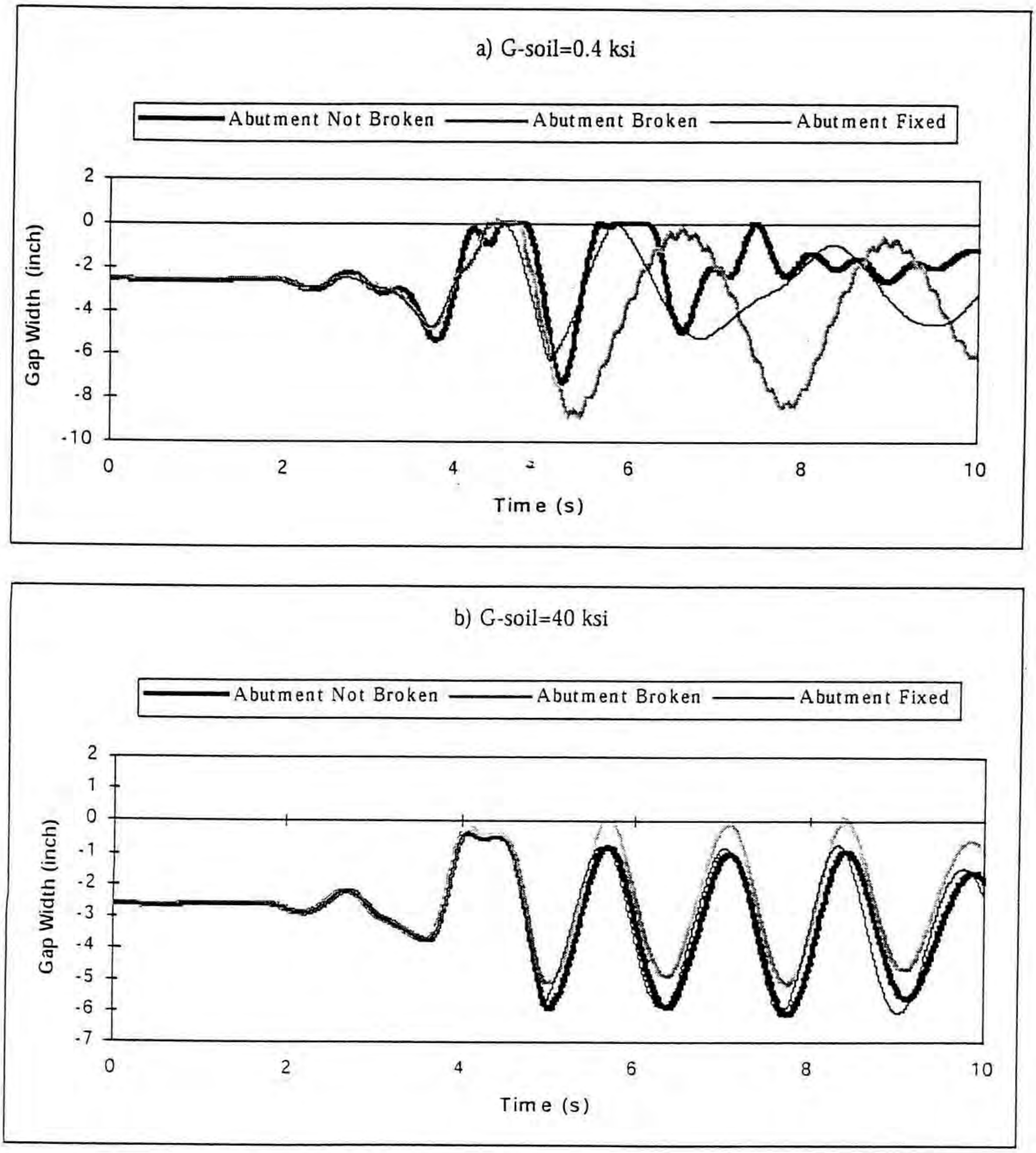

Figure 4-21 Gap width time histories for Bridge-2 ,abutment#2. Different SSI model under Parkfield earthquake. (2-D model, μ =0.6 at bearings PGA=0.18g)

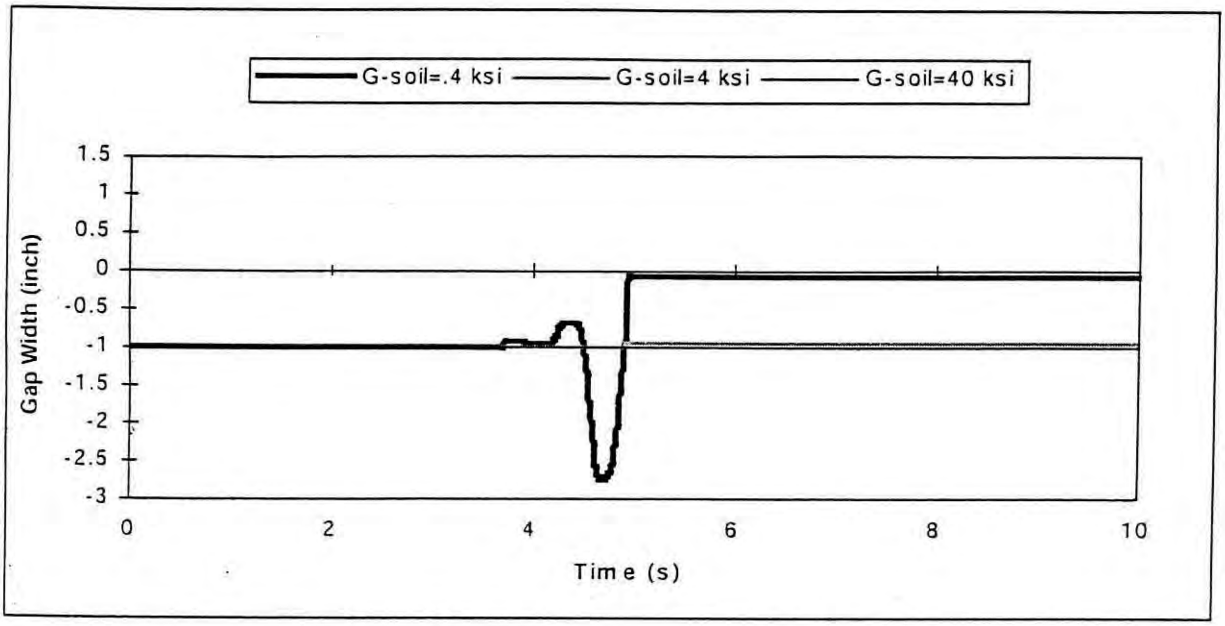

Figure 4-22 Gap width time histories for Bridge-3 ,abutment#2. Different soil shear moduli under Parkfield earthquake. (2-D model, μ =0.6 at bearings PGA=0.18g)

CHAPTER 5

RESULTS OF 3-D ANALYSIS AND COMPARISON BETWEEN 2 AND 3 DIMENSIONAL ANALYSIS

5.1) GENERAL

In this chapter, the results of nonlinear 3-D time history analyses are presented first. These analyses are performed under two sets of earthquake records (Parkfield and El-Centro) with PGAs of 0.18g and 0.4g. Later in this Chapter, the results of 3-D analyses are compared to those for 2-D models and AASHTO specifications.

5.2) RESULTS OF 3-D NONLINEAR TIME HISTORY ANALYSIS

Three-dimensional modeling makes it possible to model the skewness of the bridges. This will significantly affect the bridge dynamic behavior, including reduction in vibrating periods and coupling of mode shapes in three major directions (i.e., longitudinal, transverse and vertical). As a result of the skewness, pier columns show axial load variations under longitudinal earthquake excitation, which in turn affects the nonlinear behavior of the columns at plastic hinge locations.

Generally, detailed distribution of seismic forces among various components of the abutment is complex and will require 3-D finite element analysis, which is beyond the scope of the study. Impact forces are resisted by the approach slab, the backfill soil, and friction at the base of the abutment footings. Therefore, actual value of shear at the juncture of the backwall and breast wall, which determines backwall failure, can not be determined based on the frame models used. However, it is clear that the higher the level of impact forces the higher the shear demand at this critical section.

In the 2-D analyses impact forces reached as high as 20 times the back wall shear capacity (under low intensity earthquakes of 0.18g PGA). This necessitated the need to model backwall failure in the 2-D analyses, and as it was shown in the previous chapter the case of failed backwall resulted in the most critical performance in terms of low C/D ratios. An advantage of 3-D model is a better representation of impact between bridge components. The reason is that in 3-D models impact forces are distributed over the width of decks and are considerably less than those obtained from 2-D models. In a distributed model the impact is less sudden (i.e., rather than one intense impulse there are several impulses of lower intensity). Furthermore, for the 3-D models even under higher input PGAs the damaged abutment did not show a significant effect on the bridge responses. That is, unlike the 2-D case, bridge response did not increase for damaged abutments. This can be seen in Table 5-1, which shows selected responses of Bridge-1 and Bridge-3 for two abutment-modeling conditions under Parkfield earthquake scaled to PGA of 0.4g. As is seen, the damaged abutment condition does not have a significant effect on increasing the bridge responses and even in some cases shows a decreasing effect (e.g., plastic rotation demands of the Bridge-1 pier columns). The reason for this is coupling between the responses in the transverse and longitudinal directions. Therefore, in the 3-D study only a few cases of damaged abutment condition were considered, and for most cases the abutment is assumed intact.

5.2.1) 3-D Response of Bridge-1

Skewness and low lateral concrete confinement of the pier columns are among the special characteristics of this bridge.

Under PGA of 0.18g, Bridge-1 has C/D ratios larger than 1.0 for most cases. The only condition that leads to pier column failure is a model with elastic bearings (i.e., no failure at bearings). In an actual situation, it is very likely that the fixed bearings will fail under impact forces, even at a PGA as low as 0.18g. This is because of the low shear capacity of the connecting bolts. Consequently, the post-failure behavior of the bearings will be defined by Coulomb-friction between the decks and their supports. This will cause dissipation of energy through friction/damping. Figure 5-1 shows the time histories of the resultant shear force demand in pier columns of Bridge-1 considering both elastic bearings and μ =0.6 at the bearings. It can be seen that the maximum shear force demand for pier columns is higher in the case of elastic bearings than the cases of failed bearing (μ= 0.6 and 0.2). This can also be observed in Table 5-2, which shows the minimum C/D ratios for Bridge-1 under earthquakes scaled to PGA of 0.18g. As it is seen, pier column force and plastic rotation demands decrease significantly by for failed bearings.

To investigate the effect of higher ground motion acceleration, cases of 0.4g PGA were also considered. The summary of the minimum C/D ratios for this value of PGA is shown in Table 5-3, where it is seen that the columns' shear demands greatly exceed the shear capacities).

5.2.2) 3-D Response of Bridge-3

Because this bridge has well-confined concrete pier columns and relatively large number of columns at each pier bent, good seismic performance is expected for low intensity earthquakes. Therefore, this bridge was first analyzed under PGA of 0.4g, and then for critical cases analyses were performed for the lower PGA of 0.18g.

Table 5-4 shows the minimum C/D ratios for Bridge-3 components under earthquakes scaled to PGA of 0.4g. Also, Table 5-5 shows the C/D ratios under 0.18g earthquakes for critical cases.

5-3) COMPARISON BETWEEN 3-D AND 2-D MODELS

As it was mentioned before, 3-D modeling has the additional capabilities of modeling skewness, distribution of impact forces within the deck width, and exact mean of combining longitudinal and transverse earthquake forces in bridge components.

Following are the description of these features:

1) In any skewed bridge, skewness significantly affects the dynamic characteristics and nonlinear responses of the bridges. Mode shapes in three major directions are coupled, in other word the bridge longitudinal and transverse responses are not separable. Table 5-6 shows periods of the Bridge-1 for 2-D (longitudinal) and 3-D models for G-soil=4 ksi. As is seen as a result of coupled mode shapes shorter periods were obtained for 3-D models. Also as a result of the skewness, axial loads at pier columns show significant variation. This is shown in Figure 5-2 and is seen that this variation was not captured in 2-D models.

2) The level of impact force in 3-D models is considerably less than the impact level for 2-D models. Impact force is the reason for the backwall failure at the abutment. Table 5-7 presents the impact forces on the Bridge-1 abutments for one of the modeling cases. As is seen, the total impact force at abutment # 2 in 3-D model is reduced to the one-third of the 2-D model.

3) There is more abutment interaction with the superstructure response in 3-D models. This is because in the transverse direction the roller bearing are also fixed, causing the abutments to be an integrated part of the bridge even when the gaps are open. For skewed bridges the 3-D response is further coupled in longitudinal and transverse directions.

4) Based on 3-D analyses for skewed bridges the effect of backwall failure is not as significant as it is for the 2-D case. This is due to the coupling mentioned above. In the Tables 5-1, and 5-8, where the effects of backwall failure for 3-D and 2-D cases are shown, respectively. As seen, in Table 5-8 for the 2-D model there is an increase, as high as 100%, for plastic rotation demands for damaged backwall case, while in the 3-D model (Table 5-1) plastic rotation demands have even decreased for the case of damaged backwall.

5) The pier column flexural deformation in the plane of the pier bent is double curvature, therefore, higher plastic shear force is associated with the pier bent plastic hinge sway mechanism (i.e., Vp=2*Mp/h rather than Mp/h for single curvature bending). In columns with low lateral reinforcements (e.g., Bridge-1) the shear failure would be a potential hazard if curvature ductility demand exceeds 4. At this level of curvature demand there is a substantial decrease in concrete shear capacity . Table 5-9 demonstrates a comparison between shear capacities and demands, which were obtained from 3-D and 2-D (longitudinal) models. It should be noted that in current AASHTO codes effect of curvature ductility demand on shear capacity is not recognized.

5-4) COMPARISON OF THE 3-D ANALYSIS RESULTS AND AASHTO'S SINGLE MODE METHOD

For comparison purposes it is instructive to evaluate the response of bridges assuming that there won't be closure of any gap. This assumption is needed so that the response under uniformly distributed load, per Single-Mode Spectral Method, is independent of the intensity of the load. Employing a model of Bridge-1 with G-soil=4 ksi, the seismic forces using this method are determined for both longitudinal and transverse directions. The calculated periods and base shear coefficients are shown in Table 5-10. Periods in both directions obtained based on this method are in good agreement with those from 3-D computer model. The equivalent static seismic forces determined based on the Single-Mode-Spectral method are then applied to the 3-D model of the Bridge-1 based on the distribution specified for this method in AASHTO. The resultant force for each pier is a combination of longitudinal and transverse forces as described in the codes (100% + 30% of maximum responses in two perpendicular directions). Figure 5-3 shows the Bridge-1 pier shear demand based on this combination rule along with the results of time history analyses. Based on AASHTO to obtain the design forces the elastic forces are divided by the member response modification factor (R). This is a simplified and approximate way for considering the nonlinear response of the bridge. Based on

AASHTO-LRFD specifications AASHTO (1994) the modification factor for multi-column bents varies from 1.5 to 5 depending on the bridge importance category. Referring to Figure 5-3, where to simplify comparison R is assumed equal to unity, it is apparent that the AASHTO design force for the left pier would be much smaller than the demand obtained by 3-D analysis. With R equal to one, the two are comparable, thus, the design force when R is applied would be smaller by this factor. One reason for this is that dominant modes of response have periods between 0.3 to 0.8 seconds where the AASHTO response spectrum (RS) yields lower forces than the earthquake records used in the 3-D analyses. Another reason is incompatibility in application of an elastic spectrum (along with R factor to account for nonlinear action) to a nonlinear stiffening system. That is, current design guidelines use elastic spectrum and account for nonlinear behavior through response modification factor R, which are based on studies of nonlinear SDOF systems with elastic-plastic load-deformation characteristic.

The response of bridges is initially stiffening due to closure of gaps. Another important point to consider is that in design of new bridges due to application of response modification factor, the seismic displacement demand would be larger. This in turn will cause more abutment interaction in the bridge responses.

The pushover analysis is a graphically useful method in calculating the demands for bridge elements. Figure 5-4 shows the pushover analyses of Bridge-1 in longitudinal and transverse directions. By comparing the AASHTO RS (0.18g) with the pushover curves displacement and force demands for the entire bridge can be determined. The total displacement demands in longitudinal and transverse directions for PGA of 0.18g, as seen in Figure 5.4, are about 4.9" and 2.2", respectively. These displacements are in the range of those obtained from 3-D analyses (e.g., 3.2" and 2.8" under El Centro earthquake and elastic bearings). But for higher PGA of 0.4g this agreement of the results does not hold. As seen in Figure 5-4 displacement demands in longitudinal and transverse directions are about 10" and 6", respectively. These displacements are not in the range of the computed displacements by 3-D analyses (e.g., for Parkfield earthquake and elastic bearings these displacements are 5.8 and 3.4, respectively, which are about half of those obtained by pushover analysis). This shows that the obtained results from pushover analyses are not always in good agreement with the results obtained by nonlinear time history analyses. The difference becomes more when there is more nonlinearity involved in the bridge responses as a result of stronger earthquakes.

5-5) SUMMARY

Based on a comprehensive 3-D analysis on two multi-span simply supported bridges (Bridge-1 and Bridge-3) the following conclusions can be made with regard to their 3-D seismic response:

1) Under PGA of 0.18g, except in the case of elastic bearings (i.e., no failure at the bearings), no damage is observed for Bridge-1 by C/D ratio less than one. Bolts connecting steel bearings to the girder or concrete seat are expected to fail even under low intensity earthquakes due to low shear capacity. This failure acts like a fuse and will reduce the demands on the rest of the bridge. In Bridge-1 the most critical C/D ratio belongs to the pier column shear and the deck sliding.

2) Bridge-1 pier columns under PGA of 0.4g have shown shear failure with C/D ratio as low as 0.2. This was mostly due to low lateral reinforcements in the pier columns.

3) Bridge-3 has shown high C/D ratios for earthquakes scaled to 0.18g PGA, and no damage was observed even when the bearings are assumed to remain elastic. In reality it is except at that the bearings will fail due to low shear capacity at the connecting bolts. The main reasons for better performance of this bridge are that the concrete columns are well confined and that several columns are each pier bent.

4) Despite better confinement, Bridge-3 in moderate soil (G = 4ksi) will also sustain failure under 0.4g PGA due to shear failure in the columns.

5) Very stiff soils enhance the restraining action of the abutments in limiting bridge displacements, which may lead to no impact between decks. On the other end, very soft soils have less rotational restraining at the base of pier columns causing low curvature ductility demand and less damage. The most critical cases generally occur for models with moderately stiff soils. Note that this is the case only when there is high input acceleration (e.g., 0.4g PGA). For lower PGA, since abutment interaction is minimal, stiffer soil causes higher demand at pier columns.

6) Geometric and response characteristics, such as skewness and distributed impact, have a significant effect on dynamic response and can only be represented by employing a 3-D model. Therefore, for seismic evaluation of MSSS (Multiple Span Simple Supported) bridges even under low PGA the use of 3-D models are more appropriate.

7) The response spectrum used in AASHTO specifications may result in unconservative demands for bridge elements. Among the reasons for this, following can be mentioned:

a) Contribution of periods between 0.3 to 0.8 seconds, where the AASHTO response spectrum (RS) yields the lower forces than the employed earthquake records.

b) Stiffening dynamic behavior of the bridge due to gap closure has different characteristics that are not considered in development of AASHTO response spectrum. Therefore, use of nonlinear time history analysis should be considered for critical bridges.

8) Pushover analysis is an efficient tool for estimating displacement demands but the obtained results are not always in good agreement with those obtained from nonlinear dynamic analyses. This lack of agreement becomes more significant especially for strong earthquake motions where the response becomes more nonlinear.

The beneficial effect of bearing failure must be emphasized. As the time history results show, the most critical situation arises when the bearings are assumed to remain elastic (e.g., consider Table 5-2). Obviously, this beneficial effect of bearing failure is due to consequent energy dissipation through friction at the bearings. The advantage and critical importance of this mechanism of behavior (i.e. bearings acting like a fuse) warrants experimental investigation to validate. It is important to ensure that the pull out of bearing seat on the abutments and cap beams are prevented. That is, bearing failure must occur rather than concrete seat failure.

Table 5-1 **Selected responses of the 3-D bridge models under Parkfield earthquake (alt-1) for two different abutment-modeling conditions (G-soil = 4 ksi and elastic bearings)**

Bridge Name	PGA	Location	Displacement (inch)		Plastic Rotation (rad)	
			Whole Abut.	Damaged	Whole Abut.	Damaged
Bridge-1	0.18g	Pier # 1	X 3.07 Y 1.25	X 2.50 Y 1.78	0.012	0.001
		Pier # 2	X 4.34 Y 1.22	X 4.34 Y 2.06	0.004	0.002
	0.40g	Pier # 1	X 4.10 Y 3.25	X 5.17 Y 3.10	0.017	0.013
		Pier # 2	X 5.60 Y 2.60	X 6.30 Y 3.07	0.013	0.009
Bridge-3	0.40g	Pier # 1	X 1.07 Y 0.69	X 1.17 Y 0.73	- 0	0.010
		Pier # 2	X 4.98 Y 2.30	X 3.94 Y 2.54	0.021	0.022
		Pier # 3	X 2.05 Y 1.35	X 2.07 Y 1.57	0.018	0.014

Notes:

1) Displacements are for the middle of the pier bents

2) Plastic rotations are at the pier column ends.

Table 5-2 The minimum C/D ratios for Bridge-1 under PGA of 0.18g (3-D Model)

G-Soil	C/D ratios for		
	Pier col. Shear (y-y, z-z)	**Plastic Rot. (y-y, z-z)**	**Deck Sliding (longitudinal)**
0.4	(0.8,1.3) EL–2, μ = NY Above ratios change to (2.0,3.3) for μ = 0.6	(1.3, 1.3) EL –2, μ=NY Almost zero demand for μ= 0.6	1.1 PF-1, μ= NY
4.0	(0.4,1.3) EL –1, μ = NY Above ratios change to (1.3,2.5) for μ = 0.6	(2.5, 1.3) PF –1, μ= NY Almost zero demand for μ= 0.6	1.6 PF-1, μ= 0.6
40.0	(0.4,1.7) EL –1, μ = NY Above ratios change to (1.3,2.5) For μ = 0.6	(1.4, 1.4) EL –2, μ = NY Almost zero demand for μ = 0.6	1.8 PF-1, μ= 0.2

Notes:

1) El and PF indicate El Centro and Parkfield earthquakes. 1 and 2 refer to alternatives one and two of earthquake component
2) μ is the frictional coefficient at failed bearings.
3) Deck sliding C/D ratios are obtained from the gap opening responses over pier columns and abutments.

Table 5-3 The minimum C/D ratios for Bridge-1 under PGA of 0.4g (3-D Model)

G-Soil (ksi)	C/D ratios for		
	Pier col. Shear (y-y,z-z)	Plastic Rot. (y-y,z-z)	Deck Sliding (longitudinal)
0.4	(0.4,1.0) EL –2, μ = NY (0.4,0.9) EL-2, μ= 0.6 (0.6,1.3) EL-2, μ = 0.2	(3.3,0.9) EL-2, μ=NY *Above ratios change to (1.7, 1.4) for μ= 0.6*	1.0 EL-2, μ= 0.2
4.0	(0.2,0.8) PF –1, μ = NY (0.3,1.1) EL-2, μ = 0.6 (0.5,0.8) EL-1, μ = 0.2	(3.3,0.9) EL-2, μ=NY *Above ratios change to (1.7, 3.3) for μ= 0.6*	1.2 EL-2, μ= 0.2
40.0	(0.3,1.3) EL –2, μ = NY (0.4,0.8) EL-1, μ= 0.6 (0.5,1.0) EL-1, μ = 0.2	(5.0,0.8) EL-1, μ=NY *Above ratios change to (5.0, 1.4) for μ= 0.6*	1.3 EL-2, μ = 0.2 & 0.6

Notes :

1) El and PF indicate El Centro and Parkfield earthquakes. 1 and 2 refer to alternatives one and two of earthquake component
2) μ is the frictional coefficient at failed bearings.
3) Deck sliding C/D ratios are obtained from the gap opening responses over pier columns and abutments.

Table 5-4 The minimum C/D ratios for Bridges –5 under PGA of 0.4g (3-D Model)

G-Soil (ksi)	C/D ratios for		
	Pier col. Shear (y-y,z-z)	**Plastic Rot. (y-y,z-z)**	**Deck Sliding (longitudinal)**
0.4	(1.7,2.0) EL –1, μ = NY (1.1,1.4) EL-1, μ= 0.6 (0.83,1.0) EL-1, μ = 0.2	(5.5) EL-2, μ = 0.2 ~(10,10) for most cases	1.3 EL- 2, μ= 0.2
4.0	(0.9,1.0) EL –1, μ = NY (1.0,1.1) EL-1, μ = 0.6 (0.9,0.9) EL-1, μ= 0.2	(5.10) EL-2, μ= NY ~(10,10) for most cases	1.6 PF-1, μ = NY
40.0	(1.4,1.7) PF –1, μ= NY (2.0,1.7) EL-1, μ = 0.6 (1.4,1.3) PF-1, μ= 0.2	(24.7,10) PF-1 , μ= 0.2 ~(10,10) for most cases	2.9 EL-1, μ = 0.2

Notes :

1) El and PF indicate El Centro and Parkfield earthquakes. 1 and 2 refer to alternatives one and two of earthquake component
2) is the frictional coefficient at failed bearings.
3) Deck sliding C/D ratios are obtained from the gap opening responses over pier columns and abutments.

Table 5-5 The C/D ratios for Bridge-3 under PGA of 0.18g for selected cases (3-D Model)

Selected case	**C/D ratios for**		
	Pier col. Shear (y-y,z-z)	Plastic Rot. (y-y,z-z)	Deck Sliding (longitudinal)
G-soil = .4 ksi EL-1, μ= 0.2	**(10,10)**	**~0.0**	**3.7**
G-soil = 4 ksi EL-1, μ = 0.2	**(2.5,2.5)**	**~0.0**	**6.7**
G-soil= 40 ksi PF-1, μ= 0.2	**(3.3,5)**	**~0.0**	**7.7**

Notes :

1) EL and PF indicate El Centro and Parkfield earthquakes. 1 and 2 refer to alternatives one and two of earthquake components sets.

2) μ refers to frictional coefficient at bearings.

3) Deck sliding C/D ratios are obtained from the gap opening responses over pier columns and abutments.

Table 5-6 Bridge-1 periods obtained by 3-D and 2-D models (G-soil = 4 Ksi)

Model	Longitudinal		Transverse
	Pier # 1	Pier # 2	
3-D	1.10	1.67	0.52
2-D (Longitudinal)	1.40	2.26	N/A

Notes :

In 3-D models the mode shapes are coupled and presented periods are for the dominate mode shapes in longitudinal and transverse directions.

Table 5-7 Comparison of the impact forces on the Bridge-1 abutment backwalls obtained from 2-D and 3-D models (Elastic bearings, G-soil = 4ksi, Parkfield record (alt-1), PGA = 0.18g)

Abutment No.	2-D	3-D Model	Backwall Shear Capacity
1	0	0+3002+597 = 3,.599	2*1675 = 3,350
2	23,299	527+5964+694 = 7,510	

Notes:

1) Since the approach slab supports the abutment back wall, two shear surfaces are considered for capacity calculations.
2) For 3-D models, the total impact force is equal to the summation of the links envelope responses.

Table 5-8 **Selected responses of the 2-D bridge models under Parkfield earthquake for two different abutment modeling conditions. (G-soil = 4 ksi, and elastic bearing)**

Bridge Name	PGA	Location	Displacement (inch)		Plastic Rotation (rad)	
			Whole Abut.	Damaged Abut.	Whole Abut.	Damaged Abut.
Bridge-1	0.18g	Pier # 1	X 3.1	X 3.1	0.0013	0.0013
		Pier # 2	X 4.2	X 4.2	0.001	0.001
	0.40g	Pier # 1	X 5.8	X 8.6	0.011	0.021
		Pier # 2	X 6.07	X 10.4	0.0067	0.0195
Bridge-3	0.40g	Pier # 1	X 2.2	X 2.1	~0	~0
		Pier # 2	X 4.3	X 4.3	0.0088	0.0088
		Pier # 3	X 4.7	X 7.0	0.0067	0.0254

Table 5-9 **Comparison of the shear C/D ratios obtained from3-D and 2-D (longitudinal) models in Bridge-1 pier columns. (G-soil =4ksi, Elastic bearings, Parkfield EQ (alt-1), PGA=0.18g)**

Model	Curvature ductility demand	Shear Demand	Shear Capacity	Shear C/D
3-D	6.5	269	133	0.5
2-D	1.5	119	315	2.7

Table 5-10 **Bridge-1 periods and base shear coefficients obtained by the AASHTO single mode method (PGA = 0.18g, S= 1.2, G-Soil =4 ksi, Open Gaps)**

	T (sec)	Cs
Long. Pier # 1	1.15	0.24
Long. Pier # 2	1.71	0.18
Transverse	0.61	.36

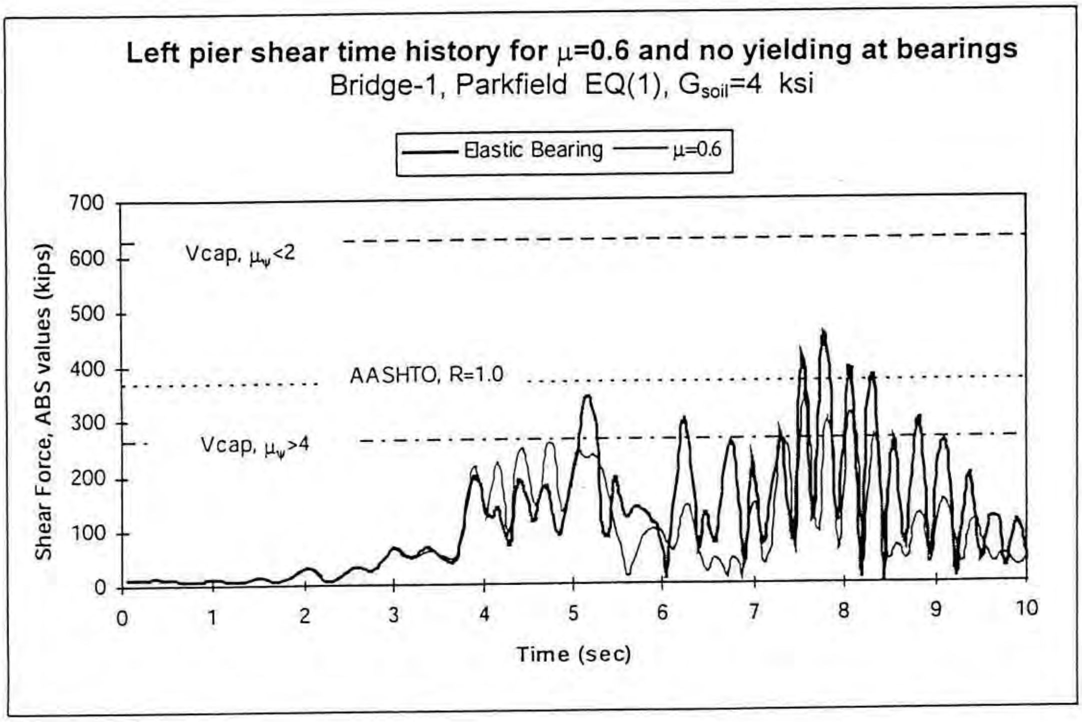

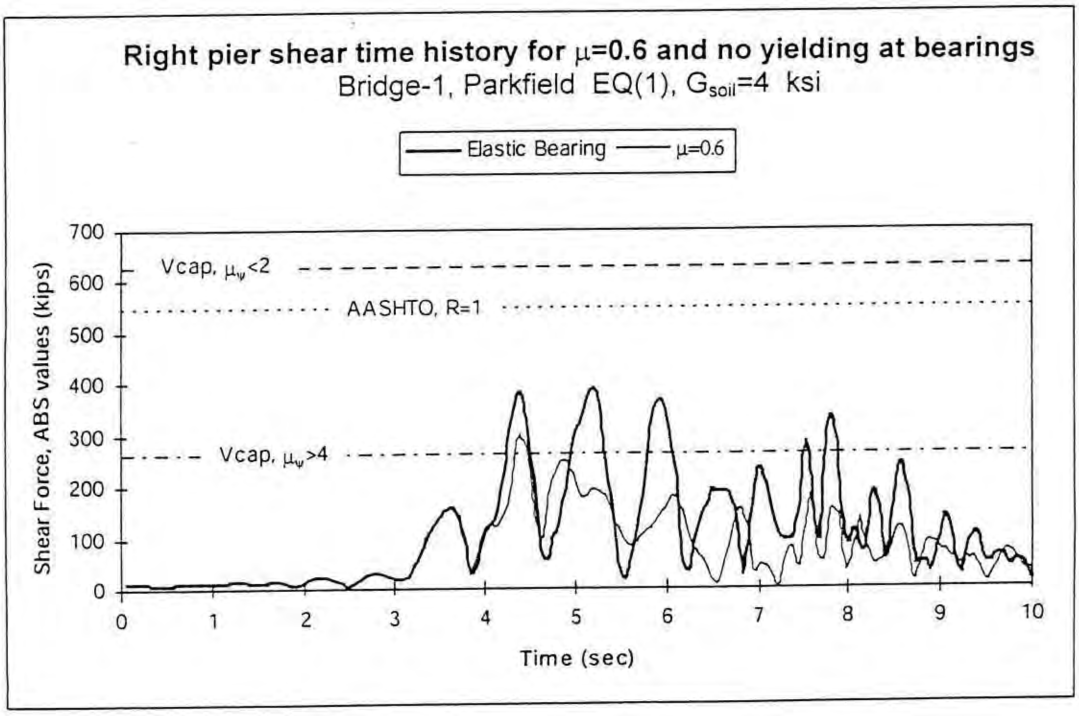

Figure 5-1 Bridge-1 time histories of resultant shear force demand at pier columns

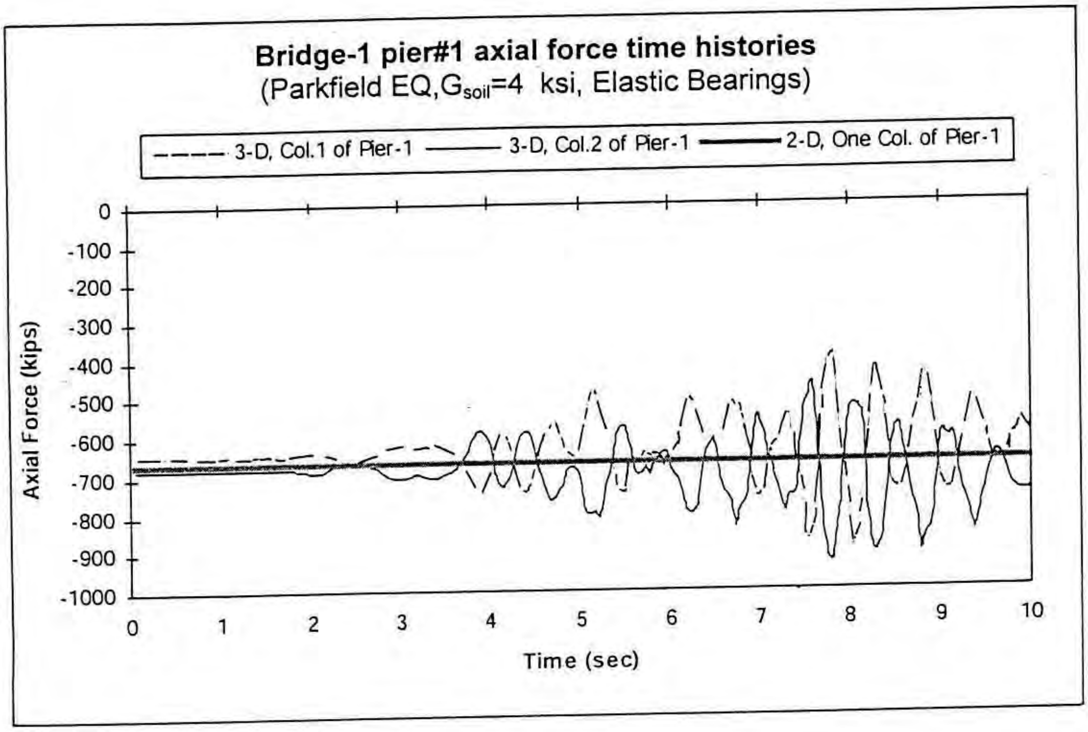

Figure 5-2 Axial force time histories of the Bridge-1 pier #1 columns 2-D and 3-D models. (G_{soil}=4 ksi, Parkfield Record (alt-1),Elastic Bearings)

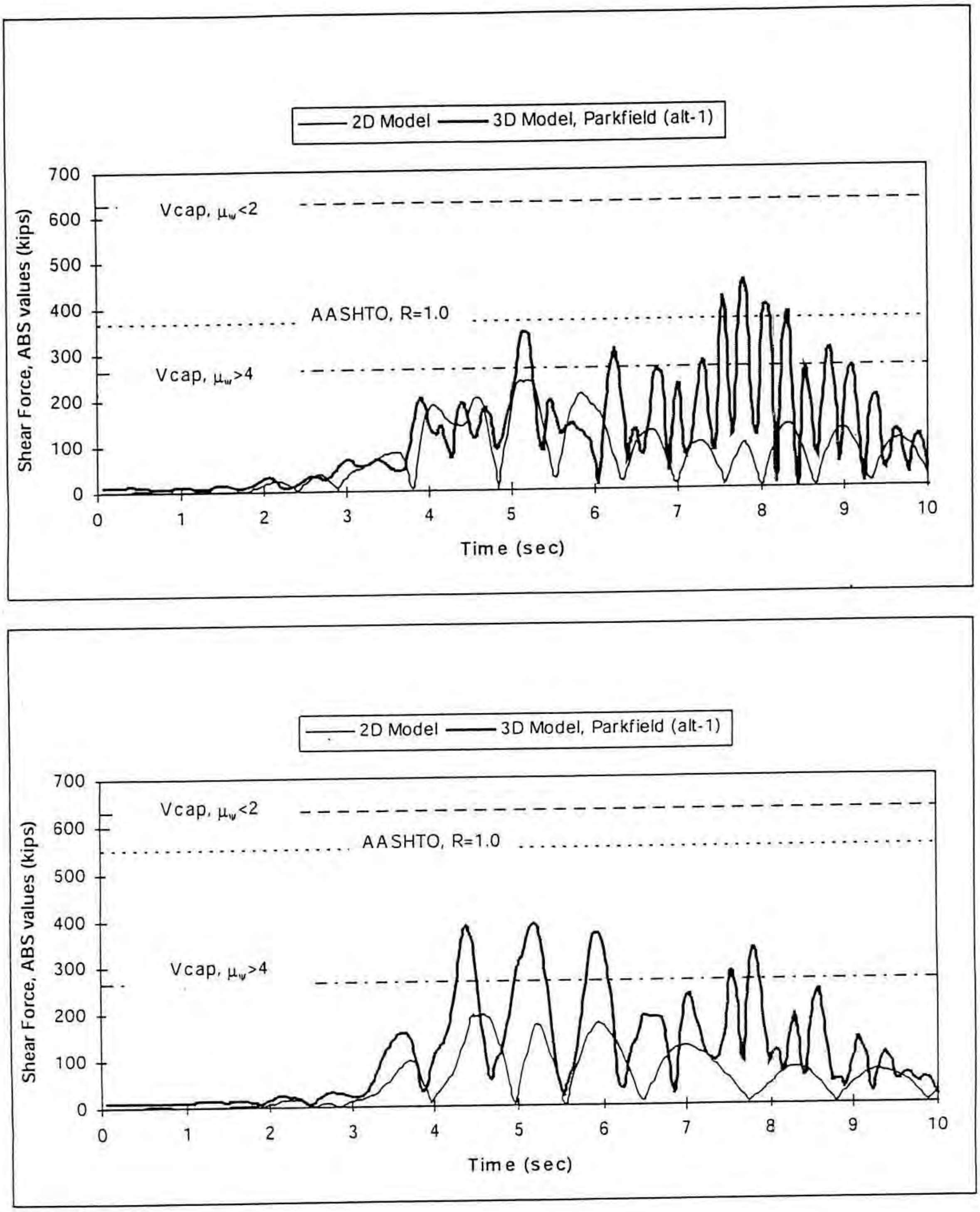

Figure 5-3 Pier column shear time history comparison of Bridge-1 for 2-D and 3-D models.
(Parkfield (alt-1)record, G_{soil}=4 ksi, Elastic bearings)

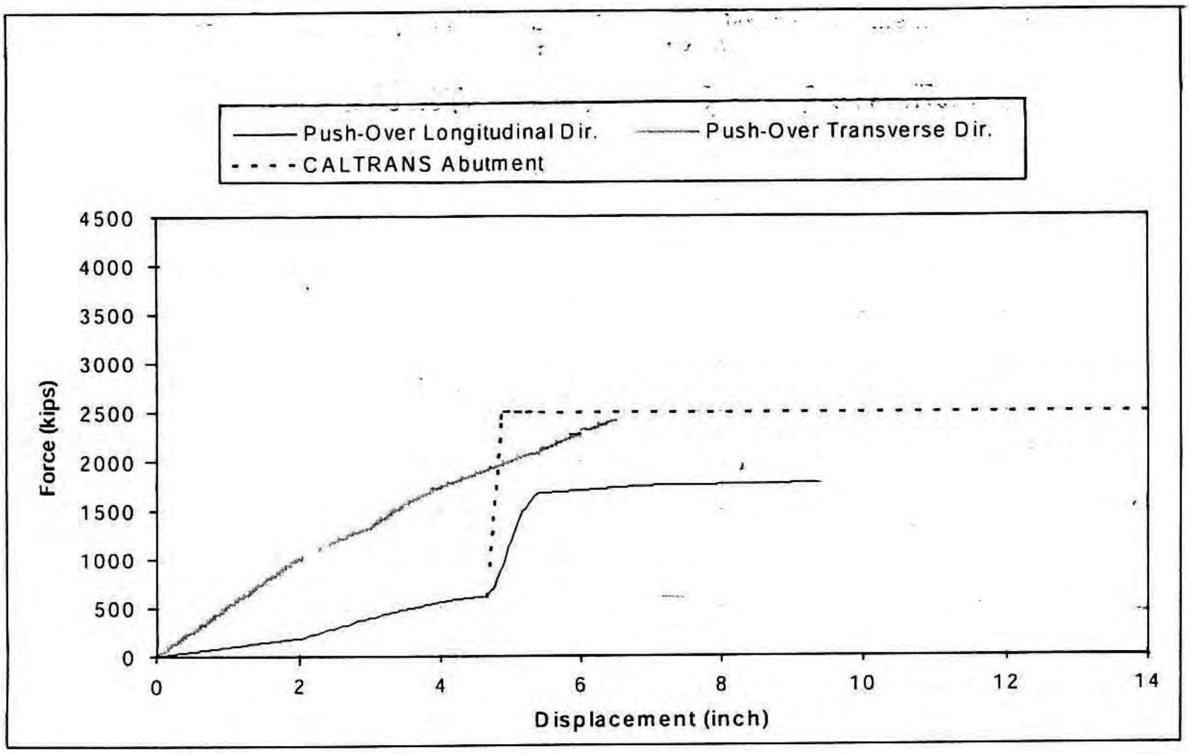

Figure 5-4 push over analysis for Bridge-1 (3-D model, Gsoil = 4 ksi)

CHAPTER 6

CONCLUSION AND RECOMMENDATIONS FOR FURTHER STUDY

6.1) CONCLUSIONS

In this study, seismic responses of three model bridges are analyzed by varying the different important properties (i.e. stiffness of soil, bearing performances) for both 2-Dimensional and 3-Dimensional models. Based on the results of extensive and systematic study, the following conclusive conclusions can be drawn from the study:

- Plastic rotation demand is affected by soil-structure interaction, under earthquakes strong enough to involve free standing abutments in the bridge dynamic response (here PGA=0.4g), the demand is higher for medium soil than softer and stiffer soils.

- Soil structure interaction (SSI) has an effect on seismic effect on seismic response in the longitudinal direction and dynamic analysis of bridge should explicitly consider SSI.

- The failure at the fixed bearing will lower the shear demand in column and abutments.

- Very stiff soils enhance the restraining action of the abutments in limiting bridge displacement, which may lead to no impact between decks. On the other end, very soft soils have less rotational restraining at the base of pier columns causing low curvature ductility demand and less damage. The most critical cases generally occur for models with moderately stiff soils. For lower PGA since abutment interaction is minimal, stiffer soil causes higher demand at pier column.

- Due to low lateral reinforcements in the pier columns shear failure has been absorbed with shear force C/D ratio low. Better confinement in columns can increase shear C/D.

- The interaction between abutment and superstructure is relatively more in 3-D models than that of 2-D models.

- The effect of backwall failure in 3-D model is not as significant as it is for 2-D models.

6.2) RECOMMENDATIONS FOR FURTHER STUDY:

The following recommendations for further study can be made from the present research:

- SSI study may be performed for bridges with pile foundation.

- Extensive experimental and observation work can be performed for identification of soil-structure interaction phenomena through utilization of data from earthquake response, forced vibration tests and microtremor observation of real data.

- Analysis may be performed using appropriate finite elements and shape function for modeling the infinite medium.

- Site response factors may be evaluated for different bridge sites.

- Extensive parametric studies varying span length, girder geometry and materials, can be done for SSI of bridges.

- Seismic response of integrated Abutment Bridge may be performed.

- More detailed analysis of deck vibration may be performed.

- Non linear behavior of pier and abutment was studied in this research using simple linear pier model. The behavior of pier can be made more realistic by Clough's degrading stiffness relationship or representing it by trilinear model.

- Different Bangladesh bridge in seismically vulnerable zone can instrumented and seismic response can be compared with theoretical analysis.

REFERENCES

AASHTO Standard Specifications for Highway Bridges, 15th Edition, 1992, Published by the AASHTO, Washington, D.C.

AASHTO LRFD Bridge Design Specifications, Customary U.S. Units, 1 st Edition 1994, published by the AASHTO, Washington, D.C.

Apsel, R.J. and Luco, J.E. (1983). "On the Green's functions for a layered half space": Part II, Bulletin of the Seismological Society of America 73, pp 931-951.

Apsel, R.J. and Luco, J.E. (1987). "Impedance functions for foundations embedded in a layered medium: an integral equation approach", *J. Earthquake Engrg. Struct. Dynamics*, 15(2), 213- 231.

Baranov,V.A. (1967). "On the calculation of excited vibrations of an embedded foundation", Voprosy Dinamiki i Prochnosti,No.14, Polytechnical Institute of Riga,pp.195-209.

Bathe, K.J. and E. Wilson (1976) "Numerical Methods in Finite Element Method", Prentice Hall, Inc. Englewood Cliffs, New Jersey, USA.

Beredugo, Y. and M. Novak (1972). "Coupled horizontal and rocking vibrations of embedded footings", Canadian Geotechnical Journal 9, pp. 477-497.

Bielak, J. (1976). "Modal analysis for building- soil interaction", ASCE 102, No. EM5, pp. 771-786

CALTRANS, Bridge Design Aids 14-1, California Department of Transportation, Sacremento, CA, October, 1989.

Clough, R.W. and Penzien, J. (1993). Dynamics of Structures, 2nd ed., McGraw Hill, NewYork, NY.

Cooley, J. W. and Tukey, J. W. (1965) "An Algorithm for the Machine Calculations of Complex Fourier Series," *Mathematics of Computation*, Vol. 19, No. 90, pp. 297-301.

Dominguez, J. (1978a). "Dynamic stiffness of rectangular foundations", Report No. R78-20, Department of Civil Engineering, Massachusetts Institute of Technology, Cambridge, Mass. USA.

Dominguez, J. (1978b). "Response of embedded foundations to traveling waves", Report No. R78-24, Department of Civil Engineering, Massachusetts Institute of Technology, Cambridge, Mass, USA

DRAIN-2DX Preliminary Element User Guide, by: V. Prakash, G.H. Powell, D.D. Campbell, F.C. Filippou. Structural Engineering, Mechanics and Material, Department of Civil Engineering, University of Berkeley, California, December 1994.

DRAIN-3DX Element Description and User Guide, by: G.H. Powell and S. Campbell. Structural Engineering, Mechanics and Material, Department of Civil Engineering, University of Berkeley, California, Report No. UCB/SEMM-94/08, December 1994.

FHWA (1986) Seismic Design of Highway Bridge Foundations Vol. II: Design Procedures and Guidelines, Report No. FHWA/RD-86/102, Federal Highway Administration, June 1986.

FHWA (1995) Seismic Design Manual for Highway Bridges, Publication No. FHWA-RD-94-052,Federal Highway Administration, May 1995.

Ganev, T, F. Yamazaki, and T. Katayama (1995a). "Observation and numerical analysis of soil-structure interaction of a reinforced concrete tower", Earthquake Engineering and Structure Dynamics 24, pp. 491-503.

Ganev, T, F. Yamazaki, T. Katayama and T. Ueshima (1995b). "Soil-structure interaction of a containment model in Hualien, Taiwan", Proceedings of the Twenty third JSCE Earthquake Engineering Symposium, pp. 397-400, Tokoyo, Japan.

Gazetas, G. (1983). "Analysis of machine foundation vibrations state of the art", Soil Dynamics and Earthquake Engineering , pp. 2-42

Goel, Rakesh K., and Chopra A. K. (1997) "Evaluation of Bridge Abutment Capacity and Stiffness during Earthquakes," Earthquake Spectra, Volume 13, No. 1, pp. 1-23, February, 1997.

Gutierrez. J. A. (1976). "A substructure method for earthquake analysis of soil-structure interaction", Report No. EERC 76-9, Earthquake Engineering Research Center, University of California, Berkeley, USA.

Gutierrez, J.A. and A.K. Chopra (1977). "Evaluation of methods for earthquake analysis of soil –structure interaction" , Proc. 6th World Conference of Earthquake Engineering 4, pp. 1-6, New Delhi, India.

Harada, T.K. Kubo and T. Katayama (1981). "Dynamic soil- structure interaction analysis by Continuum Formulation Method", Report of the Institute of Industrial Science 29, University of Tokyo, Japan.

Hayashi, y. and I. Takahashi (1992). "An efficient time- domain soil structure interaction analysis based on the dynamic stiffness of an unbounded soil", Earthquake Engineering and Structural Dynamics 21, pp. 787-789.

Iwan, W. D. (1967) "On a class of models for the yielding behavior of continuous and composite systems," *Journal of Applied Mechanics,* ASME, Vol. 34, pp.612-617.

Kausel, E, and J.M. Roesset (1974). "Soil- structure interaction problems for nuclear containment structures", Proceedings of the ASCE Power Division Specialty Conference, Denver, Colorado, USA.

Kramer, S. L. (1996). *Geotechnical Earthquake Engineering*, Prentice Hall, Upper Saddle River, New Jersey, pp. 254-280.

Luco, J.E. and H.L Wong (1986). "Dynamic response of a hemispherical foundation embedded in a viscoelastic half-space", ASCE 112, No. EM 12, pp. 1363-1374.

Luco J.E. and H.L. Wong (1987) "Seismic response of foundations embedded in layered half-space", Earthquake Engineering and Structural Dynamics 15, pp. 233-247.

Luco J.E. And R.J. Apsel (1983). "One the Green's functions for a layered half space : Part I", Bulletin of the Seismological Society of America 73, pp. 909-929

Lysmer, J. F. Ostadan, M. Tabatabaie , S. Vahdani and F. Tajirian (1988). "SASSI, A Systeem for Analysis of Soil-Structure Interaction", User's Manual, The university of California at Berkeley, USA.

Maroney, B., B. Kutter, K. Romstad, Y. H. Chai, and E. Vanderbilt (1994)"Interpretation of large scale bridge abutment test results," Proceedings, 3 rd Annual Seismic Research Workshop, California Department of transportation, Sacramento, California.

Mita, A. (1986). "Dynamic response of embedded foundations :a hybrid approach", *Report No.ORI 86-06,Ohsaki Research Institute,*Shimuzi Corporation,Japan.

Mita, A. and J.E. Luco (1987). "Dynamic response of embedded foundations : a hybrid approach", *Computer methods in applied mechanics and engineering* 63, pp. 233-259

Resisser, E and H.F. Sagoci (1944). " Forced Torsional Oscilations of and elastic half-space " Journal of Applied Physics 15, pp. 652-662.

Roesset. J. M. Whitman R.V. and R. Dobry (1973). "Modal analysis for structures with foundation interaction", ASCE 99, No. ST3, pp. 399-416.

Rashidi, S., and M. Ala Saadeghvaziri (1997). "Modeling and Effect of Impact on Seismic Response of Multi-Span Bridges," Computers and Structures, Vol. 64, No. 5/6, 1997..

Saadeghvaziri, M. Ala, S. Rashidi (1997) "Seismic Retrofit and Design Issues for Bridges in New Jersey," Transportation Research Records, No. 1594, TRB, Nov., 1997.

Schneider, J.F., Abrahamson, N.A., Somerville, P.G., and Stepp, J.C. (1990). "Spatial variation of ground motion from EPRI's dense accelerograph array at Parkfield, California," *Proc. 4th U.S.*

Seed, H.B. and Lysmer, J. (1980). "The seismic soil-structure interaction problem for nuclear facilities," *in* Soil-structure interaction: the status of current analysis methods and research, J.J

Safak, E. (1991). "Identification of linear structures using discrete-time filters," *J. Struct. Engrg.*, ASCE, 117(10), 3064-3085. 208

Saadeghvaziri, M. Ala, and S. Rashidi (1988) "Effect of Steel Bearings on Seismic Response of Bridges in Eastern United States," Proceedings, 6 th U.S. National Conference on Earthquake Engineering, Seattle.

Siddharthan Raj V., M. El-Gamal, E. A. Maragakis(1997) "Stiffnesses of abutments on spread footings with cohesionless backfill," Canadian Geotechnical Journal, Vol.34, pp. 686-697, 1997.

Sugito, M. (1995) "Frequency-dependent equivalent strain for equi-linearized technique," Proceedings of the First International Conference on Earthquake Geotechnical Engineering, Vol. 1, A. A. Balkena, Rotterdam, the Netherlands, pp. 655-660.

Tsai, N. C., and Housner G. W. (1970) "Calculation of Surface Motions of a Layered Half-Space," *Bulletin of the Seismological Society of America,* Vol. 60, No. 5, pp. 1625-1651.

Timoshenko, S.P. and Goodier J.N. (1951). "Theory of elasticity", McGraw-Hill Book Co. New York, USA.

Seismic Retrofitting Manual for Highway Bridges, Publication No. FHWA-RD-94-052, May 1995 Hognestad, E., "A Study of Combined Bending and Axial Load in Reinforced Concrete," University of Illinois Experiment Station, Bull. Series No. 339, November 1952.

Wolf, J.P. (1985). "Dynamic soil-structure interaction", Prentice Hall, Inc, Englewood Cliffs, N.J. 07632, USA.

Wolf J.P. (1994) "Foundation vibration analysis using simple physical models", Prentice Hall, Inc, Englewood Cliffs, N.J. 07632, USA

Wilson, John, and B. S. Tan (1990) "Bridge Abutments: Formulation of Simple Model for Earthquake Response Analysis," Journal of Engineering Mechanics, ASCE, Vol. 116, No. 8, pp. 1828-1837, August, 1990.

Zimmerman, R. M., and R. D. Brittain. (1979) "Seismic response of multi-simple span highway bridges." In: Proceedings of the 3 rd Canadian Conference on Earthquake Engineering, Montreal, 1979. Pp. 1091-1120